A Mathematical Model of Bovine Metabolism and Reproduction: Application to Feeding Strategies, Drug Administration and Experimental Design

Dissertation

zur Erlangung des akademischen Grades
eines Doktors der Naturwissenschaften

am Fachbereich Mathematik und Informatik
der Freien Universität Berlin

vorgelegt von

Mohamed Omari

Berlin, March 2019

Betreuer/Erstgutachter:
Prof. Dr. Susanna Röblitz
Department of Informatics, University of Bergen, Norway

Zweitgutachter:
PD Dr. Marcus Weber
Konrad-Zuse-Zentrum für Informationstechnik Berlin (ZIB)

Datum der Disputation: 12. July 2019

Contents

Dedicated to the memory of Niklas Werner

Introduction

Over the past 50 years, reproductive physiology in dairy industry has significantly changed to adapt to high milk production, [123, 33]. A few weeks after calving, modern high-yielding dairy cattle in intensive production systems give around 40 liters of milk per day. This is a high amount that comes at a cost. High-producing cows are highly susceptible to disease, show metabolic disorders and fertility problems [33, 39, 123], see Fig 1. Early culling and smaller lifetime milk production are the consequences [221]. Countermeasures have already been taken, and the trend of breeding cows with ever increasing peak milk yield – prevalent for decades – may have come to an end. Optimizing lifetime milk production has proven to be more beneficial for both economic as well as environmental reasons [35].

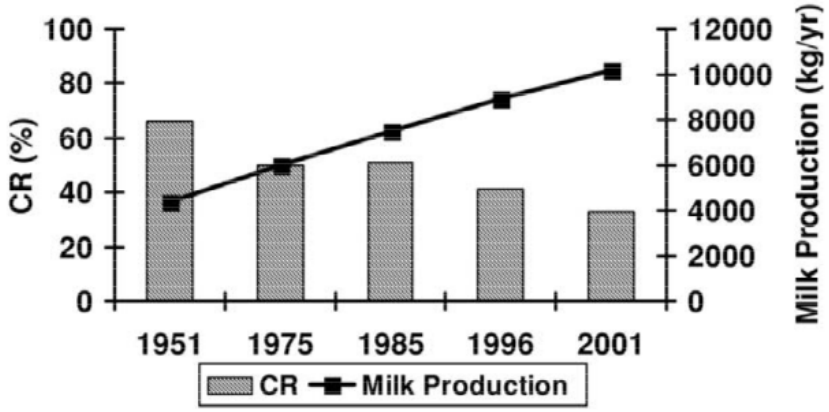

Figure 1: **Milk production and fertility in dairy cows.** The inverse relationship between conception rate (CR%) and annual milk production of Holstein dairy cows in New York. Data from Butler et. al, [33].

The most critical time period for a cow's health and her future performance is the periparturient period and the period of early lactation [217, 218]. During that time, the cow mobilizes body reserves because of her inability to meet energy demands

solely from the feed energy consumed. This state is referred to as negative energy balance (NEB) [155], see Fig 2.

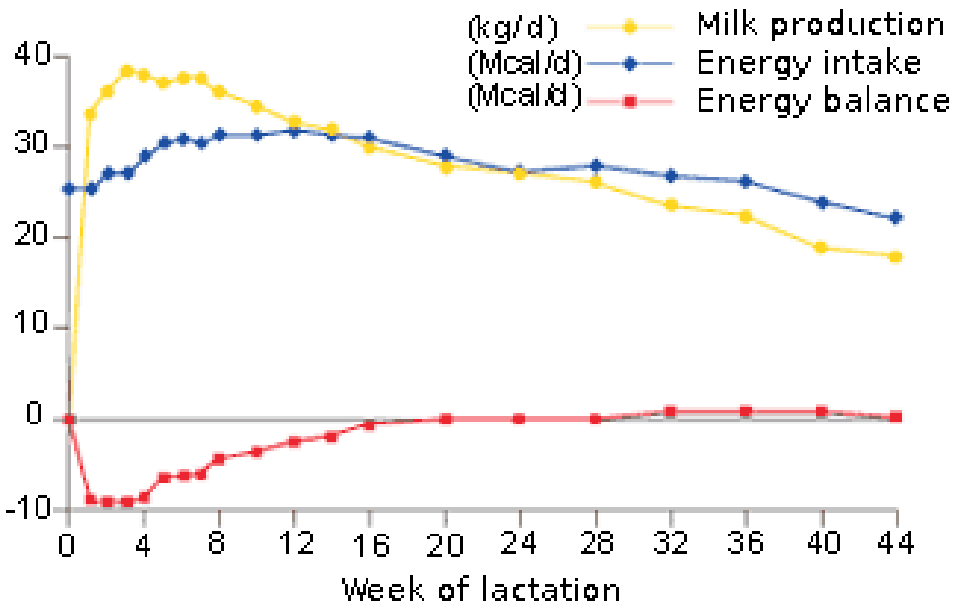

Figure 2: **Relationship between energy intake and requirements for a lactation in high producing dairy cows.** This figure shows that during the first weeks of lactation, cows are in a negative energy balance and are using body energy reserves to meet their needs. A zero net energy balance (i.e., intake sufficient to meet requirements) was not achieved until a point in lactation where milk production decreases. Figure from Baumann et. al, [9].

For ruminants, the energy content in feed cannot be increased without limits due to the fermentative character of the digestive system [44]. High energetic feed with little fiber leads to an imbalance of microbes, rumen acidosis, and may even cause severe illness and death. Nevertheless, targeted feeding strategies are able to extenuate the NEB and to ensure animal health and welfare [218, 173, 96].

A number of experimental and clinical studies were performed to examine the relationship between the metabolic status and the fertility of cows, both in qualitative and in quantitative manners, e.g., [57, 167]. Reduced nutrition intake was observed to delay the onset of puberty in beef heifers [188, 50, 229], to change the growth pattern of the dominant follicles (maximal diameter, persistence, number of follicular waves) [146], and to increase the period to conception postpartum

[227, 171, 182]. Studies in the postpartum period of dairy cows showed that the NEB is strongly correlated with low concentrations of glucose, insulin and *IGF*-1 in the blood [11, 30, 124]. Changes in the secretion of gonadotropins, caused by low glucose levels, lead to low *FSH* and *LH* concentrations [57, 33], whereby missing *LH* peaks cause anovulation [217], see Fig 3.

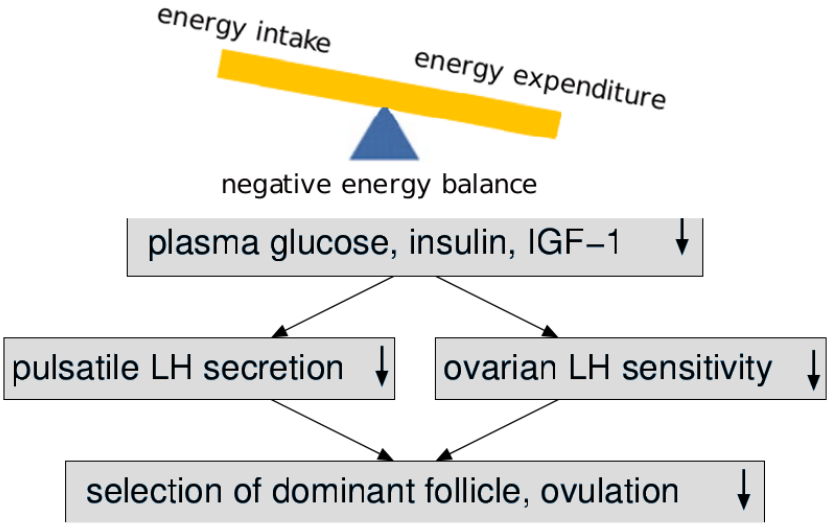

Figure 3: **Schematic illustration of the possible effect of NEB on the fate of dominant follicle.** NEB is characterised by reduced concentrations of glucose, insulin and *IGF*-1 in the blood. This in turn reduces the pulsatile *LH* secretion as well as the ovarian *LH* sensitivity, which results ultimately in ovulation failure.

On the other hand, it was reported that good feed management, e.g., nutritional manipulation that causes increased insulin [77], reduces the incidence of non-regular estrous cycles, often being associated with low average concentrations of insulin in the blood [75].

In general, the mechanisms that result in a reduced fertility are not completely understood, although a close relationship to the glucose-insulin metabolism is widely supported. Therefore, to improve practical reproduction such as pregnancy rate along with milk production simultaneously, a systems biology approach can be adopted to seek better understanding of the mechanisms linking nutrition to fertility and milk production. Thus, as an attempt to contribute to the efforts performed for the improvement of fertility in dairy cows, this thesis focuses on the role of nutritional impacts in improving the reproductive performance in dairy cows.

Particularly, this thesis focuses on the investigation of the impact of glucose, as part of the feed and as one of the main energy sources of the body, on the estrous cycle dynamics in dairy cows. Thus, to be able to explore various feeding scenarios, the aim is to develop a mathematical model that represents metabolic processes as well as reproductive regulation. This model can allow us to analyse the impact of glucose originating from the feed on the reproductive hormones and the follicular development. In addition, the model can be used to simulate and design feeding and therapeutic strategies that may aid in reducing animal experiments.

Outline

In Chapter 1, a short overview of mathematical modelling in general is provided. Moreover, some basics of modelling approaches and numerical modelling techniques that are employed for developing and simulating a mathematical model in system biology are also introduced. The second part of Chapter 1 focuses on presenting some technical tools borrowed from Bayesian inference and information theory. These tools are used for the simulation and application of the mathematical model of metabolic and reproductive regulation in Chapters 4 and 5.

In Chapter 2, the development of a mathematical model, called *the MetRep model* throughout this thesis, which combines reproductive hormones and glucose-insulin dynamics within the body of the cow is described. The model is based on ordinary differential equations and relies on previously introduced models of the bovine estrous cycle and the glucose-insulin dynamics. Necessary modifications and coupling mechanisms are thoroughly discussed.

In Chapter 3, model simulation results for different nutritional regimes in lactating and non-lactating dairy cows are examined and compared with experimental studies. In particular, depending on the amount of the dry matter and its glucose content, the model quantifies reproductive hormones and follicular development over time.

In Chapter 4, an attempt to link the MetRep model to a pharmacokinetic model is performed. The coupling is based on mechanisms underlying homeostasis regulation by dexamethasone. In particular, the coupling takes into account the predominant role of dexamethasone in stimulating glucagon secretion, glycogenolysis and lipolysis and impairing the sensitivity of cells to insulin. The resulting pharmacokinetic-pharmacodynamic model simulates the effect of one single dose of dexamethasone on the physiological behaviour of the system, especially glucose metabolism.

In Chapter 5, the MetRep model is used for simulating the design of experiments. Particularly, we make use of the model, together with Bayesian inference and information theory to select the optimal design. The latter is expected to inform us about when to measure, i.e. select the optimal sampling times of measurement,

and what to measure, i.e. specify observed species. These information allow us to reduce the uncertainty in the model parameters for non-lactating cows and the uncertainty in predicting the ovulation time during postpartum for lactating cows.

Chapter 1

General Background

This chapter briefly reviews some basic concepts of mathematical modelling in systems biology as well as some numerical techniques that can be employed for developing and simulating the mathematical model throughout the next chapters of this thesis. We begin by presenting a general overview of mathematical modelling and give an example of how to translate a biological problem to a mathematical model. Then, we review some numerical tools such as the numerical integration of ordinary differential equations, sensitivity analysis, and criteria that can be used to simulate and analyse the output of a mathematical model. Subsequently, we present some technical tools of Bayesian inference and information theory that are needed for developing Chapter 5.

1.1 Some Concepts of Mathematical Modelling in Systems Biology

The word model can be defined differently in many ways. In this paragraph, the following thoughts about what is a model are inspired from [12, 62]. A model can be a simplified description or miniature conception of a real object, particular system, phenomena, etc. For instance, it may be as simple as a drawing of house plans, assembling and gluing together some materials to form an aeroplane kit, or it can be also an example for emulation or analogy used to help visualize something (e.g., an atom) that cannot be directly observed. This definition means that modelling is an activity in which we think about, lay out a detailed plan and then create models to describe how systems or objects of interest behave. There are several ways these behaviours can be described. For example, we can use words, sketches, physical models, computer programs, mathematical formulas, or often simultaneously a combination of these things. In particular, the practice of using the language of mathematics to create models is called mathematical modelling.

Mathematical modelling can be viewed as an interdisciplinary subject, where one may use whatever knowledge from mathematics and of the system of interest. Math-

ematical modelling can also be described as the art of translating real life problems from an application area into tractable mathematical formulations whose theoretical and numerical analysis provides insight, answers, and useful guidance for the originating application [101]. As described by C. Dym in his book [62], the process of constructing a mathematical model can be viewed as having three stages: observation, modelling, and prediction, see Fig 1.1. In the observation part we observe and measure what is happening in the real world. Afterwards, we gather empirical evidence, i.e. collecting data which may provide substantial information about the system of interest. Observations may be direct, as when we use our senses, or indirect, in which case some measurements are taken to indicate through some other reading that an event has taken place. Once enough information has been collected, modelling activities start here. The modelling part focus on analysing these observations and shaping them into mathematical formulas. These formulas can be expressed in terms of a set of numbers or system of equations. Typically, a mathematical model is composed of variables that describes the state of the system, parameters that can be varied under experimental conditions, and forcing functions which are external influences acting upon the system. A mathematical model can take many forms, continuous versus discrete (some models regard time as a discrete quantity while others treat it as a continuous variable), linear versus non-linear, static versus dynamic, and deterministic versus stochastic [12]. A common class of mathematical models that fall under the umbrella of deterministic dynamical systems are ordinary differential equations (ODEs). These equations describe how a quantity of interest, denoted x, changes over time. ODEs tend to contain derivatives (rates of change) of dependent variables with respect to time. Here, the initial state of the system, denoted x_0, completely determines all future states. Mathematically, an ODE is written as

$$\frac{dx(t)}{dt} = f(\theta, x(t)),\ x(0) = x_0 \in \mathbb{R}^n, \tag{1.1}$$

where $x = (x_1, \ldots, x_n) \in \mathbb{R}^n$ is called the state variable, and $\theta = (\theta_1, \ldots, \theta_d) \in \mathbb{R}^d$ is the model input parameter vector.

In the prediction part, we exercise our models to tell what will happen in a yet-to-be-conducted experiment or in an anticipated set of events in the real world. These predictions are then followed by observations that serve either to validate the model or to suggest reasons that the model is inadequate [62].

In fact, the use of mathematical modelling is not a new subject. Rather, it has been there since a long time ago, where scientists have been studying a variety of problems through mathematical models, such as the fundamental laws of force and motion published by Issac Newton in his fundamental work "Mathematical Principles of Natural Philosophy" in 1687 [150]. Nowadays, there is hardly any area of study and research, which escapes from mathematical modelling. For instance, both mathematics and computer programs are commonly used nowadays by scientists to

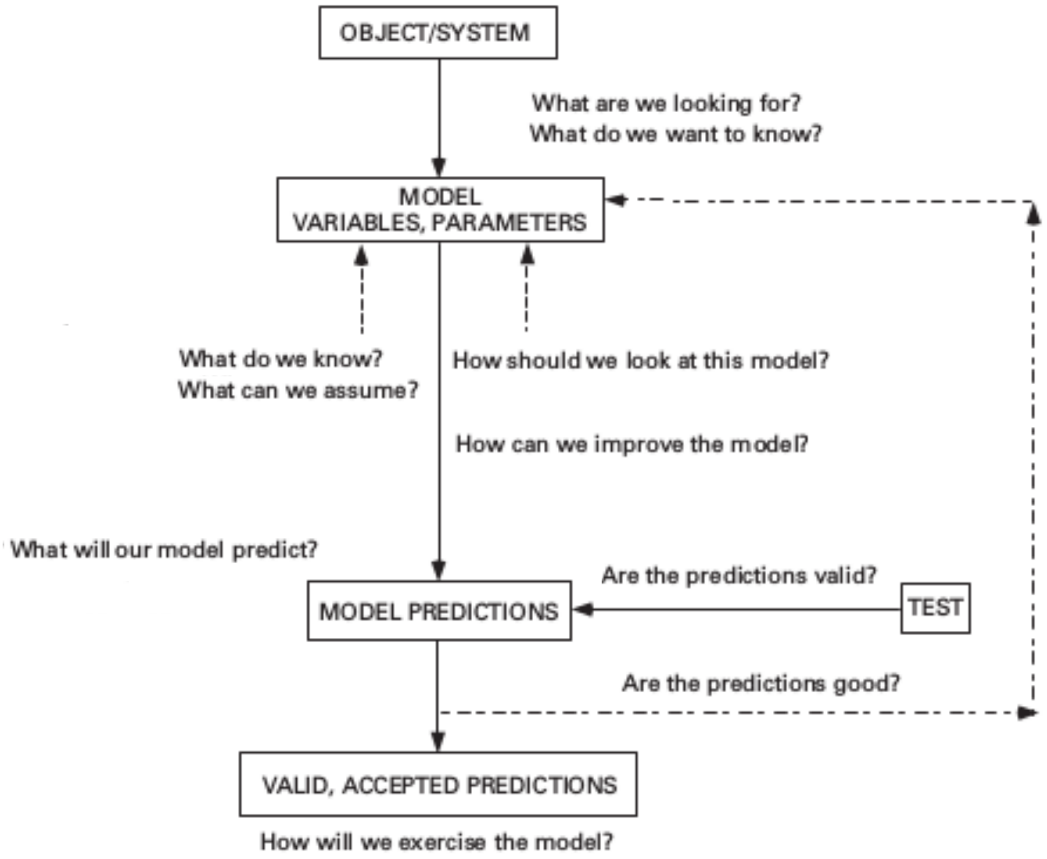

Figure 1.1: **An illustration of possible paths through the stages of modelling.** A mathematical model can be formulated and improved through the typical repeated iterations, observation, modelling, and prediction. This process of repeated iterations is one of the most useful aspects of modelling in terms of improving our understanding about how the system works (inspired from [43, 62]).

construct mathematical models for biological, social, economical, or whatever system. In addition, due to the rapid development of computers during the last 50 years, it becomes now possible to solve and simulate these mathematical models that could hardly be imagined a couple of decades ago.

It is very important to point out that since every person has different scientific knowledge and a subjective manner of looking at problems, some persons may formulate different models for the same system. Here, it is worthwhile to mention that models should be constructed in a simple manner, yet reproducing the true process behaviour. This idea was also attributed to A. Einstein: ***A model should be as simple as possible, but not simpler***. In addition, models should be easy to use and reveal everything about the internal cause and effect relationships

within the process [12]. Unfortunately, there is no accurate or perfect model that would represent a system of interest. This is also pointed out by G. Box [20]: ***Essentially, all models are wrong, but some are useful.*** As a matter of fact, one is always faced with the trade-off between accuracy, flexibility and cost. Since each model would be formulated for a specific task to a prescribed accuracy, unfortunately there is no definite "algorithm" to construct a mathematical model that will work in all situations, rather an adaptive alteration of the model is always considered. For this reason, increasing the accuracy of a model generally increases cost and decreases flexibility. Usually, the ultimate goal in constructing a model is to obtain a "sufficiently accurate" and flexible model at a lower cost [12]. In the end, mathematical models can be limited in predictions due to possible shortage of knowledge about the system. However, it is clear that their ability to simulate, and to some extent predict real-world systems provides a distinct advantage. Especially, as computing power becomes cheaper, mathematical modelling becomes an increasingly cost-effective to direct experimentation.

The mathematical modelling in systems biology is relatively new discipline. The end of 20th century was known for tremendous technological and scientific breakthroughs. These discoveries advanced new developed experimental techniques in systems biology, which prompted the emergence of many mathematical models. These mathematical models have been constructed within newly created subdisciplines such as computational biology and bioinformatics, which are at the crossroads of biology, physics, chemistry, informatics and mathematics. These models have been used for testing hypotheses about the underlying processes of complex biological systems.

Complex biological systems consist of several components which interact to control the functioning of building blocks of life. In human and animal, for example, the metabolic system is comprised of several organs, hormones and enzymes that interact together to digest, absorb, process, transport, and excrete the nutrients that are essential to life [48]. The endocrine system particularly consists of glands that produce hormones regulating metabolism, reproduction, and growth-decay of organisms. To model, simulate and predict the dynamical changes of these interacting components over time, mathematical skills can play a crucial role in elucidating and understanding the biological mechanisms behind these complex interactions within the system.

As mentioned earlier, observing and measuring what is happening in the system of interest is the first step to perform before constructing a model. For biological phenomena, a common starting point in constructing a model is to make use of collected observations, measurements, as well as existing scientific knowledge to come up with a graphical representation (also called conceptual model or flowchart) that roughly reflects the biological mechanisms one aims to model. In fact, this preliminary step is probably one of the most challenging task in modelling. It requires

the collaboration from mathematicians and biologists, yet they all use the same approach, or language, housed within the scientific method they share. The aim of this highly interdisciplinary task is to formulate a clear description of the complex biological system. In other words, the task is to define the prevailing processes controlling the system, and also to discuss and decide about the level of model complexity to consider. The chosen graphical representation should be reliable and computationally plausible. Usually, this graphical representation is iteratively updated throughout the modelling process.

After formulating a comprehensive graphical representation of the problem, the translation of biological processes to mathematical formulas can be done in different ways. This depends on the dynamical behaviour of the system, e.g. deterministic or stochastic. For instance, if we assume that every substance in the system, denoted x, is a continuous variable and no randomness is taking place, the evolution of the system from one state to another can be represented by a system of differential equations.

Typically x is a concentration, but x could also represent a density or the number of molecules. The change of x, Δx, per time interval Δt depends on the *gain* rate r_+ at which x is generated. In this case, the rate of generation reflects all processes that lead to an increase in x, i.e. synthesis, production. It depends also on the *loss* rate r_- at which x is removed. The loss rate includes all processes that lead to a decrease in the value of x, i.e. clearance, release, and decay. Additional rates, denoted g, that may describe for example possible complex formation or chemical modification can be considered. The rate of gain, loss and g are a non-negative functions that need to be specified. More formally we can model the change of x by the following,

$$\frac{\Delta x(t)}{\Delta t} = r_+ - r_- \pm g\,. \tag{1.2}$$

Instead of considering finite time intervals Δt, we will consider the change in an infinitesimal small time interval dt, such that,

$$\frac{dx(t)}{dt} = r_+ - r_- \pm g\,. \tag{1.3}$$

When $dx(t)/dt = 0$, then we say that the system reaches an equilibrium point, also referred to as steady state. The mathematical expression of each rate depends on its dynamical change over time. For instance, sometimes the *gain* term is simply a zero-order rate, i.e. the rate is apparently independent of the change of the concentration of x, e.g. a constant input into the system. It can also be expressed in terms of first-order rate, that is, a linear term which depends only on a synthesis rate constant and the current concentration of x. In other situations, the *gain* term can be expressed as a non-linear rate, which still depends on the current concentration of x. Some commonly used non-linear rates are the Hill functions which are

an extension of the Michaelis-Menten equation. The so called Hill functions were introduced by A. V. Hill in 1910 to describe the equilibrium relationship between oxygen tension and the saturation of haemoglobin [90]. Thereafter, they have been widely used in biochemistry, physiology, and pharmacology to analyse the binding equilibria in ligand-receptor interactions [225]. The Hill functions are often used to model some processes when quantitative biological mechanisms are unknown, but information about qualitative regulation such as stimulations or inhibitions between substances are available. The derivation of the Hill functions is introduced in the following.

In chemical kinetics, the law of mass action kinetics states that the rate of the reaction is proportional to the product of reactant concentrations [65]. For a simple reaction as the following,

$$S \xrightarrow{k_0} P \tag{1.4}$$

where a substance P is produced from a substance S with a reaction rate constant $k_0 \geq 0$, the two ODEs that describe the kinetics are,

$$\frac{dx_S}{dt} = -k_0 \cdot x_S \quad and \quad \frac{dx_P}{dt} = +k_0 \cdot x_S, \tag{1.5}$$

where x_S and x_P are quantities, e.g. concentrations or number of molecules, of the substances S and P, respectively.

Now let us consider the following reversible reaction,

$$A + nB \underset{k_-}{\overset{k_+}{\rightleftharpoons}} A_{nB}, \tag{1.6}$$

where k_+ and k_- are the rate constants and n is the order of reaction with respect to B, which for example describes the binding of n ligand molecules B simultaneously to the receptor A. The ODE that describes the dynamical change of the quantity $x_{A_{nB}}$ over time would be as,

$$\frac{dx_{A_{nB}}}{dt} = k_+ \cdot x_A \cdot x_B^n \; - \; k_- \cdot x_{A_{nB}}, \tag{1.7}$$

where x_A and x_B are quantities, e.g. concentrations or number of molecules, of the substances A and B, respectively. In equilibrium, the reaction rate is zero, i.e. $dx_{A_{nB}}/dt = 0$, which gives

$$K_D = \frac{k_-}{k_+} = \frac{x_A \cdot x_B^n}{x_{A_{nB}}}, \tag{1.8}$$

where K_D is called the dissociation constant. Furthermore, assume now that the total quantity of binding sites exists within a steady state. Thus, the total receptors of a binding sites, bound or unbound, is constant, that is,

$$x_A + x_{A_{nB}} = x_{A_{Tot}}. \tag{1.9}$$

It follows then from the eq.(1.8) and eq.(1.9) that the fractions of bound and free molecules A are respectively given by

$$H^+(x_B) = \frac{x_{A_{nB}}}{x_{A_{Tot}}} = \frac{x_B^n}{T^n + x_B^n} \quad and \quad H^-(x_B) = \frac{x_A}{x_{A_{Tot}}} = \frac{T^n}{T^n + x_B^n}, \tag{1.10}$$

with $T^n = K_D$. The functions H^+ and H^-, defined in the eq.(1.10), are both known as Hill functions. H^+ and H^- are monotonic increasing and decreasing functions, respectively, that satisfy the following properties,

$$H^+(S) = \begin{cases} 0 & \text{if } S = 0, \\ 1/2 & \text{if } S = T, \\ 1 & \text{if } S \longrightarrow \infty. \end{cases} \qquad H^-(S) = \begin{cases} 1 & \text{if } S = 0, \\ 1/2 & \text{if } S = T, \\ 0 & \text{if } S \longrightarrow \infty. \end{cases} \tag{1.11}$$

As it can be seen from the eq.(1.11), the Hill functions are sigmoidal functions between zero and one that switch at the threshold $S = T$ from one level to the other with a slope specified by $n \geq 0$. This number controls the steepness of the curve, see Fig 1.2. If $n = 1$, the Hill function is reduced to its simpler form known as the Michaelis-Menten equation [140]. We introduce the unscaled Hill functions as

$$H^+(S, T, n) := \frac{S^n}{S^n + T^n}, \quad H^-(S, T, n) := \frac{T^n}{S^n + T^n} = 1 - H^+(S, T, n). \tag{1.12}$$

These mathematical notations, H^+ and H^- will be used throughout the modelling process in this thesis.

Whenever a Hill function is used, it is provided with another parameter α, which controls the height of the switch, or in other words, it can serves as the maximum effect. Sometimes, the available biological knowledge about the dynamic of substances comprised in a model such as in (1.3) usually consists of only qualitative information, i.e. stimulations or inhibitions between the involved substances. Thus, when necessary, the rates appearing on the right hand side of the eq.(1.3) can be modelled in terms of scaled Hill functions,

$$\widehat{H}^+ = \alpha \cdot H^+(S, T, n) \qquad \widehat{H}^- = \alpha \cdot H^-(S, T, n). \tag{1.13}$$

where $\widehat{H}^+$ model the maximum stimulatory effects and $\widehat{H}^-$ model the maximum inhibitory effects. These effects describe the regulation of mechanisms between the involved substances.

1.2 Numerical Simulations of Mathematical Models

In this section, we introduce some basic numerical tools used for the simulation of the mathematical model in this thesis. We first start by presenting the solver used

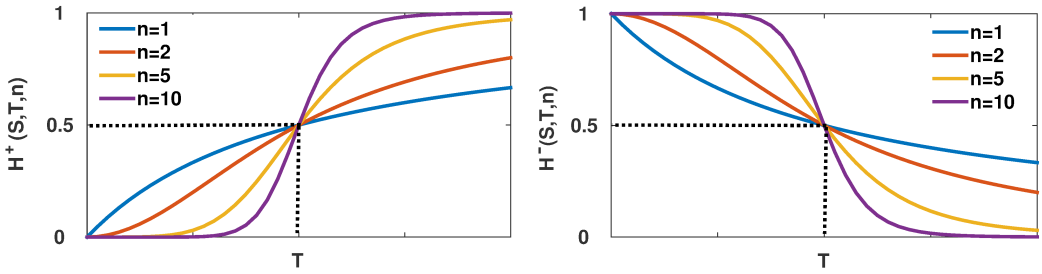

Figure 1.2: **Hill functions.** Unscaled positive and negative Hill functions with different steepness coefficients. A higher coefficient n leads to a steeper switch of the regulation.

for the simulation of the system of differential equations, and then explain the sensitivity analysis approach used for determining the model input parameters, which mostly contribute to a quantity of interest depending on the model output. Finally, we introduce a parameter identification algorithm used for searching model parameter values leading to time evolution of species concentrations that are biologically meaningful.

1.2.1 Numerical Integration of ODEs

For simple differential equations, it is possible to find closed form solutions. If the equation is of the form as eq.(1.1), the general solution would be

$$x(t) = \int f(\theta, x(s))ds + x_0. \tag{1.14}$$

In fact, many biological mechanisms are shaped into a high dimensional non-linear models. In this case, the problem has no analytical solution, thus the numerical approach is essential here to solve the problem. There are many sophisticated algorithms for doing this, but almost all are built from discretizing the differential equation and step forward in time with small steps. The simplest variant of this stepping is the Euler scheme. An equation of the form (1.1) can be converted to

$$\lim_{\Delta t \longrightarrow 0} \frac{x(t+\Delta t) - x(t)}{\Delta t} = f(\theta, x(t)), \tag{1.15}$$

where Δt is a finite time interval. Suppose Δt is fixed to a particular value h. Doing this is called discretising the continuous ODE model and h is called the discretisation step. Thus, choosing a value h for the size of every step, and set $t_n = t_0 + nh$, one step of the Euler method from t_n to $t_{n+1} = t_n + h$ is,

$$\frac{x(t_{n+1}) - x(t_n)}{h} \approx f(\theta, x(t_n)), \tag{1.16}$$

which can rewritten as

$$x(t_{n+1}) \approx x(t_n) + h \cdot f(\theta, x(t_n)). \tag{1.17}$$

The value of x_n is an approximation of the solution to the ODE at time t_n: $x_n \approx x(t_n)$. The Euler method is explicit, i.e. the solution x_{n+1} is an explicit function of x_i for $i \leq n$. Unfortunately, the explicit Euler method is an unstable numerical method when the system is stiff, therefore, a solver for stiff differential equations is needed. This ensures an appropriate approximation of the solution in any case. For this purpose, MATLAB solver *ode15s* [1] is used in this thesis, which is a variable-step, variable-order (VSVO) solver for stiff differential equations based on the numerical differentiation formulas (NDFs) of order 1 to 5. Optionally, it can use the backward differentiation formulas (BDFs).

1.2.2 Sensitivity Analysis

Sensitivity analysis aims at determining the model input parameters which mostly contribute to a quantity of interest depending on the model output. Let us denote the model input parameter vector as $\theta = (\theta_1, \ldots, \theta_d) \in \mathbb{R}^d$. The model here is an ordinary differential equation as described by (1.1) of the form,

$$\frac{dx(t)}{dt} = f(\theta, x(t)),\ x(0) = x_0 \in \mathbb{R}^n, \tag{1.18}$$

where $x = (x_1, \ldots, x_n) \in \mathbb{R}^n$ is the state variable. Let us also consider a quantity of interest, y, which can be any observable depending on the model output x,

$$y = y(x(t, \theta)). \tag{1.19}$$

This quantity can be for instance the value of a specific output variable x_j at a specific time point t, or the variance of x_j over a specific time interval. These are examples for scalar outputs. For the sake of simplicity, the study here is restricted to a scalar output y. The sensitivity of y with respect to input parameter p_i is given by

$$S_y^i = \frac{\partial y}{\partial \theta_i}.$$

To account for differences in physical units among variables and parameters, often relative sensitivities are used,

$$\hat{S}_y^i = \frac{\partial y}{\partial \theta_i} \cdot \frac{|\theta_i|}{|y|}.$$

If the exact derivative is difficult to compute, the sensitivity can be approximated by a finite difference scheme,

$$S_y^i \approx \frac{y(x(t, \theta + \Delta e_i)) - y(x(t, \theta))}{\Delta},$$

where Δ is the size of the perturbation and e_i is a vector of the canonical base. Often, Δ is a relative perturbation, i.e., $\Delta = \epsilon \cdot \theta_i$ for some small number ϵ (e.g. $\epsilon = 0.1$ corresponds to a perturbation by 10%). In this case, the relative sensitivity is approximated by

$$\hat{S}_y^i \approx \frac{y(x(t, \theta + \Delta e_i)) - y(x(t, \theta))}{\epsilon \cdot |y(x(t, \theta))|}. \tag{1.20}$$

This is a local sensitivity in the sense that it describes the influence of a specific local perturbation of parameter θ_i on the model output. Sampling Δ or sampling pairs of input and output variables would allow for a global sensitivity analysis, but this is computationally much more demanding and the results are often difficult to interpret. For details on global sensitivity analysis, the reader is referred to [54]

1.2.3 Biological Admissibility

Mathematical models describing biological systems strive to provide quantitative information about dynamical behaviour of biological species. Typically, models such as (1.1) depend on many parameters that shape the mathematical structure of the model. In a deterministic setting, the assigned *default* values of the parameters θ^*, along with the initial value x_0, control the time evolution $x(\theta^*, t)$ of quantities of interest, e.g., species, hormones. However, sometime these models require some flexibility that allows them to simulate specific personalized model behaviours, yet the resulting dynamic should be biologically meaningful. For instance, in a health-care context the aim is to individualise models in order to compute patient-specific predictions, [114]. This can be performed by assigning suitable parameter values sampled from the parameter space to the model parameters. To decide whether the assigned parameters lead to a biologically meaningful time evolution of species, we need criteria to filter out most of the parameter values leading to time evolutions that are not biologically meaningful. In this thesis, we present an approach adopted from [130]. This approach provides criteria for defining *biologically admissible parameter values* those ensuring a time evolution of species to be close enough to that of the model default parameter values. In other words, given a value θ for the model parameters, the task is to check that the time evolution of $x(\theta, t)$ is similar enough (modulo time-shifts) to that of $x(\theta^*, t)$. In particular, check if for each species x_i in the model, the time evolution $x_i(\theta, t)$ is biologically meaningful. For this purpose, we first start by introducing the following definition.

Definition. *Given two functions f and g from $\mathbb{R}$ to $\mathbb{R}$, the cross-correlation [211], denoted $< f, g > (\tau)$, between f and g is defined as,*

$$< f, g > (\tau) = \int_{-\infty}^{+\infty} f(t) g(t + \tau) dt, \tag{1.21}$$

where $\tau \in \mathbb{R}$ is the time lag. In addition, the normalised cross-correlation function, denoted $\rho_{f,g}(\tau)$, is defined as,

$$\rho_{f,g}(\tau) = \frac{< f, g > (\tau)}{\|f\| \cdot \|g\|}, \tag{1.22}$$

where $\|f\|$ and $\|g\|$ are the standard L^2 norms of f and g.

The function $\rho_{f,g}$ measures the degree to which the function f and g are correlated. In other words, it measures the similarity between the function f and shifted (or lagged) function of g with the lag τ. This allows us to compare qualitatively the dynamical behaviour of the shifted function g with the function f. Here, the higher $\rho_{f,g}$ the more similar are the function f and g, e.g., f and g have the same peaks. In particular, for a given τ, if $\rho_{f,g}(\tau) = 1$, then f is equal to g up to an amplification factor. When no lag time exists, i.e. $\tau = 0$, $\rho_{f,g}(0)$ is called the normalised zero-lag cross-correlation.

By analogy, we denote by $\rho_{\theta^*,\theta,i}(\tau)$ the normalised cross-correlation measuring the similarity between the trajectory of state variables $x_i(\theta^*)$ and $x_i(\theta)$, when $x_i(\theta)$ is subject to time-shift τ. In order to select the *biological admissible parameter values*, we consider three measures of how similar two trajectories are,

1 normalised cross-correlation: $\rho_{\theta^*,\theta,i}(\tau) = \dfrac{< x_i(\theta^*), x_i(\theta) > (\tau)}{\|x_i(\theta^*)\| \cdot \|x_i(\theta)\|}$,

2 normalised average absolute difference: $\delta_{\theta^*,\theta,i}(h) = \left| \dfrac{\int_0^h (x_i(\theta^*, t) - x_i(\theta, t))dt}{\int_0^h x_i(\theta^*, t)dt} \right|$,

3 normalised squared norm difference: $\kappa_{\theta^*,\theta,i} = \dfrac{\left| \|x_i(\theta^*)\|^2 - \|x_i(\theta)\|^2 \right|}{\|x_i(\theta^*)\|^2}$.

The normalised average differences $\delta_{\theta^*,\theta,i}$ and the normalised squared norm differences $\kappa_{\theta^*,\theta,i}$ are two measures of the average distance between $x_i(\theta^*, t)$ and $x_i(\theta, t)$, when $x_i(\theta, t)$ is subject to time-shift τ.

In the following definition, we use these functions to formalise the notion of *biologically admissible parameter values* θ with respect to a default parameter θ^*. Intuitively, θ is *biologically admissible* if the three measures above are all above or below certain thresholds.

Definition. *Let θ^* and θ be two parameters. Let $A \subseteq \mathbb{R}^+_{\neq 0}$, $B \subseteq \mathbb{R}$ be two sets of real numbers such that $0 \in B$. Given a tuple $\varepsilon = (\varepsilon_1, \varepsilon_2, \varepsilon_3)$ of positive real numbers, we say that θ is ε-biologically admissible with respect to θ^*, if there exist $h \in A$ and $\tau \in B$ such that, for all $i \in \{1, \cdots, n\}$: $(\rho_{\theta^*,\theta,i}(\tau) \geq \varepsilon_1) \wedge (\delta_{\theta^*,\theta,i}(h) \leq \varepsilon_2) \wedge (\kappa_{\theta^*,\theta,i} \leq \varepsilon_3)$.*

1.3 Some Concepts of Bayesian Inference and Information Theory

In this section, we introduce some tools needed to produce the results in Chapter 5 based on Bayesian experimental design. First, we briefly present the concept of *Kernel Density Estimation*, which is a non-parametric method for the estimation of the probability density function of a random variable from independent and identically distributed samples. Subsequently, we review the fundamental concept of the Bayesian approach and Monte Carlo integration. Finally, we combine tools from information theory and Bayesian inference to assess the information content of experimental data.

1.3.1 Kernel Density Estimation

The probability density function $p_X(x)$ describes how the probability $\mathbb{P}(X)$ of a random variable X is distributed. In other words, it shows how dense the probability is for various regions of the random variable using the relation,

$$\mathbb{P}(a \leq X \leq b) = \int_a^b p_X(x)dx, \tag{1.23}$$

where X is drawn from the probability density function $p_X(x)$ defined over the region [a,b]. The estimation of probability density functions is common in applied data analysis, where the density estimation is usually based on observed data. The observed data are usually thought of as a random sample that can be drawn from an unobservable probability density function. In practice, these samples are used to reconstruct or estimate the probability density function using either parametric or non-parametric estimators.

A parametric estimator assumes in advance the functional form of the underlying probability density function. In addition, it makes use of samples or observations to get estimates of the parameters that define the shape of the probability density function. For instance, a parametric estimator would be to assume that the shape of the probability density function being estimated is Gaussian. Then, it uses samples to obtain estimates of the mean and standard deviation of the Gaussian distribution. Some tools for parametric density estimators are Bayes estimator, maximum likelihood estimator, and least square estimator.

In contrast, a non-parametric estimation is a statistical method which does not use a priori assumptions about the shape of the underlying distribution. The term non-parametric is not meant to imply that such methods completely lack parameters, but that the number and nature of the parameters are flexible and not fixed in advance. Thus, non-parametric estimators are more flexible tools for capturing distributions where insufficient information is known a priori. Typical non-parametric density estimators include the histogram and kernel density estimators, which are

also termed as Parzen-Rosenblatt estimators [158, 174]. The first multivariate kernel density estimator was introduced by Cacoullos [36] in 1966. Since then, Kernel Density Estimators have been widely used as statistical tools to estimate unknown distributions in numerous fields with recent applications to exploratory data analysis and data visualisation [198, 148, 38, 179].

The general form of the d-dimensional multivariate kernel density estimator, denoted $\hat{p}$, for a sample of d-variate random vectors $\{x_i\}_{1\leq i\leq n}$, drawn from a density function p_X is,

$$p_X(x) \approx \hat{p}_X(x) := \frac{1}{n} \cdot \sum_{i=1}^{n} K_H\left(x - x_i\right), \tag{1.24}$$

where $x \in \mathbb{R}^d$ and $x_i \in \mathbb{R}^d$. From here on, a hat, i.e. $\hat{p}$, will always indicate an approximation. K_H is the scaled kernel function, where H is the bandwidth (or smoothing) $d \times d$-matrix which is symmetric and positive definite. K is the unscaled kernel function, which is a symmetric multivariate density and integrates to one. The scaled and unscaled kernels are related by

$$K_H(x) = |H|^{-1/2} K(H^{-1/2} \cdot x). \tag{1.25}$$

Usually, the kernel K is chosen as a product of a one-dimensional kernel smoothing function k such that,

$$K(x) = \prod_{j=1}^{d} k(x_j). \tag{1.26}$$

In this case, eq.(1.24) becomes,

$$p_X(x) \approx \hat{p}_X(x) := \frac{1}{nh_1 h_2 \cdots h_d} \cdot \sum_{i=1}^{n} \prod_{j=1}^{d} k\left(\frac{x_j - x_{ij}}{h_j}\right), \tag{1.27}$$

where the matrix $H^{-1/2}$ is a diagonal matrix with the elements of vector $(h_1, h_2, \cdots, h_d)$ on the main diagonal. A common one-dimensional kernel which is widely used is the Gaussian kernel,

$$k(x) = \frac{1}{\sqrt{2\pi}} \cdot \exp\left(-\frac{\|x\|^2}{2}\right). \tag{1.28}$$

The performance of kernel density estimators depends crucially on the bandwidth selection. In the multivariate case, the bandwidth matrix H controls both the degree and direction of smoothing, so its selection is more difficult. On the other hand, bandwidth selection in the univariate case involves selecting a scalar parameter which determines the smoothing properties of the kernel: a large bandwidth heavily smooths the sampled data while a small one provides less smoothing, see Fig 1.3.

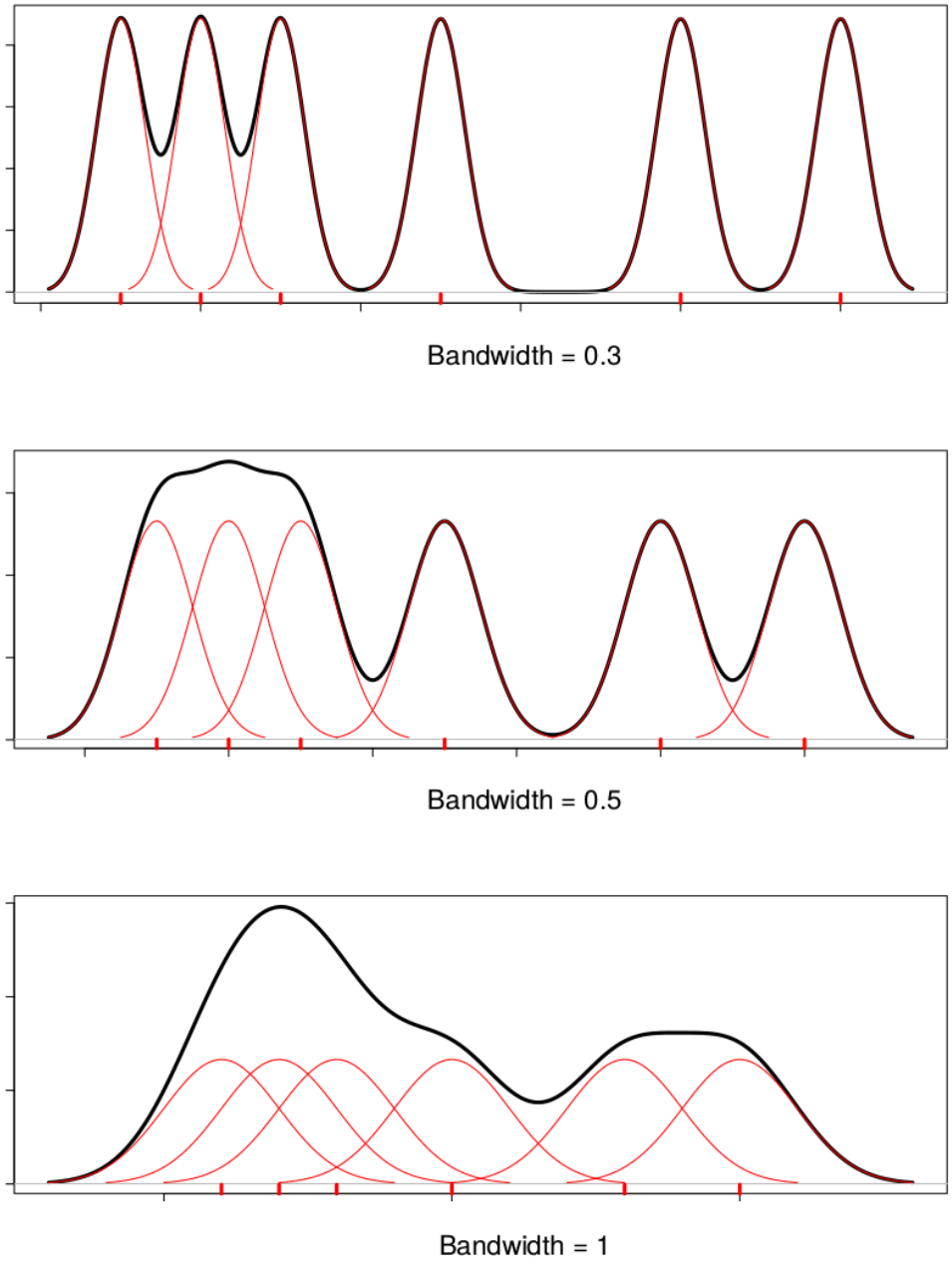

Figure 1.3: **Kernel density estimation applied to an illustrative example for three different values of the bandwidth parameter.** The red dots represent six samples from an unknown probability density function, the red lines represent the individual kernel Gaussian functions, and the full line represents the estimated probability density function that is calculated as the sum of the individual kernel functions.

1.3.2 Bayesian Formalism

In many situations, we want to know the probability of an event X occurring given that another event Z has occurred. In this case, the probability of an event X given that another event Z has occurred is called conditional probability. We define the conditional probability for continuous random variables as follows.

Definition. *Let $X : \Omega \to \mathcal{X}$ and $Z : \Omega \to \mathcal{Z}$ be two continuous random variables with the joint probability density function $p_{X,Z}(x, z)$. The conditional probability density function of X given the occurrence of the value z of Z such that $p_Z(z) > 0$ can be written as,*

$$p_X(x|Z = z) = \frac{p_{X,Z}(x, z)}{p_Z(z)}\,, \tag{1.29}$$

where $p_Z(z)$ gives the marginal density for Z, that is, the joint density $p_{X,Z}(x, z)$ marginalized over all possible x,

$$p_Z(z) = \int_{\mathcal{X}} p_{X,Z}(x, z)dx\,. \tag{1.30}$$

For notational simplicity, we omit the subscript of the probability density function (i.e. $p_X(x) = p(x)$) and we denote $p_X(x|Z = z)$ as $p(x|z)$ throughout the rest of the thesis.

Prior Knowledge

The prior distribution or prior density function is a key part of Bayesian analysis. The information contained in the prior distribution essentially reflects the knowledge or belief about uncertain quantities of interest (e.g, parameters, prediction of future responses) before some evidence is taken into account. Such knowledge could represent, for example, the order of magnitude or physiological meaningful ranges that could be taken from previous studies or experiments. Generally, the prior distribution can be based on two forms of knowledge: a subjective knowledge, which expresses the experimenter's personal belief, and an objective knowledge, where the experimenter may have information, historical data or data from experiments done prior to the one being undertaken that can be used to help formulate a prior. The use of prior knowledge in inferring a quantity of interest is formulated according to Bayes' theorem.

For two continuous random variables X and Z defined as above, Bayes' theorem is derived from the definition of conditional probability density function:

Theorem. *Let X and Z be as above. For all $z \in \mathcal{Z}$, such that $p(z) > 0$ holds,*

$$p(x|z) = \frac{p(z|x) \cdot p(x)}{\int_{\mathcal{X}} p(z|s) \cdot p(s)ds}\,, \tag{1.31}$$

Proof. The formula (1.31) can be derived immediately by inserting eq.(1.30) in the dominator of eq.(1.29) and by using the fact that $p(x,z) = p(z|x) \cdot p(x)$ (by analogy to (1.29)). □

This theorem, which is attributed to Bayes (1744-1809), tells us how to revise probability of events in light of new data. In other words, it shows us how to construct the posterior distribution $p(x|z)$ of a quantity of interest x given the observed data z, by using the so-called likelihood function $p(z|x)$ of z given x as well as the prior density function $p(x)$. Here we want to point out that for fixed z, the posterior $p(x|z)$ and prior $p(x)$ both are probability densities in X, whereas the likelihood on the other hand is not a probability density in X.

Typically, the posterior distribution, $p(x|z)$, is a complex and multidimensional functions whose computation is usually performed numerically by means of powerful (if costly) computational algorithms such as Markov chain Monte Carlo (MCMC). Moreover, in many cases, it is not possible to provide a model likelihood or it may be too slow to compute. Approximate Bayesian Computation (ABC) methods have been developed to deal with this difficulty by prescribing a surrogate measure for how plausible, for example, a particular parameter set θ is, see [209, 204, 203, 132, 190].

The computation of $p(x|z)$ can also be achieved using the *KDE* approach as explained in Section 1.3.1. The straightforward way is to estimate the joint and marginal densities and divide one by the other. In other words, if x is a l-dimensional variable of interest and z represents m-dimensional data, then the posterior distribution $p(x|z)$ can be approximated by

$$\hat{p}(x|z) = \frac{\hat{p}(x,z)}{\hat{p}(z)}. \tag{1.32}$$

To be concrete, let us suppose that we are using a product kernel as explained in Subsection 1.3.1 to estimate the joint density, and that the marginal density is consistent with it:

$$\hat{p}(x,z) = \frac{1}{n\alpha_1 \cdots \alpha_l \beta_1 \cdots \beta_m} \cdot \sum_{i=1}^{n} \prod_{j=1}^{l} k_x \left(\frac{x_j - x_{ij}}{\alpha_j} \right) \cdot \prod_{j=1}^{m} k_z \left(\frac{z_j - z_{ij}}{\beta_j} \right), \tag{1.33}$$

$$\hat{p}(z) = \frac{1}{n\beta_1 \cdots \beta_m} \cdot \sum_{i=1}^{n} \prod_{j=1}^{m} k_z \left(\frac{z_j - z_{ij}}{\beta_j} \right), \tag{1.34}$$

where k_x and k_z are one-dimensional kernels, and $(x_i, z_i)_{1 \le i \le n}$ are n-random vectors drawn from the density functions $p_{X,Z}$. Thus one needs to define the bandwidths, α_i and β_j, for each kernel.

1.3.3 Monte Carlo Integration

The solution of many problems in applied sciences can be expressed in terms of an integral function such as,

$$I = \int_{\Omega} f(x)\,dx, \tag{1.35}$$

where f is a high-dimensional function defined on the domain, Ω. In practice, it is often very difficult to evaluate this integral due to the problem of high dimensionality, or because there is no closed-form expression available using calculus. Here, numerical methods and approximations have to be employed to approximate the integral to a given degree of accuracy. Classical numerical integration methods such as the quadrature method require that the approximation of the integral is done by partitioning the integration domain into a set of discrete volumes. Thus, obtain the integral by summing the values of the weighted function. Though such a method estimates well (to a certain degree of accuracy) the integral for example in one dimension, the magnitude of the error, however, increases when the calculation is performed in a higher dimension. Instead, Monte Carlo integration can be another alternative to approximate the integral.

For the sake of simplicity, let us consider a d-dimensional function f defined on $\Omega = [a, b]^d$. Notice that the integral (1.35) can be interpreted as the expectation $\mathbb{E}(f(X))$ of the random variable $f(X)$, where X is an $\mathbb{R}^d$-valued random variable with a uniform distribution over $[a, b]^d$, meaning that its components are independent and identically uniformly distributed over $[a, b]$. The Monte Carlo approximation of the integral is then given by

$$I \approx \frac{1}{n} \sum_{i=1}^{n} f(x_i), \tag{1.36}$$

where $\{x_i\}_{1 \leq i \leq n}$ are independent observations of X, i.e., independent random observations of a $\mathbb{R}^d$-valued random variable, the components of which are random numbers. This approximation converges, by the law of large numbers, as $n \to \infty$, to the real value I of the integral. The convergence is in the probabilistic sense, that there is never a guarantee that the approximation is close to the real value I, but it converges almost surely by the law of large numbers, as $n \to \infty$. In a more general context, let us consider a function $g(x)$ that can be decomposed as a product of a probability density function $p(x)$ and another function $f(x)$ defined on Ω. Now suppose we want to evaluate,

$$J = \int_{\Omega} g(x)\,dx. \tag{1.37}$$

Similarly to the above approximation, the integral J can be defined as the expectation of $f(x)$ with respect to the density $p(x)$,

$$J = \mathbb{E}_p(f(x)) = \int_{\Omega} f(x)p(x)\,dx. \tag{1.38}$$

By drawing a large set of independent observations $\{x_i\}_{i=1}^n$ from $p(x)$, we can then approximate J by

$$J \approx \frac{1}{n} \sum_{i=1}^{n} f(x_i). \tag{1.39}$$

This quantity is referred to as Monte Carlo integration [76]. This method is often used in the Bayesian analysis to estimate posteriors or marginal distributions.

1.3.4 Information Content of Experimental Data

The role of experimental data is very essential in modelling complex biological systems. For example, experimental data may provide substantial information that help modellers in developing, testing and refining models that simulate the system of interest. However, a lack of sufficient informative data may limit the predictive performance of models and efficient statistical inference. A common task in statistical inference is the estimation of uncertainty in model parameters and model predictions using different probabilistic methods. In general, this is mainly performed via two major approaches: the frequentist and the Bayesian approach [170, 220, 215].

A commonly known drawback of the frequentist approach is that it lacks a formal framework for incorporating knowledge not represented by data. Furthermore, it has limitations in providing a proper measure of the confidence of parameters inferred from data. In contrast, the Bayesian approach which is our focus in the following discussion offers us tools to assess how well model parameters and predicted quantities are constrained by experimental data. Moreover, it makes use of newly extracted information from experimental data to update knowledge of model parameters. When data are sufficiently informative, this results in reducing the uncertainty of the model parameters and predictions. Although the main advantage of this approach is the use of available prior information, this approach, however, is prone to some limitations. For instance, it does not tell you how to select a prior distribution. In addition, it can produce posterior distributions that are heavily influenced by the prior. Moreover, it often comes with a high computational cost, especially in models with a large number of parameters.

In the Bayesian approach, the learning process, based on experimental data, is performed using Bayes' rule. If an experiment is conducted according to a design $\mathfrak{D}$, and an observation of data $z \in \mathcal{Z} \subseteq \mathbb{R}^n$ is obtained, then the prior information of a continuous random variable $x \in \mathcal{X} \subseteq \mathbb{R}^m$ is combined with the data z to form a posterior distribution $p(x|z, \mathfrak{D})$ according to Bayes' rule:

$$p(x|z, \mathfrak{D}) = \frac{p(z|x, \mathfrak{D}) \cdot p(x|\mathfrak{D})}{p(z|\mathfrak{D})}, \tag{1.40}$$

where $p(x|\mathfrak{D})$ is the prior density function, $p(z|x, \mathfrak{D})$ is the likelihood function, $p(x|z, \mathfrak{D})$ is the posterior density function, and $p(z|\mathfrak{D})$ is the evidence. It is reason-

able to assume that the prior knowledge on x does not vary with the experimental design, leading to the simplification $p(x|\mathfrak{D}) = p(x)$.

The posterior distribution contains all relevant information about the random variable X. Ideally, the data should lead to a narrow posterior such that, with high probability, the random variable X can only take on a small range of values. However, when it comes to learning about the additional amount of valuable information provided by new data, the experimenter is not only interested in the statistical confidence of the random variable X at a specific point in time, but also to measure the information gain provided by the new data. Let us assume we have two new experimental data sets, z_1 and z_2, where the content of information in data z_2 is high, whereas it is low in data z_1. If the information gain is high, the new data z_2 yield a substantial decrease in uncertainty, whereas no significant improvement would be observed if we update the prior distribution with data z_1, see Fig 1.4.

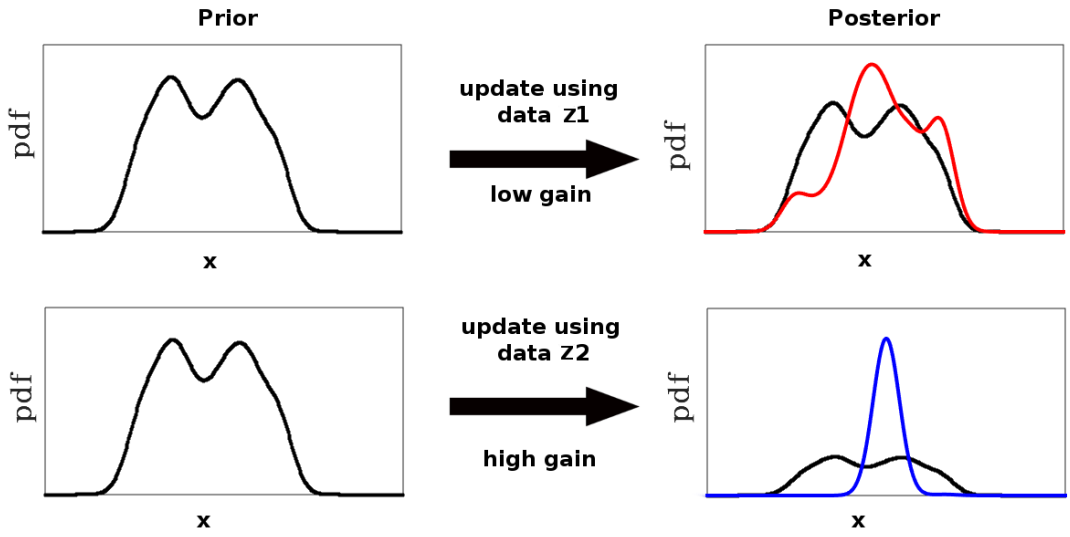

Figure 1.4: This example compares updates of probability densities. The updates are induced by two different data sets z_1 and z_2. On the top, both prior and posterior densities are similarly informative: the update yields a low information gain. This is in contrast to the bottom plot, which shows a highly informative update.

A natural question is how to evaluate the gain in information after collecting data z. Several works have been performed to deal with this question within the Bayesian and information theoretical framework [118, 194, 52, 16]. After updating the prior distribution $p(x)$ to the posterior distribution $p(x|z, \mathfrak{D})$, the amount of information gain about X provided by a single observed data $Z = z$ is given by

$$I_{X,z} = \int_X p(x|z) \cdot [\log(p(x|z)) - \log(p(x))] \; dx. \tag{1.41}$$

Here, it is worthwhile to point out that this amount depends on one observed data z. Since the outcome of an experiment is unknown before it is performed the observed data is then random with distribution $p(z)$. This means that another observed data $z^{'} \neq z$ can be more or less informative than data z. Therefore, a natural procedure to account for all possible experimental outputs is to take the average over $p(z)$. The average information gain or the expected information gain, is then called the mutual information between X and Z, and we denote it by

$$I(X;Z) = \mathbb{E}_z \left(I_{X,z} \right). \tag{1.42}$$

Mutual information, also known as transinformation, was first introduced in classical information theory by Shannon in 1948 [185]. The mutual information can be written in a manifestly symmetric form,

$$I(X;Z) = \int \int p(x,z) \cdot log \left(\frac{p(x,z)}{p(x) \cdot p(z)} \right) dxdz, \tag{1.43}$$

where $p(x,z)$ is the joint probability density function of X and Z, and $p(x)$ and $p(z)$ are the marginal probability density functions of X and Z, respectively. Mutual information, $I(X;Z)$, describes the expected reduction of the uncertainty about X after data Z are collected in an experiment. It can be seen as a measure of the mutual dependence of two variables, both linear and non linear. We can think about the mutual information as a measure of dependency. Clearly, we have $I(X;Z) = 0$ if the variables X and Z are independent, so that $p(x,z) = p(x) \cdot p(z)$ for every x and z, which means that no knowledge is gained about the variable X when Z is measured and vice versa.

As discussed earlier, the quality of data (in the sense of information content) in reducing uncertainty is of high importance. Thus, a natural way to collect the most informative data is to design experiments for a specific purpose to save time and cost. The approach introduced above from information theory allows to select experiments that maximize the value of the resulting data. These data can be used to reduce uncertainty in parameters and predictions. Consequently, in order to decrease this uncertainty, one should maximize the mutual information over the design space $\mathbb{D}$ of all considered experimental designs to find the optimal experimental design, $\mathfrak{D}^\star$, that is,

$$\mathfrak{D}^\star \in \underset{\mathfrak{D} \subseteq \mathbb{D}}{\operatorname{argmax}} \, I(X; Z_{\mathfrak{D}}). \tag{1.44}$$

1.3.5 Estimation of Mutual Information

In this section, we focus on estimating the mutual information (i.e. eq.(1.43)) shared between two random variables X and Z. In many cases, it is possible to

provide a conditional probability density function, e.g $p(z|x)$, which represents the model likelihood. In this case, the computation of eq.(1.43) becomes possible by reformulating it in terms of the prior distribution $p(x)$, the model likelihood $p(z|x)$ and the evidence $p(z)$. For this, we employ Bayes' theorem which gives rise to the following,

$$I(X;Z) = \int_Z \int_X p(x,z) \cdot log\left(\frac{p(x,z)}{p(x) \cdot p(z)}\right) dxdz, \tag{1.45}$$

$$= \int_Z \int_X p(x) \cdot p(z|x) \cdot log\left(\frac{p(z|x)}{p(z)}\right) dxdz. \tag{1.46}$$

Typically, this integral equation has no closed analytical solution. Therefore, it must be approximated numerically. To do so, one approach is to use Monte Carlo approximation, see Section 1.3.3. The equation (1.46) can be estimated by drawing samples $\{x^{(k)}\}_{1\leq k\leq N_1}$ from the prior distribution $p(x)$ and samples $\{z^{(k)}\}_{1\leq k\leq N_1}$ from the conditional distribution $p(z|x^{(k)})$. This gives rise to the following approximation,

$$I(X;Z) \approx \frac{1}{N_1} \cdot \sum_{k=1}^{N_1} \Big(log\left[p(z^{(k)}|x^{(k)})\right] - log\left[p(z^{(k)})\right] \Big), \tag{1.47}$$

where N_1 is a large number of samples in this Monte Carlo estimate.

The evidence $p(z^{(k)})$ evaluated at $z^{(k)}$, usually does not have an analytical form, but it can be approximated using yet another Monte Carlo estimate,

$$p(z^{(k)}) = \int_X p(z^{(k)}|x) \cdot p(x) dx, \tag{1.48}$$

$$\approx \frac{1}{N_2} \cdot \sum_{q=1}^{N_2} p(z^{(k)}|x^{(k,q)}), \tag{1.49}$$

where $\{x^{(q)}\}_{1\leq q\leq N_2}$ are large number of samples, i.e. N_2, drawn independently from the prior distribution $p(x)$. Thus, by combining eq.(1.47) and eq.(1.49), we obtain the following estimate of the mutual information between the random variables X and Z,

$$I(X;Z) \approx \frac{1}{N_1} \cdot \sum_{k=1}^{N_1} \left(log\left[p(z^{(k)}|x^{(k)})\right] - log\left[\frac{1}{N_2} \cdot \sum_{q=1}^{N_2} p(z^{(k)}|x^{(k,q)})\right] \right). \tag{1.50}$$

In contrast, when it is not possible to provide a model likelihood $p(z|x)$, then it is not straightforward to estimate the mutual information as in the previous case. For this purpose, we use the non-parametric *KDE* approach as explained in Section

1.3.1. Let us assume that $(x^{(k)}, z^{(k)})_{1\leq k\leq n}$ are n-random vectors drawn from the density functions $p_{X,Z}$. Then by choosing an adequate kernel and bandwidths, the joint and marginal probability density functions of the two random variables X and Z can be approximated by $\hat{p}_{X,Z}$, $\hat{p}_X$, and $\hat{p}_Z$. Thus, eq.(1.45) can be approximated via Monte-Carlo estimation by using a large number N of independent and identically distributed samples,

$$I(X;Z) \approx \frac{1}{N} \cdot \sum_{k=1}^{N} \Big(log(\hat{p}_{X,Z}(x^{(k)}, z^{(k)})) - log(\hat{p}_X(x^{(k)})) - log(\hat{p}_Z(z^{(k)})) \Big) . \quad (1.51)$$

Chapter 2

Model Development - MetRep Model

In the last few years, mathematical models dealing with reproductive performance in dairy cows have received relatively more attention. Previous modeling efforts mainly focused on either the bovine estrous cycle [18, 195, 162, 212, 139] or the nutritional strategies [134, 8, 46], yet there are a few approaches that combine the two topics. The most recent one is by McNamara and Shields [138] who connect the reproductive cycle (given by differential equations [18, 195]) and nutrition (implemented by a rather sophisticated model called Molly [8]) via the ATP to ADP reduction reaction. Martin et al. [133] introduced an empirical model that includes nutritional effects on the reproduction. Pring et al. [162] modeled different nutritional scenarios by varying parameters in an estrous cycle model. A more conceptual model was suggested by Scaramuzzi et al. [177], where the coupling between nutrition and reproduction is realized by IGF-1, the glucose-insulin system, and leptin.

None of these models, however, captures the dynamics between nutrition, hormonal regulation, and milk yield, which are of particular interest in cows. The model introduced here aims at better understanding the involved interactions and time evolution. It includes compartments for the nutrient intake, the glucose-insulin system [14], the milk production, and the reproductive hormones [195]. Based on that model, it is analyzed how changes in dietary intake, which usually happen on the time-scale of days, affect the behavior of the estrous cycle on the scale of weeks and months.

The model that is developed in this Chapter, i.e. the MetRep model, is built on two major pillars. The one is the glucose-insulin dynamics in dairy cows, which was modeled in [14] by utilizing the Systems Biology Markup Language [95] and CellDesigner[1]. The other is the bovine estrous cycle, modeled by a system of dif-

[1] `http://www.celldesigner.org`

ferential equations (BovCycle) that quantifies reproductive hormones and other relevant compartments, representing follicles and corpora lutea [18, 195], see Fig 2.1.

The MetRep model here consists entirely of ordinary differential equations (ODEs), which are solved for problem-specific initial conditions and parameter values. The metabolic model implements the mechanisms explained in [14], which allow for simulating the time-evolution of glucose and insulin for different dietary inputs in lactating as well as non-lactating cows. The reprodcutive model (BovCycle) implements the biological feedback mechanisms between hypothalamus, pituitary gland and ovaries, which produce periodic estrous cycles of constant duration, similar to [195]. However, modifications needed to be implemented as the mechanisms suggested in [195] are not tailored to cows during pregnancy, calving and lactation. In these stages the interaction between hormones is somewhat different. To simulate the onset of lactation, oxytocin is included in the model; this hormone peaks during delivery [112], and it is required for milk ejection [79, 149, 23].

This Chapter is organized as follows. The metabolic model is described in Section 2.1. Section 2.2 presents the coupling of the metabolic model to the estrous cycle model. Necessary modifications and coupling mechanisms are thoroughly discussed.

2.1 Bovine Metabolic Model

The metabolic model to be developed in this section is based on an improved version of the glucose-insulin model in [14]. It involves six components: Glu_{blood}, Glu_{liver}, Glu_{store}, Fat, Ins, $Gluca$; see Tab 1) and, as formulated here in terms of ODEs, their explicit interaction over time. Initial conditions are chosen based on the following calculation. For a cow of weight 600 kg and body condition score 3.5, the total body fat can be estimated by 25% of the total body weight [178, 44]. That is, 150 kg is taken as initial value for Fat. Typical physiological ranges for Glu_{blood}, Ins and $Gluca$ are listed in Tab 2. As long as the initial values are within these ranges, the simulation results are not sensitive with respect to the exact value.

The model only involves the most basic mechanisms that regulate the flow of glucose through the body. It starts with the feed, continues with the digestive system and the blood, and ends up with glucose usage. Glucose and glucogenic substances are ingested with the dry matter intake (DMI). In the liver, the glucogenic substances are converted to glucose via gluconeogenesis. Glucose is used for maintanance and milk production, it is stored as glycogen or, after conversion, as fat. A detailed description of these mechanisms are presented in the following.

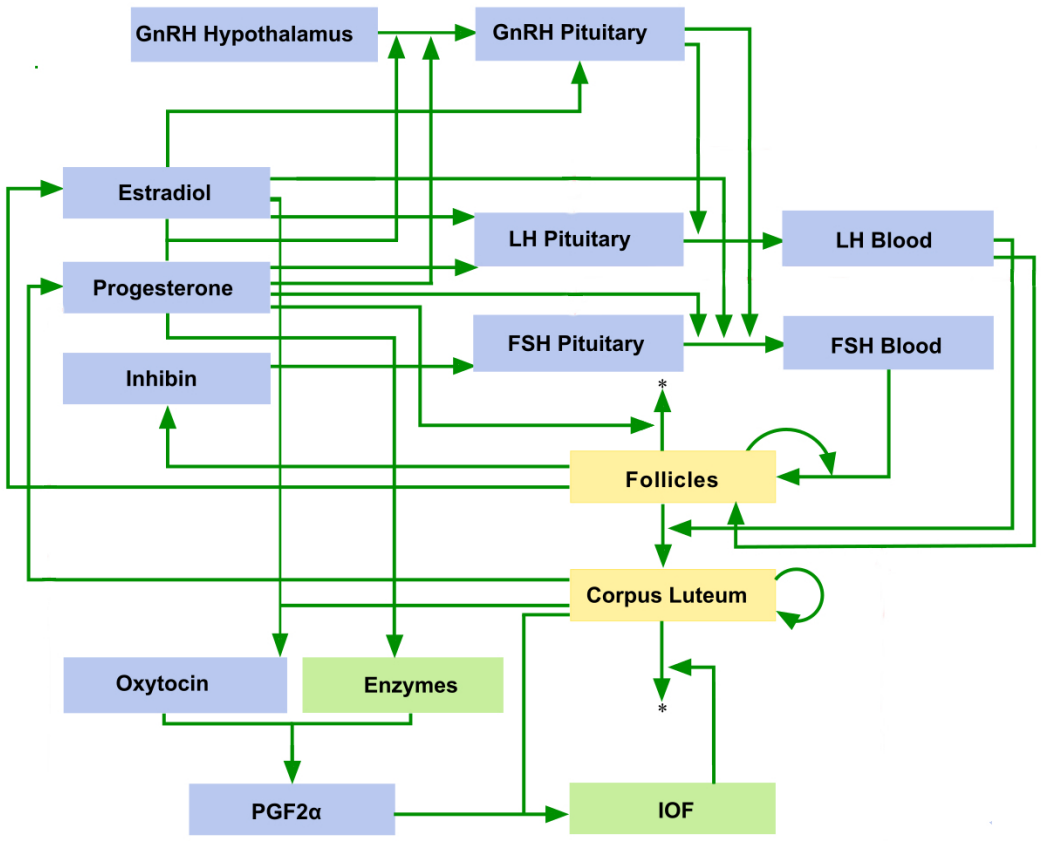

Figure 2.1: **Flowchart for the model of the bovine estrous cycle (BovCycle),** [195]. The compartments are expressed in terms of ODEs which simulates the biological feedback mechanisms between hypothalamus, pituitary gland and ovaries. The model produces periodic estrous cycles which lasts 21 days per cycle.

2.1.1 Feed Intake

The first step involves the quantification of the amount of substances in the DMI that are either available for gluconeogenesis in the liver or directly absorbable as glucose into the blood. There exist empirical formulas that estimate the DMI needed to meet the energy requirements; these formulas are based on the cow's body weight (BW) and the net energy (NE) of the diet; see, e.g., [44]. Throughout the thesis, a standard cow with body weight 600 kg is considered, and the value for DMI of 11700 gram per day (g/d) is adopted from [14]. This value also results from a formula in

[44], assuming a diet's net energy of 1.32 Mcal/kg.[2]

Ruminants digestion involves fermentation, which makes consumption of a high-fiber diet possible and necessary [115, 55]. In the default setting, the fraction of glucose and glucogenic substances in the DMI, glu_{pool}, is assumed to be 8% of the total DMI,

$$glu_{pool} = c_0 \cdot DMI\,, \tag{2.1}$$

where c_0 is a mass-fraction parameter (with default value $c_0 = 0.08$) that allows for varying the total amount of glucose and glucogenic substances that can be extracted from DMI. This fraction combines glucose precursor substances such as short chain fatty acids, which are converted to glucose in the liver by gluconeogenesis, as well as glucose that can directly be absorbed from the digestive tract into the blood [106, 128, 55]. In the cow, only very little glucose is available for direct absorption from the digestive tract [22]. From the total amount of glucose and glucogenic substances in the DMI (glu_{pool}), the portion of glucose was estimated to be less than 10% [147, 15, 230], whereas up to 90% of glu_{pool} are glucogenic substances.

The flow of absorbable glucose that goes directly to the systemic circulation is incorporated into the model via the rate

$$glu_{feed-bl} = c_1 \cdot glu_{pool}\,. \tag{2.2}$$

The flow of glucose precursor substances that are converted to glucose by gluconeogenesis in the liver is incorporated into the model via the rate

$$glu_{feed-gng} = (1 - c_1) \cdot glu_{pool}\,. \tag{2.3}$$

The default parameter value is $c_1 = 0.08$ (see Tab 4). It is assumed here that there is no loss from the glucose pool (the flows sum up to $1 \cdot glu_{pool}$), i.e., the processes take place with 100% efficiency. If some loss was included here, the simulation results presented further below would be the same but correspond to higher values of c_0 (the amount of glucose and glucose precurser substances in the feed). These processes are illustrated in Fig 2.2.

2.1.2 Insulin and Glucagon

The blood glucose concentration is maintained at normal levels primarily through the action of two hormones, namely insulin and glucagon. Any elevation in the blood

[2] In [44], the following formula was proposed for growing, non-lactating Holstein heifers.

$$DMI = \big(-0.1128 + 0.2435 \cdot NE_M - 0.0466 \cdot NE_M^2\big) \cdot \frac{BW^{0.75}}{NE_M}\,,$$

where DMI is in (kg/d), BW is the body weight (kg) and NE_M is net energy of diet for maintenance. NE recommendations are stated in the range between 1.24 and 1.55 Mcal/kg.

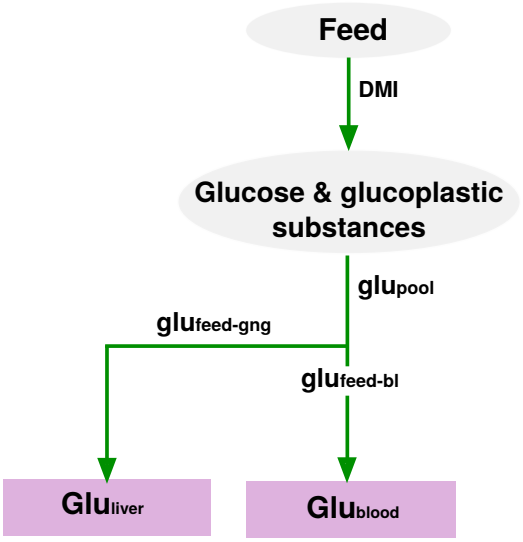

Figure 2.2: **Feed intake process in dairy cows.** This figure illustrates glucose input provided by DMI. The amount glu_{pool} is the fraction of glucose contained in the DMI as glucose and glucogenic substances. This amount of glucose can be transported to the blood circulation via the digestive tract (rate $glu_{feed-bl}$) and gluconeogenesis process (rate $glu_{feed-gng}$).

glucose concentration leads to the production of insulin in the pancreatic beta cells. Insulin promotes glucose uptake in target cells, e.g., those in the liver, muscles and fat tissue, and it promotes the conversion of glucose to glycogen (glycogenesis) in the liver [21]. When the glucose blood concentration is low, the pancreatic alpha-cells produce glucagon. Glucagon increases the plasma glucose concentration by stimulating the generation of glucose from non-carbohydrate substrates (gluconeogenesis) and the breakdown of glycogen to glucose (glycogenolysis) in the liver [21]. The mechanisms describing the change of insulin and glucagon concentrations are illustrated in Fig 2.3.
In the model here, the dynamics of the blood insulin and glucagon concentrations are determined by their secretion rates (ins_{sec}, $gluca_{sec}$) and their degradation rates (ins_{deg}, $gluca_{deg}$),

$$\frac{d}{dt}Ins = ins_{sec} - ins_{deg}, \quad \frac{d}{dt}Gluca = gluca_{sec} - gluca_{deg}, \tag{2.4}$$

with linear degradation rates

$$ins_{deg} = c_3 \cdot Ins, \quad gluca_{deg} = c_5 \cdot Gluca. \tag{2.5}$$

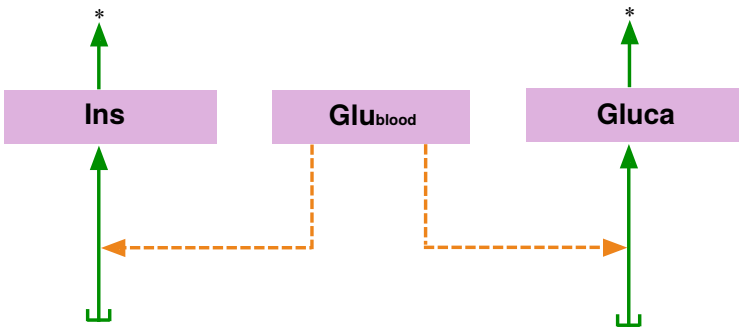

Figure 2.3: **Insulin and Glucagon processes.** The change of insulin and glucagon concentrations are glucose-dependent. When the glucose blood concentration is high, the pancreatic beta-cells produce insulin. When the glucose blood concentration is low, the pancreatic alpha-cells produce glucagon. The stars describes the degradation process of insulin and glucagon.

It is assumed that the insulin secretion rate increases when the glucose concentration in the blood is above a certain threshold value (T_1 = 0.5 g/L = 2,77 mmol/L), whereas the glucagon secretion rate decreases whenever the glucose concentration in the blood is above that threshold value (T_2 = 0.5 g/L = 2,77 mmol/L),

$$ins_{sec} = c_2 \cdot H^+(Glu_{blood}, T_1, 10), \quad gluca_{sec} = c_4 \cdot H^-(Glu_{blood}, T_2, 2). \tag{2.6}$$

Threshold kinetics were selected to account for rapid adaptivity, which is an important mechanism to keep the plasma glucose concentration within the physiological range. There are no reference values for the individual rate constants $c_{2,3,4,5}$, but their values were chosen such that a constant glucose blood concentration of $Glu_{blood} = T_1 = T_2 = 0.5$ g/L (resulting in a Hill function value of 0.5) would give rise to constant insulin and glucagon concentrations that are within the physiological range, namely $0.5 \cdot c_2/c_3 = 20$ mU/L and $0.5 \cdot c_4/c_5 = 100$ ng/L, respectively, compare Tab 2.

2.1.3 Glucose Production and Storage in the Liver

When the glucose blood level rises above a certain threshold (T_3 = 0.45 g/L = 2,77 mmol/L), insulin promotes the absorption of glucose from the blood into liver cells (rate glu_{bl-lv}). This mechanism is illustrated in Fig 2.4.
The rate glu_{bl-lv} is mathematically described by

$$glu_{bl-lv} = c_6 \cdot H^+(Glu_{blood}, T_3, 10) \cdot Ins\,. \tag{2.7}$$

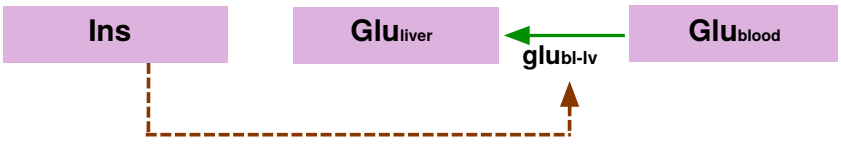

Figure 2.4: **The absorption of glucose blood into the liver.** When nutritional supply with glucose is high, insulin promotes the absorption of glucose from the blood into liver cells.

Insulin also stimulates the conversion of glucose available in the liver (Glu_{liver}) to glycogen (glycogenesis rate glu_{lv-st}). It is assumed here that this rate decreases when the cow produces more than a certain amount of milk (threshold $T_4 = 10$ L) per day in order to make more glucose available for milk production. In addition, the rate glu_{lv-st} is switched off when the glycogen store, Glu_{store}, reaches the maximal carrying capacity $K = 1000g$[3]. The equation that describes this process is given by

$$glu_{lv-st} = c_7 \cdot H^{-}\left(Milk, T_4, 2\right) \cdot \left(1 - \frac{Glu_{store}}{K}\right) \cdot Glu_{liver} \cdot Ins\,. \tag{2.8}$$

In addition, insulin promotes the absorption of glucose into fat cells and its conversion into triglycerides via lipogenesis. It is assumed here that this process is enhanced once the glycogen storage Glu_{store} is full (threshold $T_6 = 1000g$). Again, similar to the glycogenesis rate glu_{lv-st}, the rate is assumed to decrease when the cow produces more than a certain amount of milk (threshold $T_5 = 10$ L) per day,

$$glu_{lv-fat} = c_8 \cdot H^{-}\left(Milk, T_5, 1\right) \cdot H^{+}\left(Glu_{store}, T_6, 10\right) \cdot Glu_{liver} \cdot Ins\,. \tag{2.9}$$

When nutritional supply with glucose is insufficient, the glucagon concentration increases and stimulates the breakdown of glycogen to glucose in the liver (glycogenolysis) to maintain blood glucose homeostasis [84]. This process is assumed to slow down when the glycogen store is below a certain threshold ($T_7 = 10g$),

$$glu_{st-lv} = c_9 \cdot H^{+}\left(Glu_{store}, T_7, 10\right) \cdot Gluca\,. \tag{2.10}$$

In this case, i.e., when the glycogen store falls below a threshold ($T_8 = 10g$), glucagon additionally stimulates the breakdown of lipids into glycerol and free fatty acids (lipolysis) in adipose tissue and the conversion of glycerol into glucose via

[3] Berg et al. [13] estimated that 2% of the weight of the muscle tissue is formed by glycogen, and 10% of the liver weight. Is was also estimated that for a cow with 600 kg body-weight the mass of muscle, liver and kidney is around 280 kg, whereof 9 kg is liver weight [159]. According to these numbers, the liver stores about 900 g glycogen.

gluconeogenesis in the liver. This rate is assumed to slowly decrease whenever the total body fat becomes smaller than a certain threshold ($T_9 = 150$ kg),

$$glu_{fat-lv} = c_{10} \cdot H^{-}\left(Glu_{store}, T_8, 10\right) \cdot H^{+}\left(Fat, T_9, 1\right) \cdot Gluca\,. \tag{2.11}$$

These processes are illustrated in Fig 2.5.

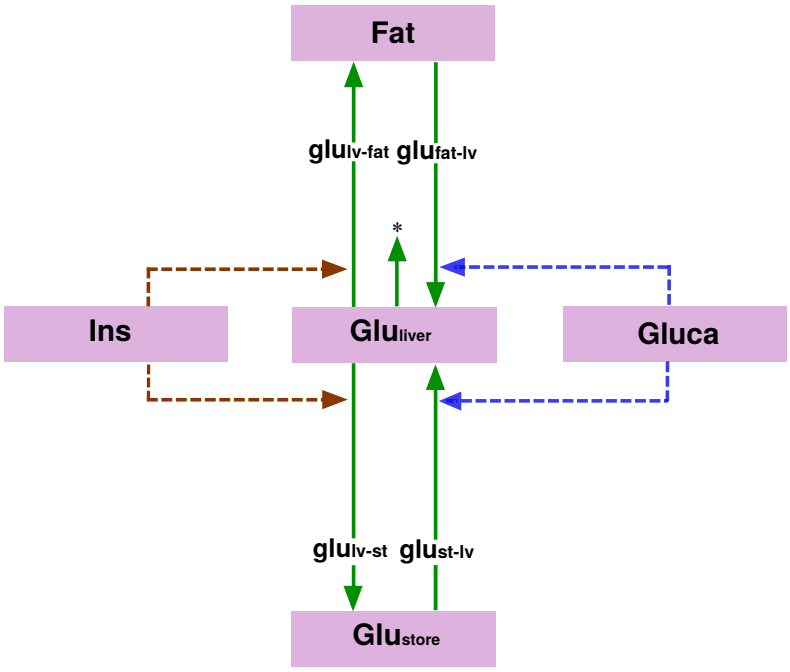

Figure 2.5: **A schematic illustration of the interaction between glucose in the liver, glucose in the store and fat.** When nutritional supply with glucose is high, insulin stimulates the conversion of glucose available in the liver (Glu_{liver}) to glycogen (glycogenesis rate glu_{lv-st}). Insulin also stimulates the absorption of glucose into fat cells and its conversion into triglycerides via lipogenesis (rate glu_{lv-fat}). When nutritional supply with glucose is insufficient, the glucagon concentration increases and stimulates the breakdown of glycogen to glucose in the liver (glycogenolysis, rate glu_{st-lv}). In addition, glucagon stimulates the breakdown of lipids into glycerol and free fatty acids (lipolysis) in adipose tissue and the conversion of glycerol into glucose via gluconeogenesis (rate glu_{fat-lv}) in the liver.

Finally, glucagon stimulates the release of glucose synthesized in the liver (Glu_{liver}) into the blood, see Fig 2.6. This can be modelled by the following equation,

$$glu_{prod} = c_{11} \cdot Glu_{liver} \cdot Gluca. \tag{2.12}$$

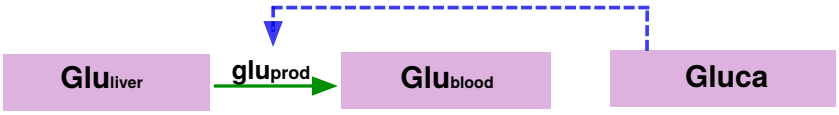

Figure 2.6: **Glucose production.** When nutritional supply with glucose is insufficient, the glucagon concentration stimulates the glucose production in the liver.

In the equations above, threshold kinetics were selected for Glu_{store} to differentiate between full end empty store, without modifying the rates in dependence on the actual amount of glycogen in the store.

There are no reference values for the rate constants c_6 to c_{11}. They were fitted manually such that the simulation results qualitatively agree with the results reported in literature.

2.1.4 Glucose Utilization

All organs and tissues of dairy cows use glucose [55]. Glucose provides energy for maintenance and production. In the milk producing dairy cow, glucose utilization is dominated by the requirements of the mammary gland for milk synthesis [168]. These requirements increase rapidly right after parturition[6]. The process of glucose utilization is illustrated in Fig 2.7

Glucose utilization is modelled here in terms of two different sink terms, one from Glu_{liver},

$$glu_{lv-usage} = c_{14} \cdot Glu_{liver}, \tag{2.13}$$

and one from Glu_{blood},

$$glu_{bl-usage} = c_{12} \cdot H^{+}\left(Glu_{blood}, T_{10}, 10\right) + c_{13} \cdot Milk. \tag{2.14}$$

The sink term from Glu_{blood} accounts for maintenance (1st term) and milk production (2nd term). Maintenance refers to glucose utilization by non-mammary tissues including brain and skeletal muscle, but excluding liver. For example, glucose that is stored in skeletal muscle as glycogen cannot be released back into the bloodstream due to the absence of glucose-6-phosphatase. It is assumed here that the glucose consumption for maintenance decreases when the glucose blood level drops below a certain threshold ($T_{10} = 0.5$ g/L = 2,77 mmol/L). The second term accounts for glucose utilized for milk production, including substance and energy. The variable *Milk* quantifies the daily milk yield in kg/day, whereas the parameter $c_{13} = 72$ g/kg

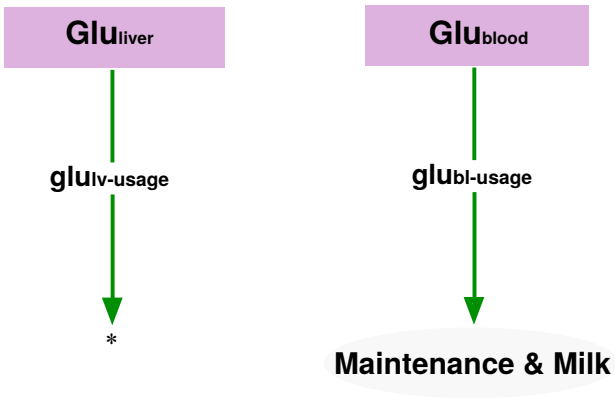

Figure 2.7: **Glucose Utilization.** Glucose utilization is described by two terms, $glu_{bl-usage}$, $glu_{lv-usage}$. The first one accounts for maintenance of brain and skeletal muscle, but excluding liver. The rate $glu_{bl-usage}$ also increases when cows produce milk (milk production). The second term, $glu_{lv-usage}$, accounts for glucose utilized for the liver maintenance.

[107] quantifies the amount of glucose (in gram) per kg of milk. Hence, the mammary glucose requirement in a cow with a daily milk yield of 40 kg would be about 3 kg per day. There is no reference value for the non-mammary glucose requirement, but according to the literature [168] this value should be significantly lower (here, $c_{12} = 1$ kg/day was chosen).

2.1.5 The System of Differential Equations

The interactions of the metabolic processes we have discussed above are combined into a compartmental model and illustrated in Fig 2.8. Flows and regulatory mechanisms are summarized in Tab 3. The final set of ordinary differential equations

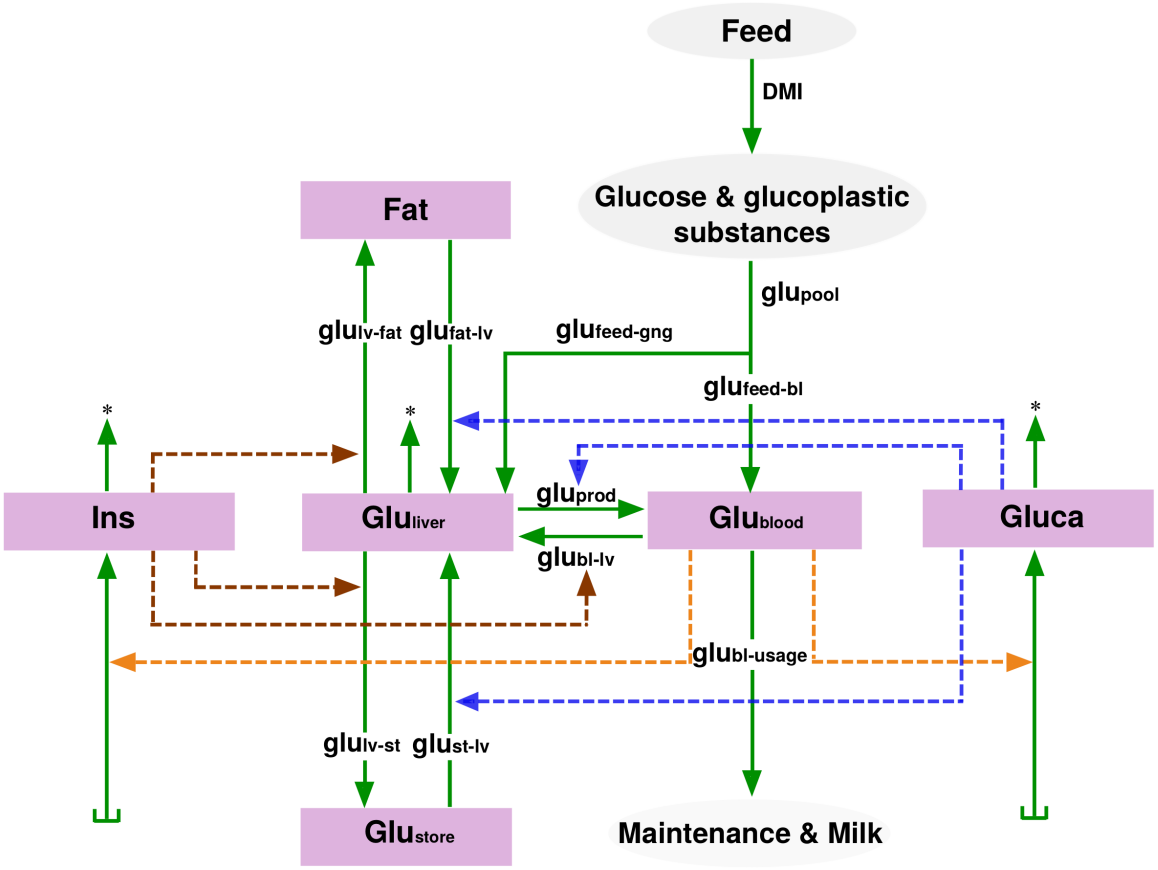

Figure 2.8: **Schematic representation of the metabolic model.** The pink boxes indicate the state variables of the model, gray ellipses indicate sources and sinks. The five compartments of the underlying ODE model are denoted by upper case letters; they have units of concentration or mass (see also Tab 1). Rates are denoted by lower case letters; they have units of gram per day (see also Tab 3).

modelling the dynamics of the glucose exchange (Fig 2.8) reads

$$V \cdot \frac{d}{dt} Glu_{blood} = glu_{feed-bl} + glu_{prod} - glu_{bl-lv} - glu_{bl-usage}, \tag{2.15}$$

$$\frac{d}{dt} Glu_{liver} = glu_{feed-gng} - glu_{prod} + glu_{bl-lv} - glu_{lv-st} + glu_{st-lv} - glu_{lv-fat} + glu_{fat-lv} - glu_{lv-usage}, \tag{2.16}$$

$$\frac{d}{dt} Glu_{store} = glu_{lv-st} - glu_{st-lv}, \tag{2.17}$$

$$\frac{d}{dt} Fat = glu_{lv-fat} - glu_{fat-lv}, \tag{2.18}$$

$$\frac{d}{dt} Ins = ins_{sec} - ins_{deg},$$

$$\frac{d}{dt} Gluca = gluca_{sec} - gluca_{deg},$$

where $V = 22.8$ L is the extracellular volume of blood [14].

2.2 Metabolic Reproductive Bovine Model (MetRep)

Several studies have shown that the metabolic status has a large influence on growing cattle and on reproductive performance in dairy cows. During negative energy balance, which can be caused, e.g., by dietary restrictions or high milk yield, a remarkable change occurs in the levels of the metabolic components IGF-1, insulin, and glucose in the systemic circulation, which in turn influences the levels of reproductive hormones and follicular development [11, 30, 124]. The aim is to reproduce these observations by coupling the metabolic model and the reproductive model BovCycle introduced in [18, 195]. The initial values for the species in the BovCycle model are listed in Tab 6. Detailed explanations of the coupling mechanisms are given in the three sections below.

2.2.1 IGF-1 and Insulin

Kawashima et al. [103] reported that IGF-1 is positively correlated with the level of feed intake. The authors argue that the plasma IGF-1 concentration increases transiently during the follicular phase and decreases during the luteal phase of the estrous cycle, i.e., IGF-1 levels decrease when progesterone ($P4$) increases. On the other hand, IGF-1 is lowest during early lactation when there is no $P4$ in circulation, and highest in late lactation [89]. In particular, a decrease in blood insulin and glucose concentrations in postpartum cattle is associated with the decrease in IGF-1 [124]. In addition, acute dietary restrictions reduce both insulin and IGF-1 concentrations in the blood [201, 217]. Even if these are only empirical observations and evidence for mechanistic relationships is missing, these observations are incorporated into the equation for IGF-1 as follows,

Figure 2.9: **Effects of *P4* and insulin on IGF-1.** Insulin positively stimulates the synthesis of IGF-1, while $P4$ negatively affects the synthesis of IGF-1.

$$\frac{d}{dt}IGF = c_{17} + c_{18} \cdot H^{-}(P4, T_{11}, 4) \cdot H^{+}(Ins, T_{12}, 10) - c_{19} \cdot IGF, \qquad (2.19)$$

where c_{17} accounts for the basal IGF-1 synthesis rate. The rate constants $c_{17,18,19}$ were determined such that the simulated IGF-1 concentrations match with the experimental data from 13 Holstein cows [103], see Fig 2.10 B. Moreover, in order to fit the simulated progesterone concentrations to the data (Fig 2.10 A), the basal

P4 production rate had to be increased from $c_{P4} = 0$ in the original model [195] to $c_{P4} = 0.1$. This is consistent with reports about baseline progesterone levels [19].

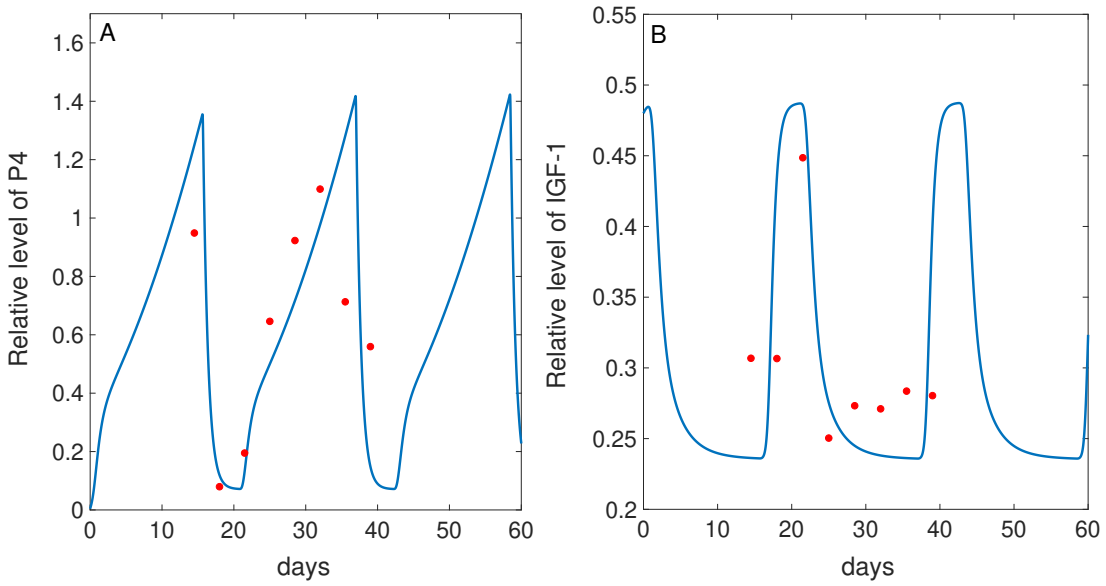

Figure 2.10: **Changes in *P4* and *IGF*-1 levels during the estrous cycle.** Growth of *P4* (A) is correlated to the decay of *IGF*-1 (B). Data of *IGF*-1 and *P4* from 13 Holstein dairy cows (red dots) were collected and kindly provided by Kawashima et al. [103].

A change in plasma *IGF*-1 has an impact on follicular cell development and responsiveness to hormonal signals. In particular, experimental studies demonstrated that reduced *IGF*-1 reduces ovarian responsiveness to *LH* stimulation [193, 124]. To include this mechanism in the model, the term in [195] that models the follicular cell responsiveness to *LH*,

$$H^+(LH_{Bld}) = c_{20} \cdot H^+\left(LH, T_{13}, 2\right),$$

was improved as follows. The *LH* blood concentration that is required for an ovarian response (threshold T_{13}) is made dependent on *IGF*-1,

$$T_{13} := hm_{IGF} = c_{21} \cdot H^-\left(IGF, T_{14}, 2\right). \tag{2.20}$$

Such a dependency was chosen because it allows for *LH* concentrations to increase in response to *IGF*-1 being below a certain threshold, T_{14}. This mechanism is essential to ensure appropriate ovarian responses to *IGF*-1.

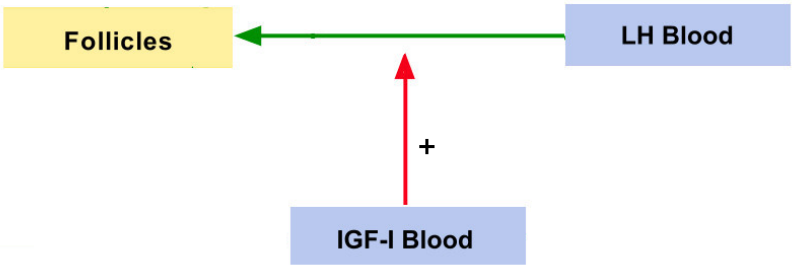

Figure 2.11: **Effect of IGF-1 on the follicular stimulation by *LH*.** An increase in IGF-1 concentration results in increased follicular responsiveness to LH.

Insulin serves as a metabolic signal influencing the release of LH and FSH from the anterior pituitary into the blood [143, 124]. This mechanisms is included in the model by a stimulatory effect of insulin on the synthesis rates of LH and FSH. The equations for LH and FSH in [195] are changed to

$$\frac{d}{dt}LH_{Pit} = LH_{syn} \cdot hp_{Ins}^{LH} - LH_{rel}, \tag{2.21}$$

$$\frac{d}{dt}FSH_{Pit} = FSH_{syn} \cdot hp_{Ins}^{FSH} - FSH_{rel}, \tag{2.22}$$

where LH_{syn}, FSH_{syn}, LH_{rel}, and FSH_{rel} are the synthesis and release rates of LH and FSH, respectively, as described in [195]. The Hill functions hp_{Ins}^{LH} and hp_{Ins}^{FSH} describe the influence of insulin on LH and FSH pituitary levels, respectively,

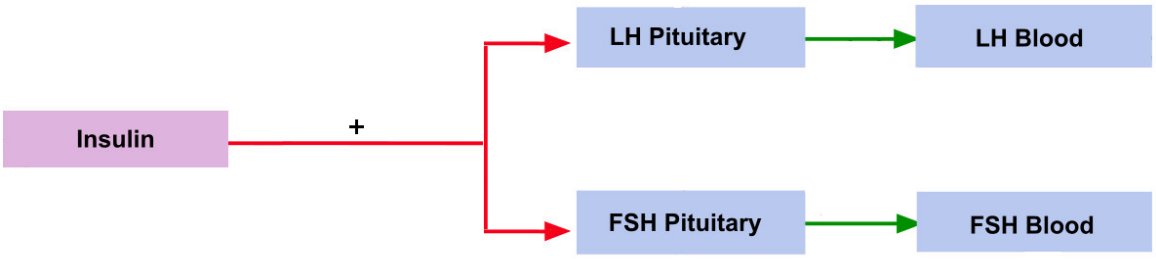

Figure 2.12: **Effect of insulin on *LH* and *FSH*.** Insulin stimulates the release of LH and FSH from the anterior pituitary. This results in increased concentrations of LH and FSH in the blood.

$$hp_{Ins}^{LH} = c_{23} \cdot H^{+}\left(Ins, T_{16}, 10\right), \tag{2.23}$$

$$hp_{Ins}^{FSH} = c_{22} \cdot H^{+}\left(Ins, T_{15}, 10\right). \tag{2.24}$$

Hence, if insulin levels drop below a certain threshold ($T_{15} = T_{16} = 21$ mU/L), the synthesis of LH and FSH halts.

Finally, the flowchart that describes the MetRep model is presented in Fig 2.13.

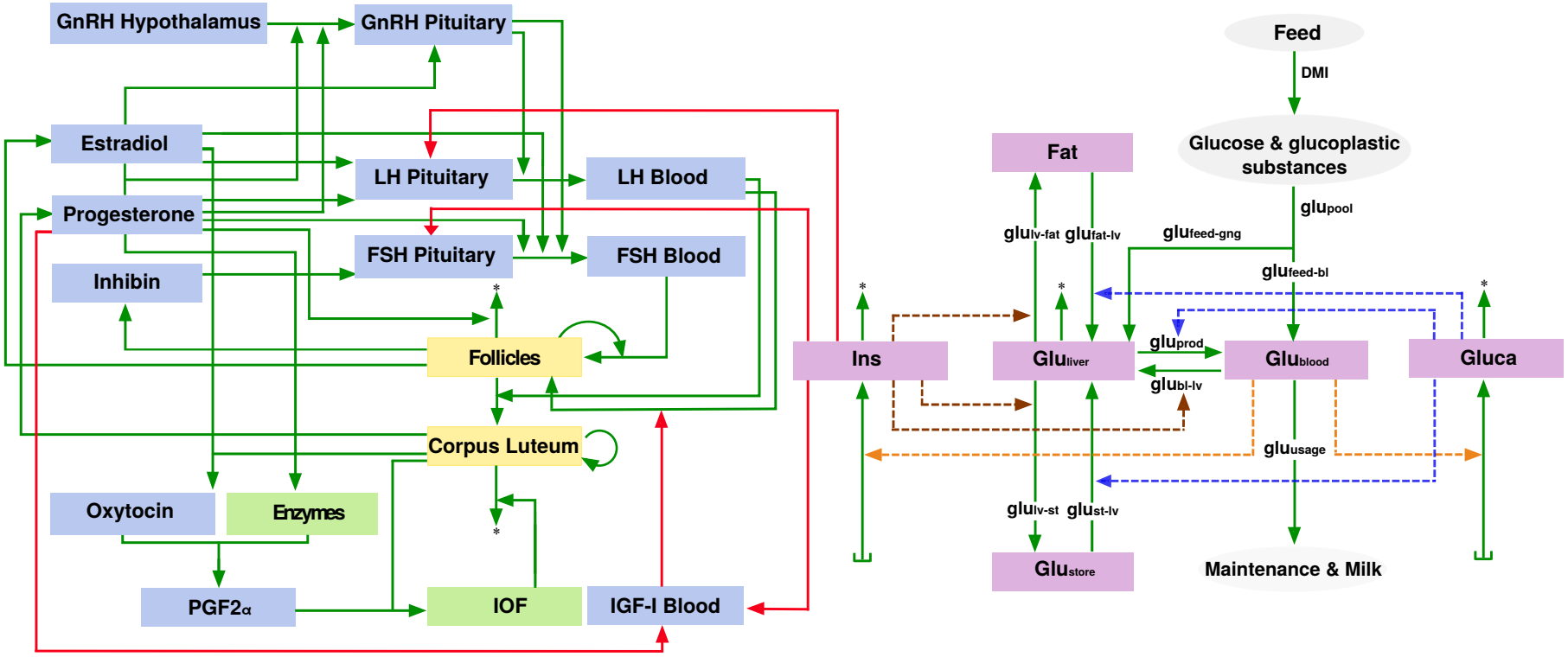

Figure 2.13: **Schematic representation of the coupled metabolic-reproductive model (the MetRep model).** The coupled model links the metabolic model (right hand side) to the bovine estrous cycle model [195] (left hand side). Red arrows depict the sites where both models are coupled. Insulin acts on the site of anterior pituitary influencing *LH* and *FSH* release to the blood circulation. Insulin stimulates *IGF*-1 levels in the blood. Progesterone inhibits *IGF*-1 secretion which in turn decreases the responsiveness of follicular cells to *LH*.

2.2.2 Lactation

Pregnancy and calving are characterized by a complex interplay of hormones. One of these hormones is oxytocin. The release of this hormone and milk yield are positively correlated [149]. Overall as well as peak concentrations of oxytocin decrease over one ongoing lactation [78]; earlier studies reported similar dynamics [141, 142, 165, 166]. According to measurements in those studies, peak concentrations of oxytocin during early lactation are more than twice the magnitude of those during late lactation.

The BovCycle model [195] does not capture changes in oxytocin concentrations during pregnancy and calving. To this end, the model was extended by introducing an additional term Oxy_{lac} into the equation of oxytocin,

$$\frac{d}{dt}Oxy = Oxy_{lac} + Oxy_{syn} - Oxy_{cle}, \tag{2.25}$$

with

$$Oxy_{lac} = c_{24} \cdot \exp(-c_{25} \cdot t^2). \tag{2.26}$$

This is the simplest form of a non-negative decreasing function, namely a Gaussian function, see Fig 2.14. The parameter value $c_{25} = 0.0007$ determines the width of the curve and was adopted to the approximate length of the early lactation period, whereas the parameter value $c_{24} = 1.5$ was fitted so that $Oxy(t)$ during early lactation is about twice as high as $Oxy(t)$ during late lactation.

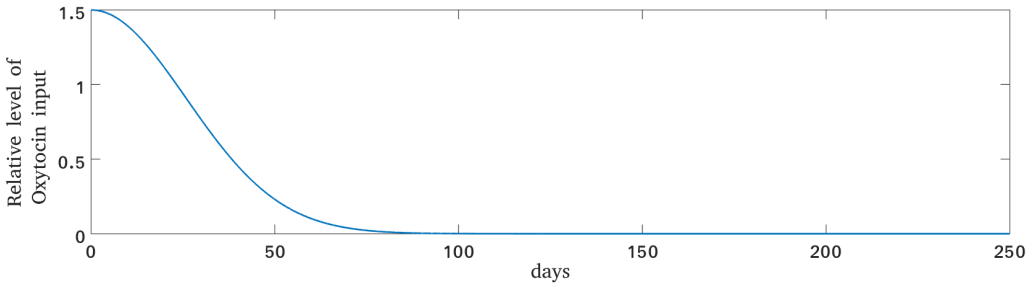

Figure 2.14: **Modelled additional oxytocin during lactation.** Plot of the additional time-dependent oxytocin source term during lactation as defined by eq.(2.26).

2.2.3 Reparametrization of the BovCycle Model

The changes in the equations of the original BovCycle model [195] required changes of some of the original parameter values in order to be able to recover regular estrous cycles. In addition, the original BovCycle model [195] was challenged with the scenario of adding exogenous oxytocin early in the cycle. In a study by Donaldson et. al [59], it was shown that daily oxytocin injections to eight non-lactating cows starting on day two of the cycle reduced the estrous cycle length to nine days. The

slow increase in plasma *P4* concentration during the first five days of the cycle was not altered significantly, but plasma *P4* concentrations decreased again to low values after day five. These results confirmed earlier studies [60, 58]. However, the original BovCycle model [195] did not reproduce these results. Hence, changes were made on parameters that describe the interaction of oxytocin and enzymes with prostaglandin $F2_\alpha$ and the interovarian factor such that the recalibrated model correctly reflects the effects of oxytocin administration on the length of the estrus cycle and plasma *P4* concentrations. Parameters that required changes are listed in Tab 7.

Chapter 3

Model Simulation - Feeding Strategies

The aim of this study is to analyze the impact of glucose availability in the feed, represented by the parameter c_0, on the estrous cycle dynamics in both lactating and non-lactating cows. For a cow of 600 kg BW, DMI at maintenance is set to its default value of 11.7 kg/d [14]. This is the reference value corresponding to 100% DMI throughout the following, and variations to this value are stated accordingly.

This Chapter is organized as follows. Section 3.1 deals with the simulation for non-lactating cows. In this section, we simulate different feeding scenarios, including short and long time dietary restrictions. The results are compared with data from literature. Section 3.2 presents the simulation results for lactating cows and compares the outcome with data from literature. Finally, the results are summarized again and limitations of the model are presented in the 3.3. The ordinary differential equations of the MetRep model were implemented and solved using the software MATLAB (release 2014b). The parameters and the initial values are listed in Tabs 1, 4, 5, 6 and 7.

3.1 Non-Lactating Cows

To model these cows, the value of *Milk* in eq.(4.6) is set to zero. The numerical experiments for acute and chronic dietary restrictions are designed according to three experimental feeding studies from Mackey et al. [127], Murphy et al. [146] and Richards et al. [172]. Since these are studies in beef heifers and anestrus beef cows, respectively, the results are expected to agree only qualitatively, not necessarily quantitatively.

3.1.1 Varying the Glucose Content in the DMI

The effect of varying glucose content in the DMI on the glucose-insulin dynamics is analyzed by changing the value of the parameter c_0 (glucose content in the DMI) between 4%, 8% and 16%. Simulation results are presented in Figs 3.1 and 3.2.

At maintenance intake, i.e. $c_0 = 0.08$, the model calculates the non-mammary usage to be slightly less then 400 gram per day (see Fig 3.2(D)). This number is in qualitative agreement with Danfær et al [47], who estimated the amount of glucose required for maintenance in a non-lactating cow with a slightly lower body weight of 500 kg to be 290-380 gram per day. The amount of glucose absorbed from the digestive tract directly into the blood is calculated to be 75 g/d (see Fig 3.2(A)). The calculated amount of glucose released from the liver into the blood is about 800 g/d (see Fig 3.2(C)). This means that the total amount of glucose available in the blood is around 875 g/d, whereas the glucose uptake into liver cells (see Fig 3.2(F)) and the non-mammary usage (see Fig 3.2(D)) sum up to the same amount. This balance between input and consumption of glucose leads to stable glucose and insulin levels in the blood (see Fig 3.1(A)(D)). In addition, this leads to stable glycogen and fat levels in the respective storage components (see Fig 3.1(B)(E)).

With increasing glucose content in the DMI ($c_0 = 0.16$), more glucogenic substances are available and lead to an increased gluconeogenesis [55]. This increases glucose and insulin concentrations in the blood, but they are still within their physiological range (see Fig 3.1(A)(D)). Excess glucose in the system is stored as glycogen or fat reserves (Fig 3.1(B)(E)). When the glucose content in the DMI is decreased to 4%, blood glucose and insulin levels decrease towards their lower physiological bounds within two days (see Fig 3.1(A)(D)), compare Tab 2. As a result, the stored glycogen and the fat reserves (see Fig 3.1(B)(E)) are reduced as well.

3.1.2 Acute Nutritional Restriction

To simulate the effect of acute nutritional restriction on the estrous cycle, a numerical experiment was designed according to the study of Mackey et al. [127], who reported about the effect of nutritional deprivation for a period of 13–15 days. Heifers with 406 ± 5 kg body weight were allocated to a diet with a DMI of 1.2% of body weight for maintenance and then reduced to a diet with a DMI of 0.4% of body weight. In the model here, this reduction to 1/3 of the default diet corresponds to a reduction in the DMI from 11.7 kg/d to 3.84 kg/d.

This acute nutritional restriction is applied immediately after ovulation. The simulation results show increased levels of *FSH* (Fig 3.3(D)), indicating a failure of luteolysis. Anovulation can be attributed to the absence of *LH* pulses (Fig 3.3(A)) and lower *FSH* levels (Fig 3.3(B)), as a result of decreased insulin levels (Fig 3.3(F)). In addition, *IGF*-1 is decreased during the dietary restriction (Fig 3.3(E)), which

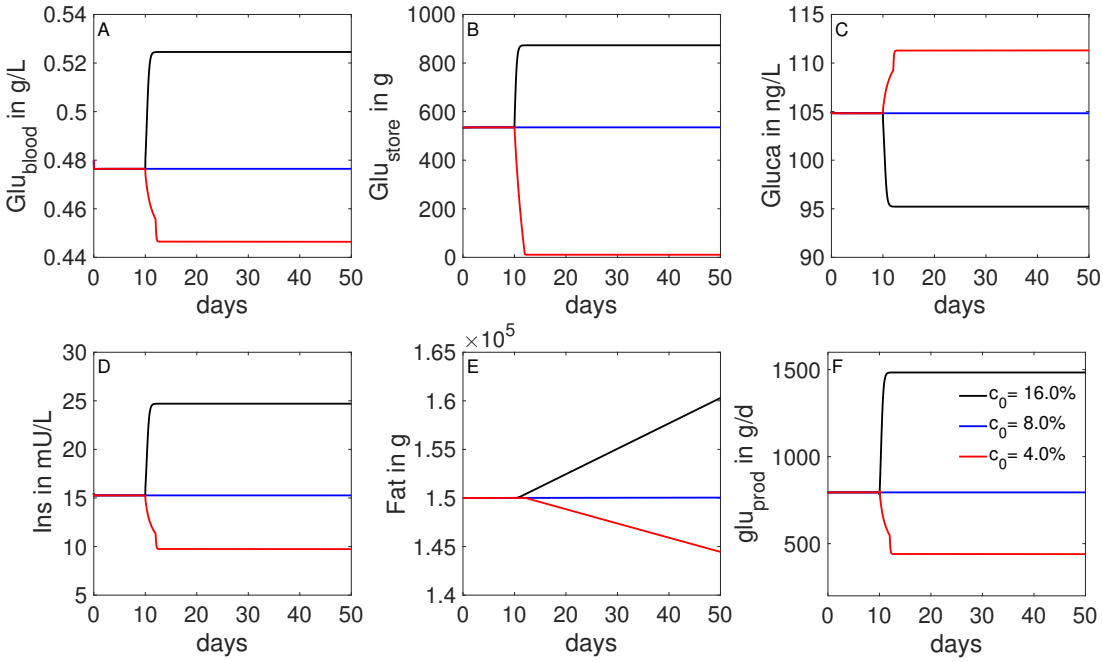

Figure 3.1: **Simulated glucose and insulin dynamics in non-lactating cows for different values of glucose content in the DMI.** The glucose content in the DMI is varied with $c_0 = \{0.04, 0.08, 0.16\}$, corresponding to 4, 8, and 16%, whereby 8 % represents the amount required for maintenance. With higher/lower glucose content in the DMI, blood levels of glucose (A), insulin (D), stored glucose (B) and fat (E), and glucose production (F) increase/decrease over time. Glucagon (C) behaves inversely to the glucose blood level (A).

negatively influences the responsiveness of follicular cells to *LH* [30].

3.1.3 Chronic Nutritional Restriction

To simulate the effect of chronic nutritional restriction on the estrous cycle, numerical experiments were designed according to the studies of Murphy et al. [146] and Richards et al. [172]. Murphy et al. [146] examined the effect of chronic dietary restriction on the estrous cycle over 10 weeks. In this study, heifers with 375 ± 5 kg body weight were allocated to a maintenance diet with an amount of DMI corresponding to 1.2% of the body weight and a reduced diet with 0.7% of the body weight. In the model here, this reduction to 58% of the maintenance diet corresponds to a reduction in the DMI from 11.7 kg/d to 6.79 kg/d. In the experiment by Richards et al. [172], multiparous non-lactating Hereford cows underwent a chronic nutritional restriction for 30 weeks. They were fed to lose 1% of their bodyweight weekly. After the restriction period, the diet was increased to 160% of

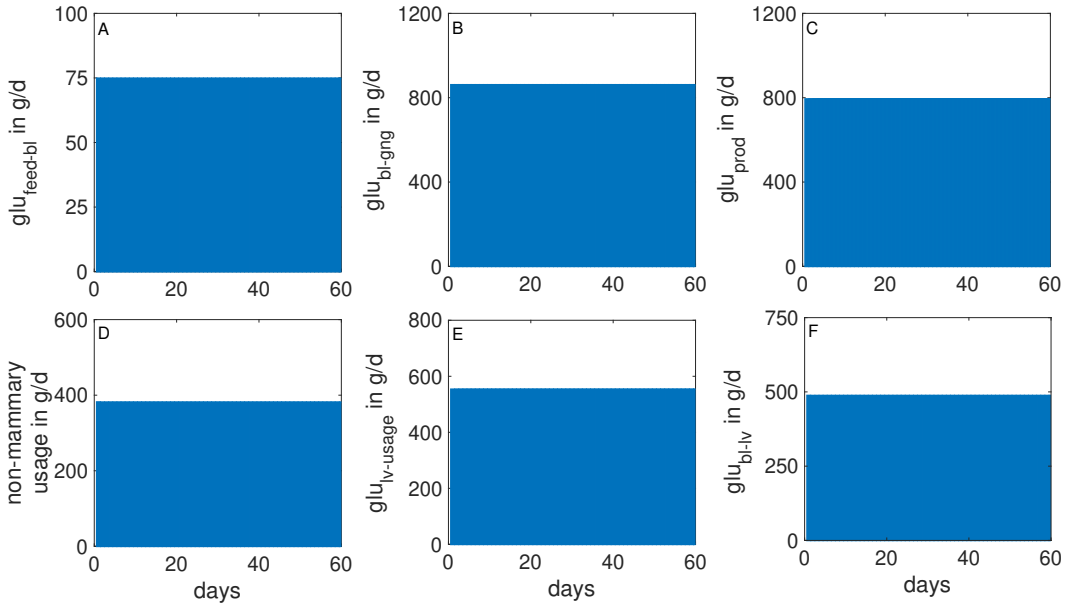

Figure 3.2: **Simulated metabolic rates in non-lactating cows at maintenance.** Glucose content in the DMI was fixed at 8%. The figure illustrates glucose input, storage, and usage in terms of the amount of glucose absorbed via the digestive tract (A), glucose generated from glucogenic substances in the feed (B), glucose released from the liver into the blood (C), glucose absorbed into liver cells (F), and glucose used for body maintenance (D) and for metabolic processes in the liver (E). At maintenance intake, the cow is able to cover the daily glucose requirement, which results in stable levels of glucose in the different compartments.

the maintenance diet.

The simulation was adapted to these two scenarios as follows. The nutritional restriction starts after ovulation. From then on, the model was simulated with 58% of the maintenance DMI within a time interval of 30 weeks. Simulation results (Fig 3.4) show that the cow exhibits normal estrous cycles over a period of 15 weeks. During the chronic restriction period, the glycogen store (Fig 3.4(G)) and the insulin in blood (Fig 3.4(F)) decrease. *LH* (Fig 3.4(A)), *FSH* (Fig 3.4(B)) and *IGF*-1 (Fig 3.4(E)) pulses decrease in frequency and amplitude, resulting in cessation of cyclicity after 15 weeks of feed restriction. The fat compartment loses around 10%. After 15 weeks, *P4* decreases to a low level for the remaining 15 weeks, indicating the onset of anestrus. *FSH* and *E2* exhibit changes in their wave patterns, that is, the number of waves per cycle increases. A similar tendency was observed in [146].

Murphy et al. [146] examined ultrasound data and serum *P4* between week 6 and 9.

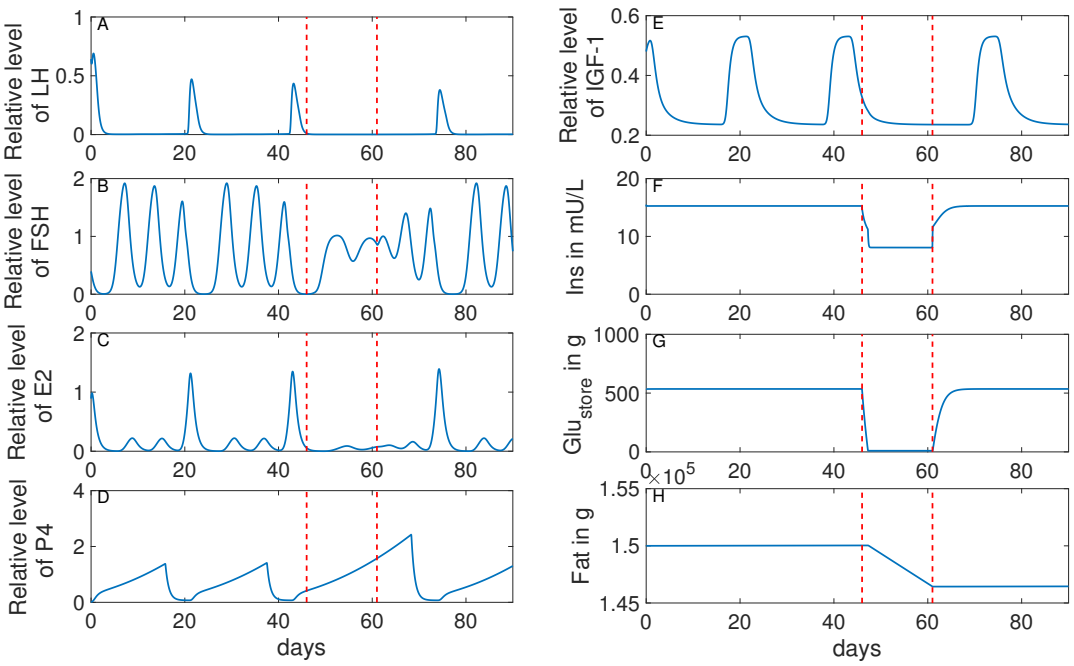

Figure 3.3: **Effect of acute dietary restriction on the bovine estrous cycle in non-lactating dairy cows.** On day 43, DMI is reduced from 100% (11.7 kg/d) to 33% (3.84 kg/d) for 15 days (the time period bounded by the two red lines). During the restriction period, one can observe a decrease of glucose in the store (G), insulin in the blood (F) and *IGF*-1 (E), an absence of *LH* pulses (A), and a decrease of amplitude in the *FSH* waves (B), leading to anovulation and failure in luteolysis with increasing *P4* (D). The cycle re-starts soon after the end of the restriction period.

They found no alteration in *CL* growth, whereas *P4* in restricted cows was numerically higher than in cows on maintenance diet. No anestrus was observed in the first 10 weeks of the restriction period, which is in agreement with the simulation results.

During the first weeks of restriction in the experiment by Richards et al. [172], *P4* concentration increased as well. After losing 24.0 ± 0.9% of their initial body weight, cows had decreased luteal activity measured via *P4*, and cessation of the estrous cycle was observed in 54% of the cows after 26 weeks. The authors reported that estrous cycles were re-initiated by week 40 in 64% of the restricted cows, feeding 160% of maintenance diet. The model predicts re-initiation of cyclicity by week 32, feeding 160% of DMI at maintenance.

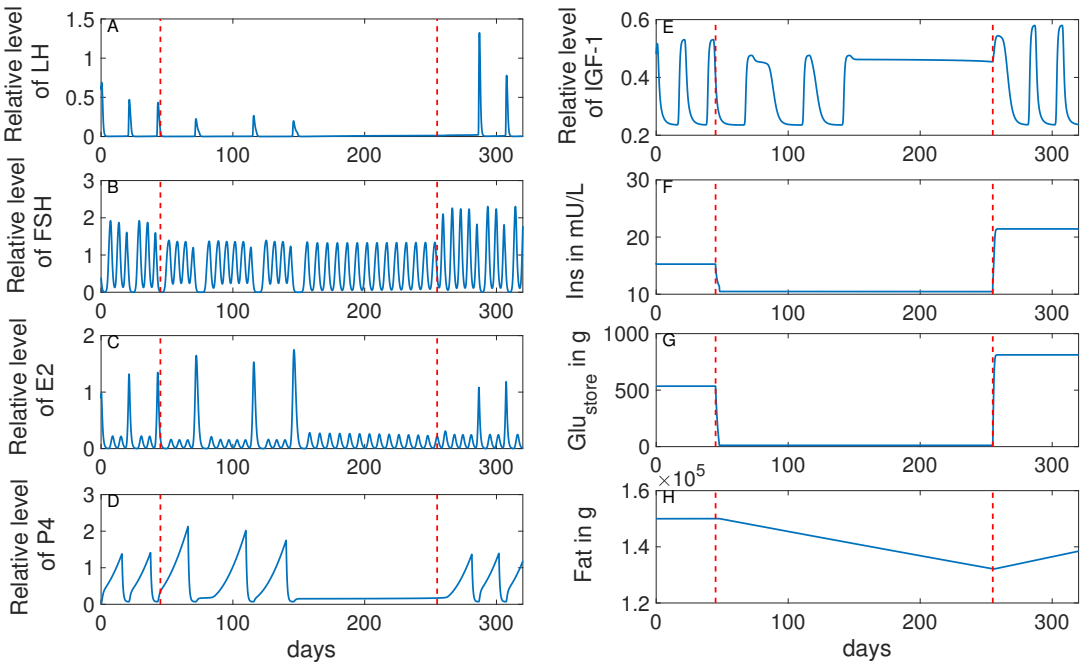

Figure 3.4: **Effect of chronic dietary restriction on the bovine estrous cycles in non-lactating cows.** DMI is reduced to 58% for 30 weeks (period between the red lines) and increased to 160% afterwards. During the restriction period, the glycogen store (G) and insulin in blood (F) decrease. *LH* (A), *FSH* (B) and *IGF*-1 (E) pulses decrease in frequency and amplitude, resulting in cessation of cyclicity after 15 weeks of feed restriction.

3.2 Lactating Cows

To investigate the effect of lactational metabolism and NEB on fertility hormones, different scenarios were simulated with the MetRep model. As model input, interpolated time series data of DMI and milk yield from a study by Friggens et al. [71] were used, see Fig 3.5. Each kilogram of milk produced requires around 72 gram glucose (parameter c_{13} in eq.(4.6) [107]. Hence, the production of 41 kg milk per day requires about 3 kg of glucose per day. This was confirmed by Reynolds et al. [169], who predicted the glucose usage for milk to be between 2500 g/d and 3000 g/d. Milk production and the provided DMI in this study were 41 kg/d and 21 kg/d, respectively, averaged over 5 Holstein cows with an average body weight of 647 kg.

Energy balance is usually calculated as energy input minus output, requiring measurements of feed intake and energy output sources (milk, maintenance, activity, growth, and pregnancy)[202]. Alternatively, the energy balance can be calculated based on changes in the body reserves, using body weight and body condition score [202, 121]. Since the model presented here does not explicitly calculate the body

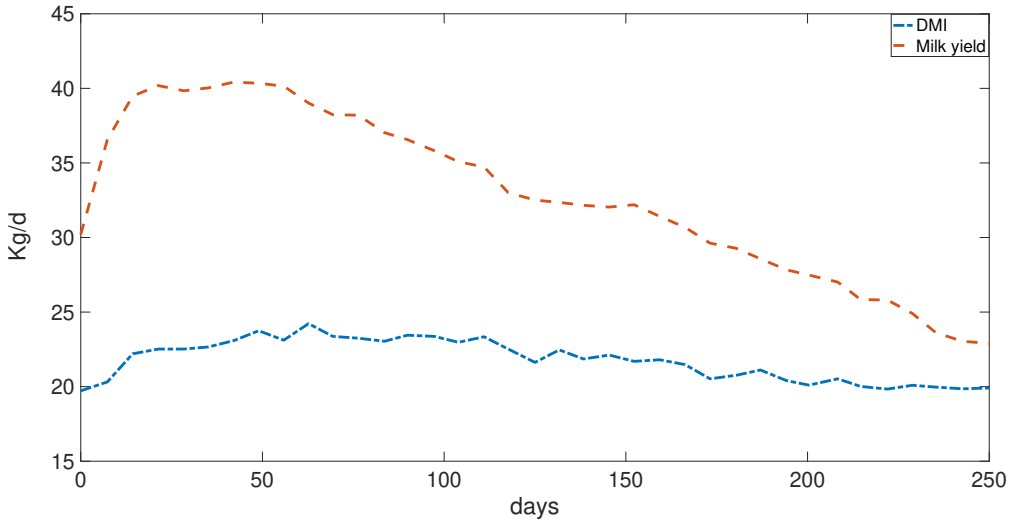

Figure 3.5: **Model input data of DMI and milk.** In this data, the highest milk yield (about 41 kg/d) can be observed 8 weeks postpartum. It coincides with the peak in the DMI (22 kg/d).

weight, the change in body fat is considered as an indicator of the energy balance,

$$\Delta_{Fat} = glu_{lv-fat} - glu_{fat-lv}. \tag{3.1}$$

This approach was also used in [222].

3.2.1 Varying the Glucose Content in the DMI

To explore the metabolic processes during lactation, simulations were performed for different values of glucose content in the DMI (parameter c_0). The results are compared qualitatively with the studies by Elliot [64] and Reynolds et al. [169]. The changes in the glucose-insulin dynamics, body fat reserves, and metabolic rates are illustrated in Figs 3.6, 3.7, and 3.8, respectively.

The simulation results clearly show a non-linear relationship between glucose content in the DMI and the values of glucose in blood and storage as well as insulin in blood at peak milk. Decreasing the glucose content in the DMI, starting from $c_0 = 0.3$, first leads to a slow decrease in glucose and insulin levels, followed by a rapid decrease if c_0 approaches the value 0.2.

For a high amount of glucose in the DMI (30%, $c_0 = 0.3$), glucose and insulin levels in the blood are maintained within their physiological range (Fig 3.6 (A), (D)). After the peak milk phase, the cow is even able to store glucose and fat (Fig 3.6 (B), (E)). Consequently, the overall energy balance is positive throughout the

lactation period (Fig 3.7 (D)). The model calculates the amount of glucose available in the circulation by direct absorption from the digestive tract (rate $glu_{feed-bl}$) to be between 500 and 600 g/d (see Fig 3.8(A)). This is in agreement with Elliot [64], who estimated that for a cow with 600 kg BW and a milk yield of 40 kg/d, the amount of glucose absorbed from the digestive tract is around 600 g glucose per day.

For medium amounts of glucose in the DMI (22.5% or 25%), glucose and insulin levels are still kept within their physiological range (Fig 3.6 (A), (D)), but the period of negative energy balance is prolonged (Fig 3.7 (B),(C)).

If the amount of glucose in the DMI is decreased even further (20%, $c_0 = 0.2$), one can observe an extended phase of negative energy balance with glucose and insulin dropping towards their lower physiological limits around peak milk (Fig 3.6 (A),(D)). High demand and low input trigger the mobilization of body reserves, represented in the model by glycogen and fat in the store (Fig 3.6 (B),(E)).

When c_0 is varied between 0.2 and 0.3, the calculated amount of glucose released from the liver (glu_{prod}) within the first 83 days post partum is 2500–4400 g/d (see Fig 3.8(C)). These numbers are in qualitative agreement with Reynolds et al. [169], who estimated the daily glucose production in the liver within the first 83 days post partum to be between 2700 and 3600 g/d. On can also observe that the mammary glucose usage gets prioritized compared to the non-mammary usage (see Fig 3.8(F,D)), and that this effect becomes more pronounced for low glucose diets.

3.2.2 The Effect of Changing Glucose in the DMI on the Estrous Cycle

The glucose content in the DMI (parameter c_0) has an effect on the estrous cycle. In the previous subsection, it was shown that decreasing c_0 from 0.3 to 0.2 prolongs the phase of negative energy balance. A decrease in blood glucose and insulin concentrations is associated with a decrease in IGF-1 [81, 213, 122]. As a consequence, elongated postpartum anestrus periods occur [32, 31, 37, 192]. Similarly, Walsh et al. [218] resumed that NEB leads to low insulin concentrations in blood, which in turn prevents an increase in IGF-1 secretion, resulting in delayed resumption of ovarian cyclicity [83].

The simulation results (see Fig 3.9) agree with those observations. Increasing the relative amount of glucose in the DMI from $c_0 = 0.2$ to 0.3 increases the IGF-1 concentration. This stimulates the responsiveness of follicles to LH, thereby shortening the postpartum anestrus interval from about 150 to 40 days (see Fig 3.10). Accordingly, the oxytocin level becomes cyclic again at the end of the anestrus interval, after having significantly decreased over the postpartum period (see Fig 3.11).

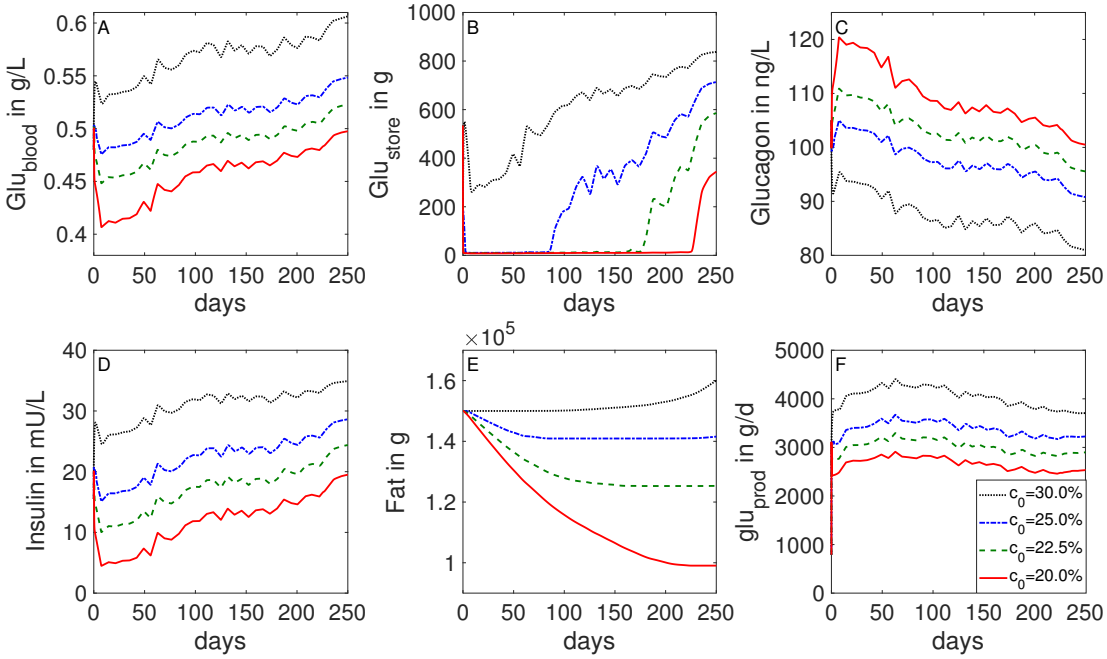

Figure 3.6: **Simulated glucose and insulin levels in lactating dairy cows for different values of glucose content in the DMI.** Time series data of milk yield and DMI from Holstein cows [71] are used as input for the model (C). Glucose and insulin dynamics were simulated with different glucose content in the DMI ($c_0 = \{0.2, 0.225, 0.25, 0.30\}$). When $c_0 = 0.2$ (corresponding to 20% glucose content), glucose levels during peak milk drop towards the physiological limit (0.39 g/L) (A). In general, low amounts of glucose lead to a rapid depletion of the store (B), accompanied by a decrease in body fat (E), indicating a negative energy balance due to high milk production.

The length of the postpartum anestrus in the simulations agrees with the literature. In studies based on postpartum progesterone profiles, it was demonstrated that 90 to 95% of post partum dairy cows have resumed ovarian cycles by day 50 after calving [156, 27, 28]. Hence, a postpartum dairy cow is considered 'normal' if it has resumed ovarian cyclicity by day 50 post partum and continues cycling at regular intervals of approximately 21 days [111].

The simulations also show that estradiol levels at the beginning of the lactation period are within their normal range. This was confirmed by several studies. The authors in [172] found that restricted nutrition leads to anovulation but does not alter estradiol blood concentrations. Although ovulation and luteal development do not occur in anestrus cows, follicular growth is not totally impaired by restricted

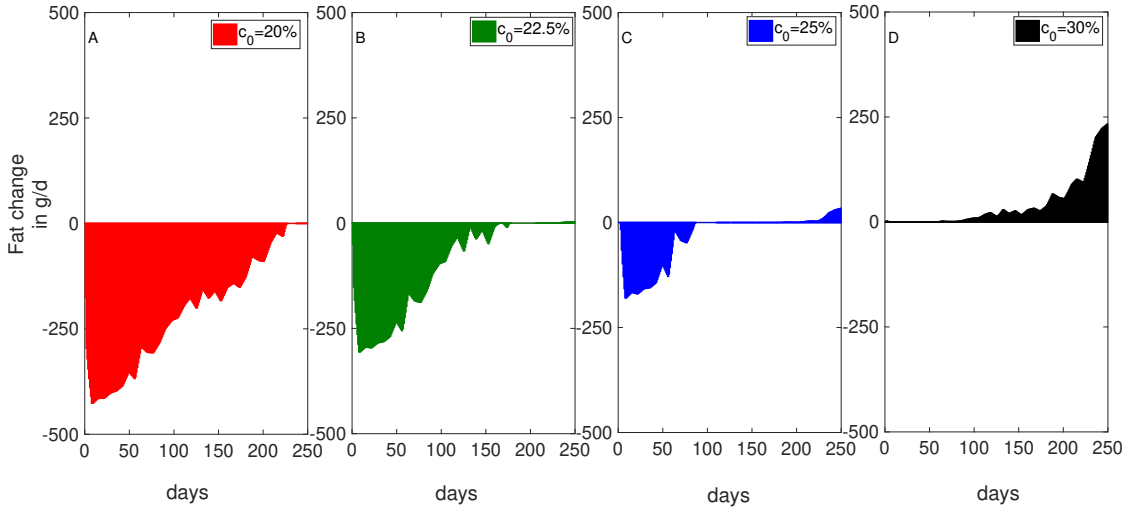

Figure 3.7: **Simulated change in body fat as an indicator of energy balance in lactating dairy cows for different values of glucose content in the DMI.** When $c_0 = 0.2$, energy balance is negative throughout the lactation period (A). When $c_0 = 0.225$ or higher, the period of negative energy balance becomes shorter (B,C). When $c_0 = 0.3$, energy balance is positive throughout the lactation period (D).

nutrient intake. In a review, Diskin et al. [57] suggested that NEB in early lactation does not affect the follicle population but does affect the ovulatory fate of the first dominant follicle. The authors summarized that low *IGF*-1 and insulin cumulatively reduce follicular responsiveness to *LH* and ultimately suppress follicular oestradiol production.

There is evidence that a good management of the diet can reduce the incidence of abnormal estrous cycles [77, 75, 162]. Improving postpartum nutrition increases the blood concentration of insulin and *IGF*-1, which ultimately enhance *LH* pulsatility [122, 11]. Higher *IGF*-1 levels during the first two weeks postpartum lead to an earlier re-start of the estrous cycle [218]. It was demonstrated in a study that providing a diet high in starch promotes an increased insulin release with a subsequent rise from 55% to 90% in the number of cows that ovulated within 50 days postpartum [77], a time interval that is considered to be an indicator for good reproductive performance [156]. In sum, resumption of cyclicity during lactation is crucial for good fertility in dairy farming. It can be influenced by feed intake, but also depends on many other factors such as uterine health, metabolic status, milk yield and overall condition.

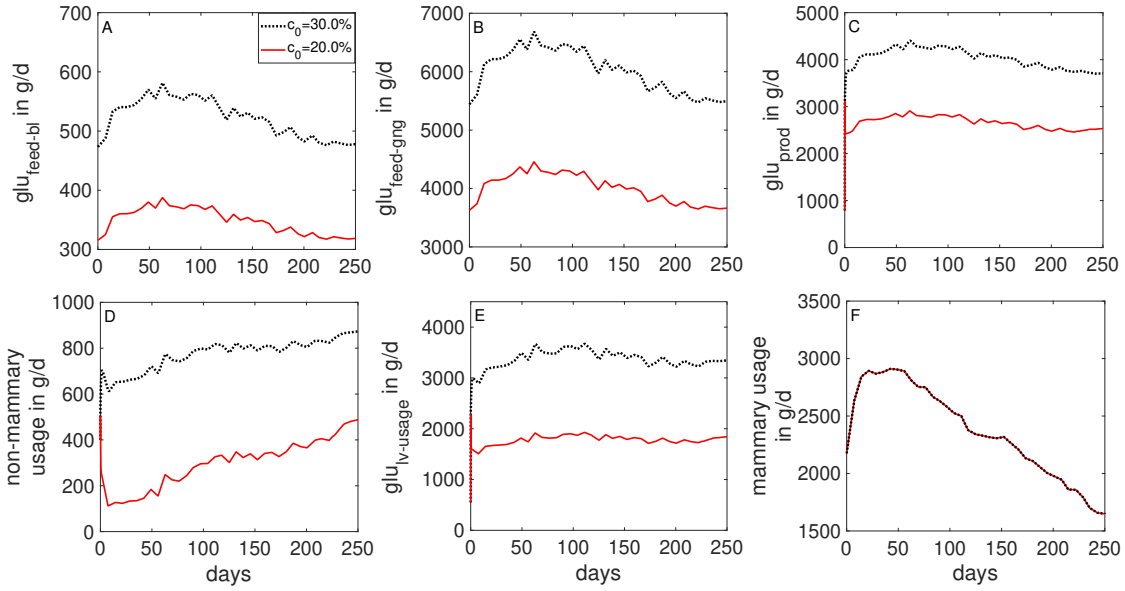

Figure 3.8: **Simulated metabolic rates in a lactating cow for different values of glucose content in the DMI.** Glucose content in the DMI was fixed at 20% (red line) or 30% (black line). During lactation, mammary glucose usage (F) gets prioritized compared to the non-mammary usage (D).

3.2.3 The Effect of Changing Model Parameters on the Estrous Cycle

A local sensitivity analysis as described in eq. (1.20), was performed to assess the influence of all model parameters on the time of first ovulation after calving, characterized by the onset of luteal activity (increased *P4* levels). For this, the observable y is chosen as the earliest time point at which the (relative) *P4*-level is larger than a threshold $T_{P4} = 1$,

$$y(x(t,\theta)) := \min_{t \geq 0}(P4(t) \geq T_{P4}).$$

Throughout the calculations, glucose content in the DMI was fixed at $c_0 = 0.25$, which resulted in an onset of luteal activity at day 50 post partum. The parameters' impact on the timepoint of ovulation is illustrated in Fig 3.12. Fig 3.12 (A) shows the change in the timepoint of first ovulation after perturbation of single parameters by +10%, whereas Fig 3.12 (B) shows the change in the timepoint of first ovulation after perturbation by -10%. Note that in the two subplots (A) and (B) only the numerator of $\hat{S}_y^i$ is plotted, since the denominator is independent of the parameter index i. The two most influential parameters are T_1 (parameter number 91) and T_{P4}^{Foll} (parameter 33, described in [195]). The first one describes the threshold of glucose in the blood to stimulate insulin secretion, while the second

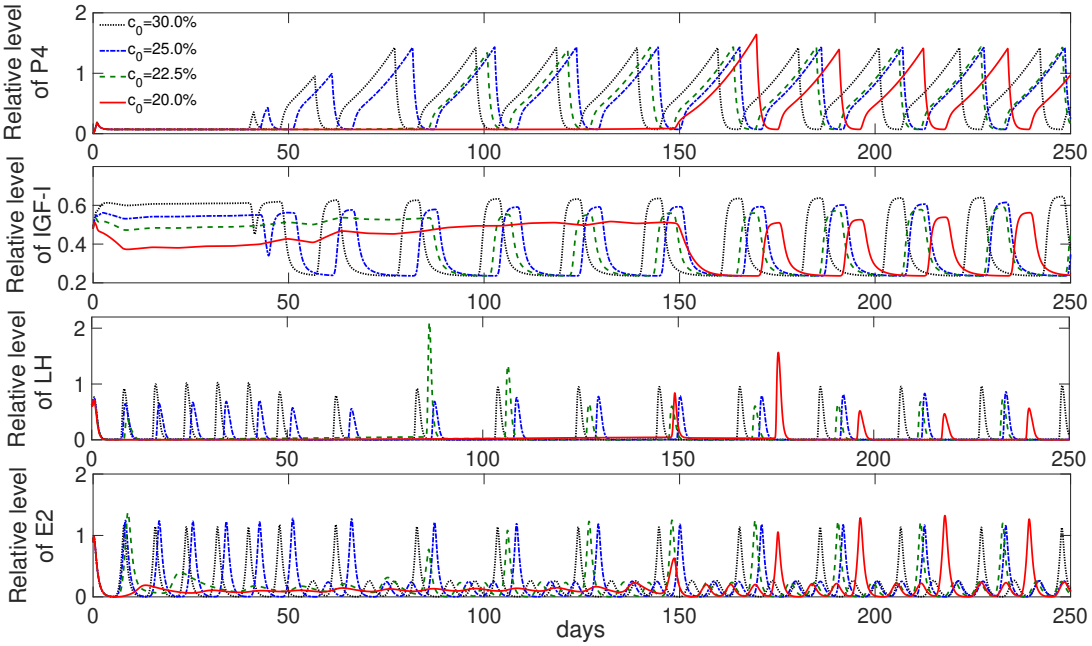

Figure 3.9: **Simulated levels of *P4*, *IGF*-1, *LH* and estradiol during lactation for different values of glucose content in the DMI.** Hormonal cycles were simulated over the lactation period for different fractions of glucose in DMI (parameter c_0). A lower glucose content results in negative energy balance (see Fig 3.7), thereby prolonging the anestrus period. A higher glucose content results in an improved energy balance, which leads to increased insulin and *IGF*-1 levels and an earlier re-start of the estrous cycle.

one is the threshold of *P4* to stimulate decrease of follicular function. A change of the parameters 91 and 33 by +10% and -10%, respectively, results in a later occurrence of ovulation (see Fig 3.12 (C)). Indeed, an increase in the value of T_1 by 10% limits the secretion rate of insulin. As insulin influences the release of *LH*, *LH* pulses are suppressed, which delays the ovulation to day ≈ 90. On the other hand, a decrease in the value of T_{P4}^{Foll} by -10% stimulates the decay of follicular function, which causes a prolongation of the anovulatory period to day ≈ 120.

3.3 Discussion

In the previous sections, the relationship between fertility and metabolism was explored based on two validated models [195, 14]. These models were slightly modified and coupled to simulate the interplay of follicular development and its hormonal regulation with the glucose-insulin system. Information about the mechanistic interactions between fertility and metabolism, if taken straight from the literature,

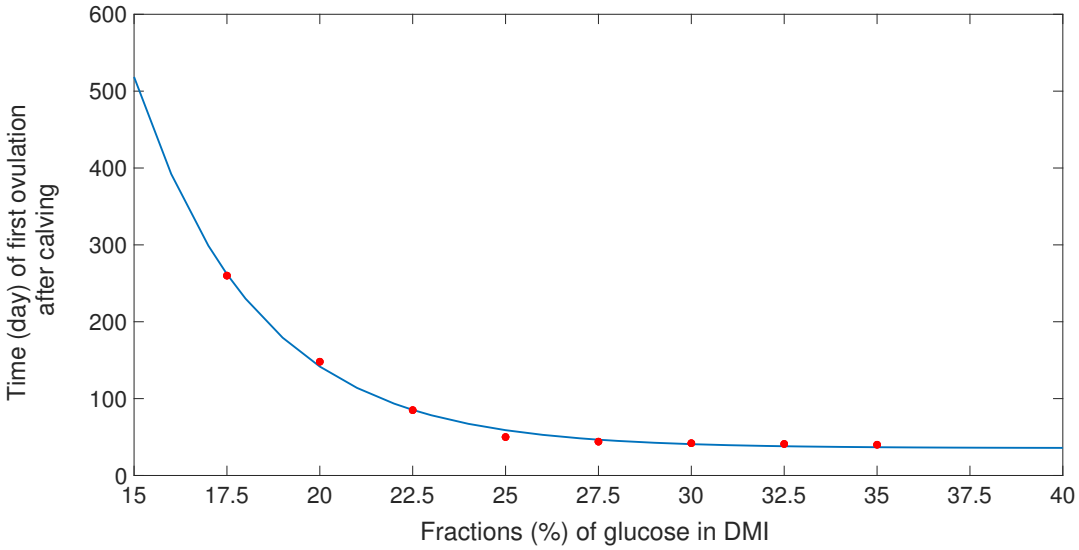

Figure 3.10: **Effect of changing the glucose content in the DMI on the time of first ovulation after calving.** Hormonal cycles were simulated over the lactation period for different fractions of glucose in DMI (parameter c_0). Simulated data (red dots), which represents the estimated incidence of first ovulation, is determined by the time of first *LH* peak followed by an increase in progesterone production above baseline. The blue line represents the fitted curve $f(x) = a \cdot \exp(-b \cdot x) + c$ to the data with $a = 45581$, $b = 0.30317$, $c = 35.644$. A lower glucose content results in a late ovulation, whereas a higher glucose content results in an early ovulation.

is sometimes contradictory and/or redundant. Therefore, only a small number of mechanisms was included, sufficient to realize the coupling of the two models.

With the coupled model, acute and chronic dietary restriction scenarios were simulated, intending to reproduce clinical study findings for non-lactating cows [127, 126, 172]. Furthermore, numerical experiments were run by varying the amount of DMI and the glucose content in the DMI for both lactating and non-lactating cows, and the effect of dietary restrictions on the estrous cycle was analyzed in lactating cows. The simulation results agree with the findings from the clinical studies, at least on a qualitative level.

Of course, the model has some limitations. Increasing (decreasing) the glucose content in the DMI, given by the parameter c_0, results in the same simulation out-

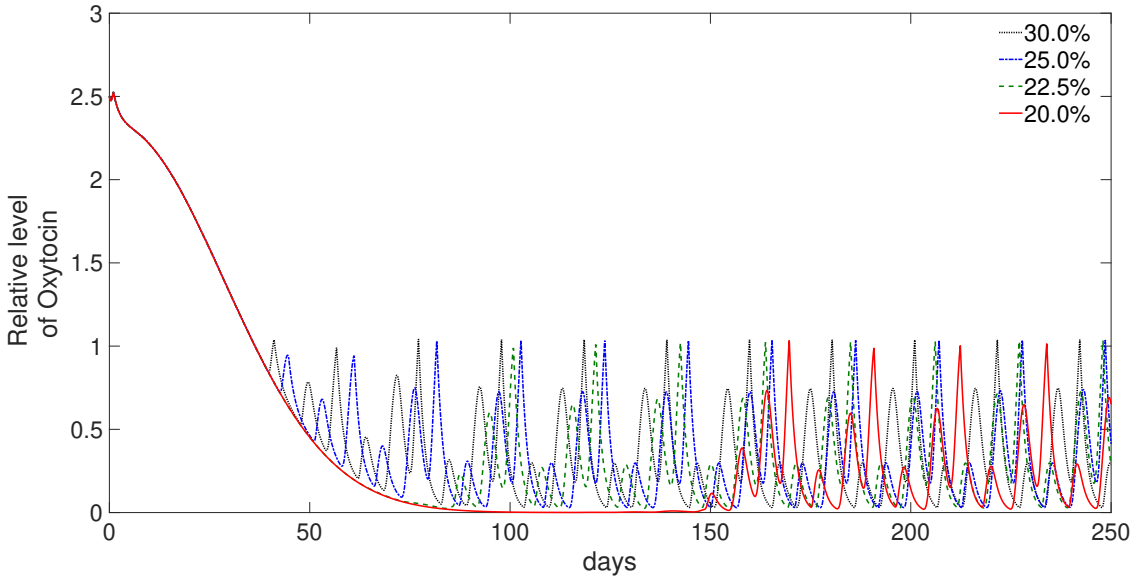

Figure 3.11: **Simulated levels of oxytocin during lactation for different values of glucose content in the DMI.** Levels of oxytocin, which are very high in early lactation, decrease with ongoing lactation and become cyclic again at the end of the anestrus period.

put as increasing (decreasing) total DMI, because only the product $c_0 \cdot DMI$ is contained in the model equations but not the individual factors. In reality, this is certainly not true. A way out would be to relate DMI directly or indirectly (e.g., via metabolic activity as in [14]) to one of the other variables. However, this would have complicated the model structure which, from the authors' point of view, is not necessary for the modeling purpose in this thesis.

Furthermore, the model presented here only describes processes in a single representative cow. In its current form, the model is not able to display inter- or intra-individual variability. However, since the implemented mechanisms are universal, variability could easily be included by adapting parameter values to individual measurements, once such measurements are available.

One could also criticize the model for its restriction to glucose as the only feed component. Hence, the protein content should be included in addition to glucose and fat to complete energetic composition of DMI. This would provide one with a more realistic nutrient supply, change of body composition and body weight as well as milk production and composition.

In addition, experimental research is gaining more and more insights into the effect

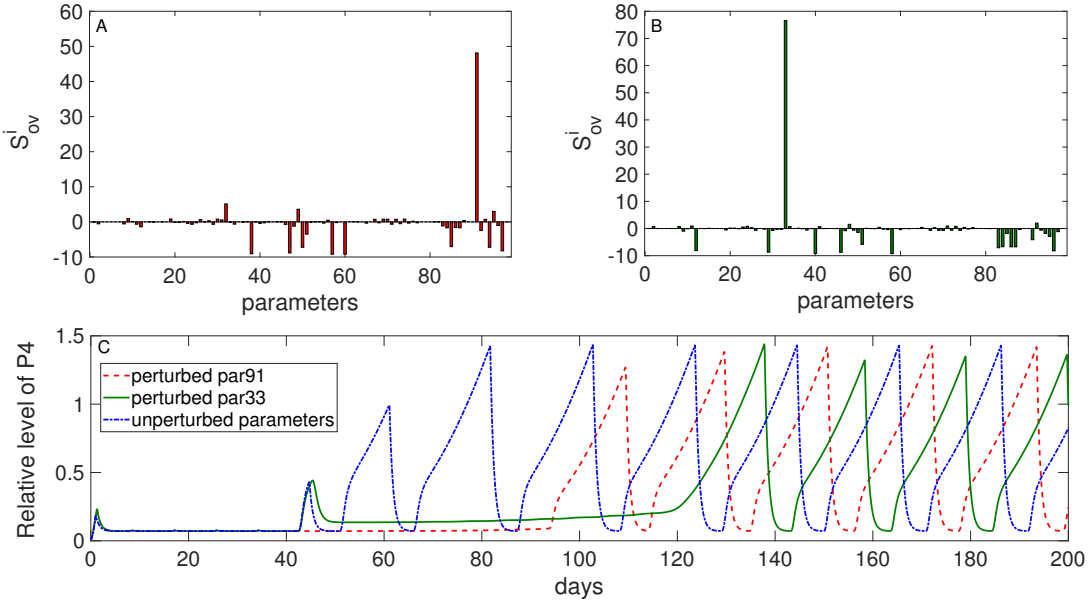

Figure 3.12: **Sensitivity analysis results for the time of first ovulation post partum.** A sensitivity analysis was performed to assess the influence of all model parameters on the time of first ovulation after calving as described by eq. (1.20). (A) shows the change in the timepoint of first ovulation after perturbation of single parameters by +10%, whereas (B) shows the change in the timepoint of first ovulation after perturbation by -10%. Note that in the two subplots (A) and (B) only the numerator of $\hat{S}_y^i$ is plotted since the denominator is independent of the parameter index i. The two most influential parameters are T_1 (parameter 91) and T_{P4}^{Foll} (parameter 33). A change of the parameter T_1 by +10% results in a later occurrence of ovulation (see Fig 3.12 (C)). On the other hand, a decrease in the value of T_{P4}^{Foll} by -10% stimulats the decay of follicular function, which causes a prolongation of the anovulatory period to day ≈ 120.

of nutrition on follicular development. With an improved follicle model, similar to the one introduced in [113], further simulations can be conducted to explore the effect of nutrition on multiple follicles in more detail.

Chapter 4

Model Application - Administration of Dexamethasone

4.1 Background

Glucose requirement in dairy cows early in lactation is dominated by the requirements of the mammary gland for milk synthesis [168]. Due to increased glucose requirements caused by milk production, high yielding dairy cows usually go through a period of negative energy balance that predisposes them at risk of developing hypoglycemia and ketosis. Hypoglycemia, which is often observed in early lactation, stimulates glycogenolysis in skeletal muscles and lipolysis in adipose tissues as an adaptation to manage the energy deficit. An increased rate of lipolysis often results in increased levels of non-esterified fatty acids in the blood, which causes an increase in its uptake by the liver. The liver can exceed its capacity to oxidize mobilized non-esterified fatty acids. Therefore, excess fatty acids are accumulated in the liver, which may impair hepatic function. This gives rise to an increase in susceptibility to disease and several health problems such as ketosis, fertility disorders, impairment of immune function [51, 61, 85, 186]. Ketosis in dairy cows is very common during the postpartum period. From a large sample size of population study (1717 cows), it was reported that the average of ketosis incidence was 43% and the peak incidence occurred at 5 days in milk [135].

Improved feeding management of cows during dry and early lactating periods has been shown to mitigate the degree and duration of negative energy balance and reduce accumulation of fatty acids in the liver [214, 17]. But if the increase of feed intake lags behind the demands for energy requirements, therapeutic intervention may be required to improve the energy balance of the cows. This treatment should regulate blood glucose and insulin concentrations in order to reduce fat mobilisation, thereby diminishing the risk of ketosis. Glucocorticoids such as dexamethasone are

commonly known to treat and regulate mammalian glucose homeostasis. In other words, they play a protective role against glucose deprivation, especially under stress and starvation [10, 67, 98, 105]. Glucocorticoids have been shown to be beneficial in the treatment of cows with clinical ketosis and fatty liver syndrome postpartum [108, 5, 189, 5, 163, 199, 226]. In particular, they are known to improve the energy balance of cows by decreasing the uptake of glucose in body tissues and by suppressing milk production [108, 226, 88, 183]. Because of their ability to promote muscle and fat catabolism, glucocorticoids also stimulate gluconeogenesis during an energy deficit [108, 136, 208]. However, the use of glucocorticoids in these animals is still controversial. This is because in addition to these beneficial effects, they may adversely result in even increased lipolysis and suppression of components of the immune system [153, 151, 191].

In the literature, there exists several pharmacokinetic-pharmacodynamic models developed for investigating the effect of glucocorticoids on rats [98, 116, 7, 197, 119]. For instance, the model in [98] quantitatively describes the induction of hyperglycemia as a result of methylprednisolone drug administration. In bovine, there are only a few studies focussing on the pharmacokinetics of glucocorticoids, e.g., dexamethasone [205, 74]. Moreover, no combined mathematical model describing the coupling of pharmacokinetic and pharmacodynamic was introduced for dairy cows. Therefore, the aim of this Chapter is to develop a mechanistic pharmacokinetic-pharmacodynamic model for dairy cows. This model simulates the effect of dexamethasone on the physiological behaviour of the system, especially glucose metabolism. "In-silico simulations" could play an important role in designing therapeutic strategies for ketosis and diseases related to the metabolic system. This can be done by varying drug and physiological parameters without performing animal experiments.

4.2 Pharmacokinetic-Pharmacodynamic Model

Dexamethasone is the main glucocorticoid drug which is used for the treatment of fatty liver syndrome or ketosis in postpartum dairy cows [51, 199]. In the following, we introduce a pharmacokinetic model for dexamethasone in dairy cows. This model is based on the existing developed pharmacokinetic models. Then, we link the pharmacokinetic model to the MetRep model to investigate the pharmacodynamic characteristics of the drug.

4.2.1 Pharmacokinetic Model

The pharmacokinetics of dexamethasone in bovine have been reported in two published experimental studies [205, 74]. In the experiment of Toutain et al. [205], four cows received dexamethasone alcohol and dexamethasone 21 isonicotinate as a solution by intravenous and intramuscular routes of 0.1 mg/kg (0.1 mg of the drug

per kg body weight). Following intravenous administration, the disposition kinetics of both formulations were described by a two-compartment open model. The half times of elimination were almost similar, 335 and 291 min, for dexamethasone alcohol and dexamethasone 21 isonicotinate. No statistically significant difference was found for all other parameters. Following intramuscular administration, no significant difference in parameters was observed between the two formulations. Peak plasma concentrations were reached at 3 to 4 hours post injection. The bioavailability, denoted by F, which is the fraction of dose that reaches the systemic circulation, was estimated to be around $F = 72\%$. Following intramuscular administration, Toutain et al. [205] described the pharmacokinetics of dexamethasone by a two-compartment model. In this model, one compartment described the distribution phase after intramuscular dosing, and the second compartment was considered to model the absorption phase into the central compartment.

In this work, we also consider an intramuscular administration of dexamethasone 21 isonicotinate, which we call in the followig dexamethasone only for the sake of simplicity. In this regard, we use the pharmacokinetic parameters reported by Toutain et al. [205] for the construction of our pharmacokinetic model. A graphical representation of this model is depicted in Fig 4.1. The figure illustrates the change of dexamethasone concentration, denoted by C, in the central compartment with the volume of distribution V_d. This change is controlled by two rate constants, k_a and CL. The first rate, k_a, describes the absorption phase, that is, the movement of the drug from its site of administration to the bloodstream. The second rate, CL, describes the volume of plasma from which the drug is totally removed per unit time. This rate can also be expressed in terms of the elimination rate and the volume of distribution, $CL = ke \cdot V_d$. The mathematical model describing the change in dexamethasone concentration is given by the following equation:

$$V_d \cdot \frac{d}{dt} C = dose \cdot F \cdot k_a \cdot e^{-k_a \cdot t} - CL \cdot C, \quad \text{with } C(t = 0) = 0, \tag{4.1}$$

where *dose* is the total amount of dexamethasone given per kg body weight (mg/kg) following an intramuscular administration.

4.2.2 Integrating the Pharmacokinetic Model into MetRep Model

To couple the pharmacokinetic model to the MetRep model, a description of glucocorticoids' mechanisms of action on the system is presented in the following along with the coupling hypotheses.

Delayed Drug Effects

To observe the effect of a drug on the system, one has to wait the time it takes for the drug to induce an effect at the site of action. This can be ascribed to several

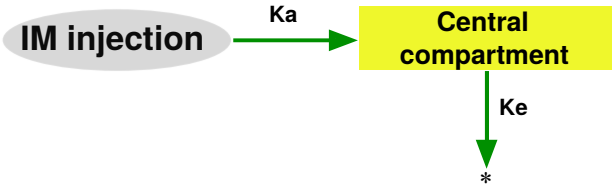

Figure 4.1: **Illustration of pharmacokinetic model.** This figure illustrates the absorption phase described by first order rate k_a of dexamethasone following intramuscular administration into the central compartment from which dexamethasone is cleared by an elimination rate of first order.

mechanisms which explain delayed effects. For instance, after administrating a dose of drug, it takes time for the drug to reach the site of action (distibution) and then to bind to its receptor, which again takes time, thus contributing to a delay in response. Moreover, it may take time for the drug to change physiological intermediate substances before the drug response is observed. Commonly, these time lags can be seen as only one delay process. When the delay is short (minutes) then the mechanism is probably a distribution process, whereas if the delay is long (hours or longer) then the mechanism is more likely to be physiological [92]. When administering dexamethasone, it is not sufficient to directly model the effect as a function of systemic concentrations in the pharmacokinetic model, rather we assume that there exists a delayed effect as it can be seen in Fig 4.5. This is because the maximum effect observed from the data is delayed compared to the maximum concentration of the drug in the plasma. To account for this delay, an additional compartment called "the effect compartment" is considered linking the blood concentration in the central compartment to the systemic effect [3, 93, 187]. The equilibrium concentration in the effect compartment, C_e, is achieved by the flow of dexamethasone concentration, C_{dxm}, from the central compartment to the effect compartment with a rate constant k_{e1} and a dissipation from the effect compartment with a rate constant k_{eo}. Here we assume that k_{eo} is equal to k_{e1}. This parametrization of the model assumes that the average concentration in the effect compartment at steady state is the same as in the central compartment. If the value of k_{eo} is large, this means that the effect compartment is rapidly equilibrating and the concentration in this compartment closely follows the plasma concentration, whereas a small value of k_{eo} means that the effect compartment equilibrates slowly and hence effects are delayed relative to plasma concentrations. The temporal change of C_e is given by the following equation,

$$\frac{d}{dt}C_e = k_{e1} \cdot C - k_{eo} \cdot C_e = k_{eo} \cdot (C - C_e)\,, \quad \text{with } C_e(t=0) = 0. \tag{4.2}$$

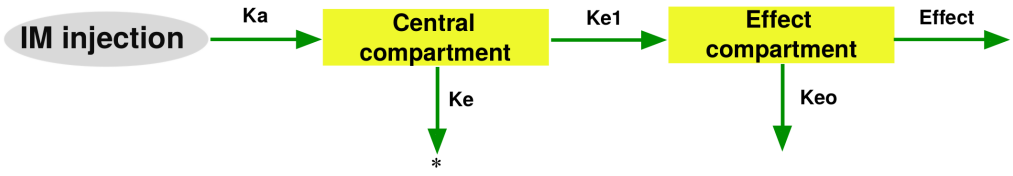

Figure 4.2: **Combined pharmacokinetic and effect compartment.** This figure shows the link of pharmacokinetic model with effect compartment to describe the indirect effect of drug at the site of action caused by the time lag. The central compartment is linked to the effect compartment with a rate constant k_{e1}. The elimination term from the effect compartment with a rate constant k_{eo} is assumed to be equal to k_{e1}.

Glucocorticoid Effects

Several studies have analyzed the role of glucocorticoids in regulating glucose metabolism. In both human and animals, a common findings is that increased glucocorticoids induce peripheral insulin resistance by increasing hepatic glucose output and reducing the peripheral glucose uptake [56, 98, 108, 144, 224]. One mechanism by which glucocorticoids reduce glucose uptake is the inhibition of the insulin signalling cascade [108, 144, 161, 200, 208]. In contrast, reduced glucocorticoids signalling improves insulin-stimulated glucose uptake in peripheral tissues. At the level of alpha cells, this decrease would be regarded as glucose shortage in the system, which augments the responsiveness of alpha cells, thereby triggering glucagon secretion [131]. Studies in man and rats [131, 136, 164, 228] have reported that glucocorticoids increase glucagon secretion from alpha cells.

A second major effect of glucocorticoids on glucose metabolism is that glucocorticoid excess can increase glucose production by stimulating proteolysis, lipolysis and hepatic gluconeogenesis. In particular, glucocorticoids increase the release of amino acids by decreasing protein synthesis and increasing the breakdown of proteins in several tissues. This leads to an increased update of hepatic amino acids uptake, which serve as gluconeogenic precursors. In addition, glucocorticoids also increase the availability of gluconeogenic substrates by stimulating glycerol release from fat cells. The abundance of gluconeogenic precursors enhances hepatic gluconeogenesis, which results in an increase in glucose production particulary in case of an energy deficit [136, 208]. Glucocorticoid-stimulated proteolysis, lipolysis and hepatic gluconeogenesis can be mediated by glucagon. The major target for glucagon is the liver where glucagon stimulates gluconeogenesis, but it also stimulates proteolysis and lipolysis. Exton et al [68] reported that glucocorticoids stimulate gluconeogenesis by glucagon. The authors showed that subcutaneous injection of dexamethasone 30 min prior to perfusion restored glucagon activation of gluconeogenesis as revealed

by increased glucose production and synthesis of glucose and glycogen from lactate. On the other hand, glucocorticoid deficiency showed to markedly impair the ability of glucagon to stimulate gluconeogenesis or glycogenolysis [136].

While the effect of glucocorticoids on alpha cells is to increase plasma glucagon levels, their effects on beta cells, on the other hand, are conflicting [108, 110]. Different results have been reported by in vitro studies in rats, mice and man treated with glucocorticoids, where insulin secretion was measured afterwards. These studies reported either increased [24, 102, 129, 219], unchanged [42, 45, 69, 110, 184, 100, 207], or decreased [120, 25, 49, 63, 80, 104, 110, 152] insulin secretion. These discrepancies cannot easily be explained and it seems that effects of glucocorticoids on beta cells function are highly dependent on the dosage and duration of administration, the experimental animal model and susceptibility of the population under investigation [97, 110]. However, some studies speculated that glucocorticoid treatment acutely (within less than one day) inhibits insulin secretion [120, 53, 104, 110, 152, 208], whereas, pancreatic islets isolated from healthy rats after more prolonged treatment (several days) with dexamethasone or hydrocortisone showed either unchanged or increased glucose-stimulated insulin secretion [152, 219, 208]. Chronic exposure likely results in beta-cell dysfunction in susceptible individuals [208, 196].

In dairy cows, results from some studies indicate that treatment with dexamethasone has the ability to enhance the metabolism of glucose and insulin. For instance, a single dexamethasone injection of 20 mg induced a sharp increase in blood glucose concentration and then a quick return to normal level [154]. Results from Kusenda et al. [109] reported that the mean plasma glucose and insulin concentrations increased one day after treatment and were significantly even higher the second day in cows treated with a single dexamethasone injection of 0.04 mg/kg compared with control cows. In addition, the authors added that dexamethasone administration induced peripheral insulin resistance. Hammon et al. [86] reported an increase in both plasma glucose and insulin concentrations observed in calves treated with a single dexamethasone injection of 0.03 mg/kg. Jorritsma et al. [99, 199], observed in their studies a significant increase in the mean plasma glucose and insulin levels on the second day after treatment with a single dexamethasone injection of 0.02 mg/kg in cows fifteen days after calving versus the controls. This findings supported early work of Wierda et al. [226]. The same finding has been reported by van der Drift et al. [206] in a study where healthy Holstein-Friesian dairy cows in late pregnancy received a single dexamethasone injection of 0.02 mg/kg.

The effect of dexamethasone on reducing milk in dairy cows is well documented in the literature [226, 88, 183]. For example, in an experiment by Shamay et al. [183], a single intramuscular dose of 40 mg dexamethasone in multiparous cows at mid-late lactation caused a 45% reduction in milk yield after 24 hours. Milk yield then started to rise, but it took additional five days to return to the initial level. The decrease in milk yield was ascribed the ability of dexamethasone to reduce

glucose uptake in body tissues as well as the mammary gland, which leads to an insulin resistance state [88].

Coupling Hypotheses

Based on the aforementioned mechanisms, we couple the pharmacokinetic model described above to the MetRep model, which incorporates glucose-insulin interregulations. From the above discussion, it is clear that glucocorticoids act on the alpha and beta cells, body tissues, mammary gland as well as the liver. However, the results from different studies about the action of glucocorticoids on insulin secretion in rodents and man are still contentious. As discussed previously, studies in dairy cows indicated an elevation in insulin level following a single dexamethasone injection. In addition, it is known that the effects of glucocorticoids counteract those of insulin, which enhances glucose uptake in peripheral tissues. Thus, to allow glucocorticoids to exert their responses, glucocorticoids need to antagonize insulin actions. Because of this, we rule out the possibility of glucocorticoids acting on insulin secretion in this work. Thus, we couple the two models according to the following hypothesis.

We assume that a rise in dexamethasone concentration stimulates glucagon secretion from pancreatic alpha cells, see Fig 4.3. The stimulation of glucagon secretion in turn will augment the availability of gluconeogenic precursors and enhance hepatic gluconeogenesis. On the other hand, glucocorticoids reduce insulin-stimulated glucose uptake in body tissues. In lactating cows, we assume that dexamethasone induces milk reduction by impairing glucose uptake in the mammary gland, see Fig 4.3. All these effects are mathematically expressed by altering the secretion term of glucagon represented by $gluca_{sec}$ in eq.(2.4), glucose uptake in body tissues represented by glu_{lv-st} (eq.(2.8)) and glu_{lv-fat} (eq.(2.9)), and the sink term of milk production in eq.(4.6), respectively to:

$$gluca_{sec-dxm} = gluca_{sec} \cdot effect_{dxm-gluca}, \tag{4.3}$$

$$glu_{lv-st-dxm} = glu_{lv-st} \cdot effect_{dxm-bt}\,. \tag{4.4}$$

$$glu_{lv-fat-dxm} = glu_{lv-fat} \cdot effect_{dxm-bt}\,, \tag{4.5}$$

$$glu_{milk-usage} = c_{13} \cdot Milk \cdot effect_{dxm-bt}\,, \tag{4.6}$$

where

$$effect_{dxm-gluca} = \left(1 + E_{max} \cdot \frac{C_e^{10}}{C_e^{10} + C_a^{10}}\right), \tag{4.7}$$

and

$$effect_{dxm-bt} = \left(1 - \frac{C_e^7}{C_e^7 + C_b^7}\right). \tag{4.8}$$

Here E_{max} is the parameter representing the maximum possible stimulation of glucagon secretion $gluca_{sec}$. The constant C_a is the drug-specific parameter representing the concentration required for half-maximal stimulation of glucagon secretion. The constant C_b is the drug-specific parameter representing the concentration required for half-maximal inhibition of glu_{lv-st}, glu_{lv-fat} and glucose uptake in the mammary gland. A full description of the combined pharmacokinetic and pharmacodynamic model of the system is depicted in Fig 4.4.

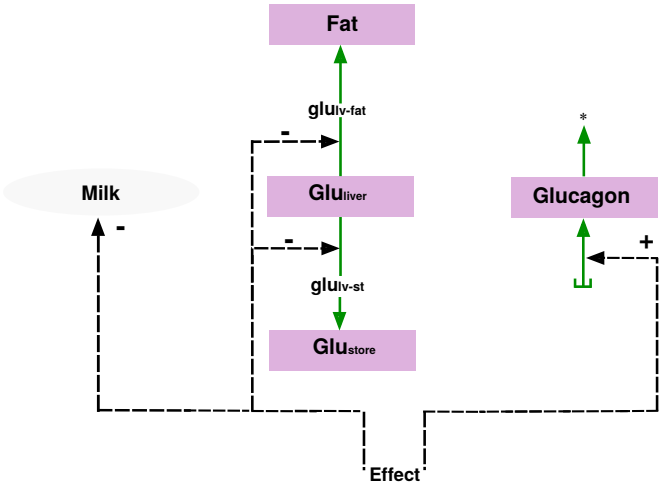

Figure 4.3: **Representation of possible drug effects on pancreatic cells and body tissues and mammary gland.** A rise in drug concentration stimulates glucagon secretion from pancreatic alpha cells and reduces glucose uptake into peripheral tissues, represented by glu_{lv-st} and glu_{lv-fat}, as well as uptake into mammary gland. The green arrow with a star represents the decay term of glucagon.

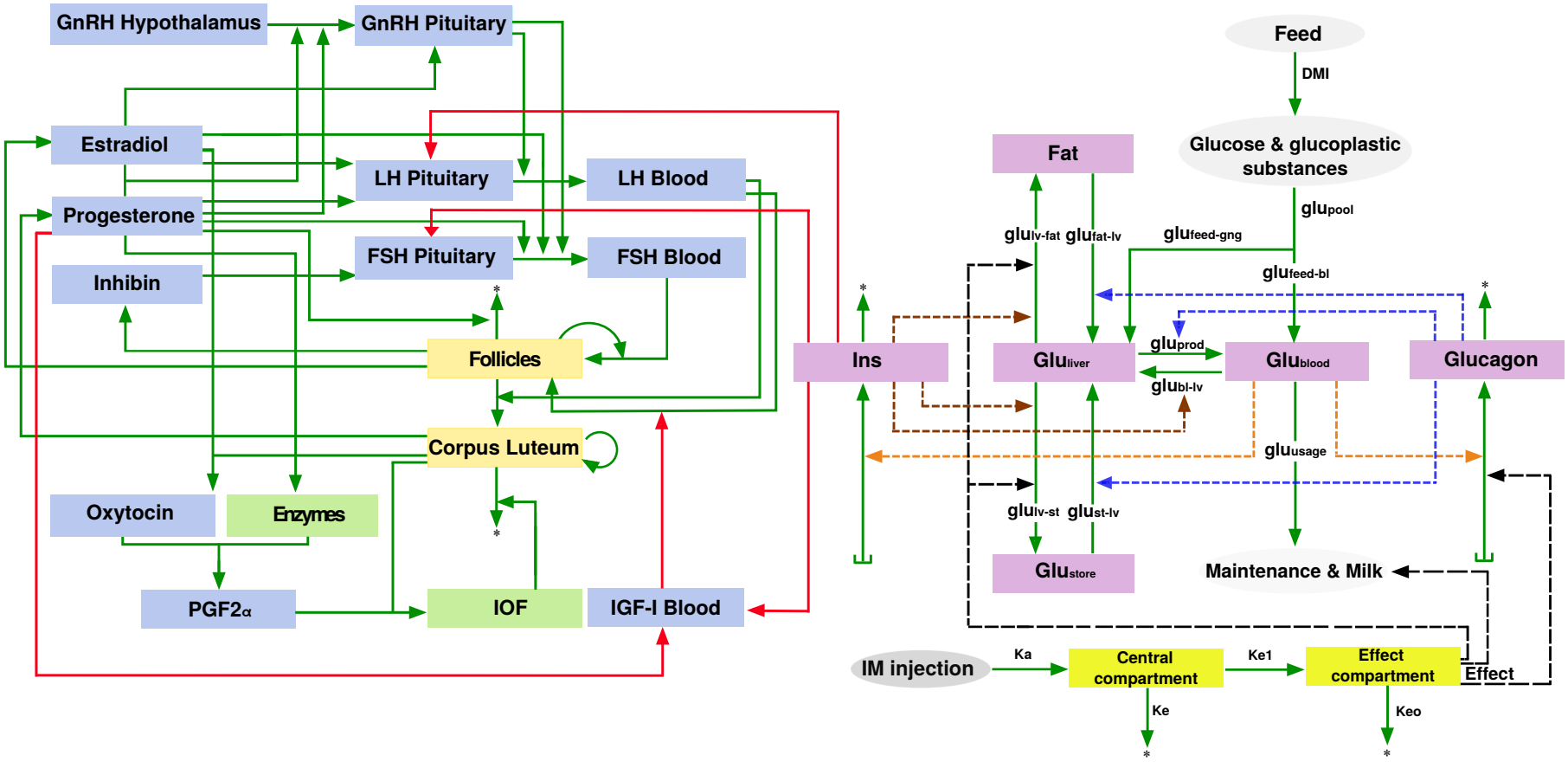

Figure 4.4: **Combined pharmacokinetic and pharmacodynamic model**. This figure illustrates the proposed scenario linking pharmacokinetic model with pharmacodynamic model, where the black dashed arrows describe the stimulatory and inhibitory effects on pancreatic alpha cells and body tissues.

4.3 Simulation Results

In this section, we present the simulation results of the combined pharmacokinetic and pharmacodynamic model. We start by presenting the simulation results of the pharmacokinetic model for intramuscular administration of one single dose of dexamethasone of 0.02 mg/kg. Particularly, we explore the effect of administration on the dynamical behaviour of the model components in non-lactating cows. Subsequently, we examine the effect of administrating one single dose of dexamethasone on the resumption of cyclicity of the estrous cycle during the postpartum period in lactating cows. Simulation results in non-lactating cows are compared with data of glucose and insulin concentration from 6 non-lactating cows that received 0.02 mg/kg dexamethasone 21 isonicotinate by the intramuscular routes, see Fig 4.5. It can be seen from Fig 4.5 that concentrations stay steady post drug administration until around 12 hours after which a trend of increase is observed and a peak is achieved at around 20 hours thereafter. However, we assume that the peak concentrations are already reached at around 18 hours since there are measurements missing for a time period of almost 5 hours. In addition, we assume that concentrations continue to decrease after 22 hours until return to the baseline.

4.3.1 Pharmacokinetics of Dexamethasone

As mentioned earlier, following intramuscular administration, the dexamethasone pharmacokinetics were described by a two-compartment model. The change in concentration C of dexamethasone in the central compartment as well as C_e in the effect compartment are expressed by eq.(4.1) and eq.(4.2), respectively. For a cow of weight 600 kg and a dose rate of 0.02 mg/kg, we consider an intramuscular administration of 12 mg dexamethasone. Only a fraction, F = 72%, of the dose reaches the systemic circulation. The parameter values used to simulate eq.(4.1) and eq.(4.2) are shown in table 4.1. Simulation results are depicted in Fig 4.6. As we can see, the plasma concentration of dexamethasone in the central compartment, C, increases up until around 3 hours post injection. At approximately 4 hours, the concentration reaches its maximal value of $C_{max} \approx 8.7$ ng/ml and then subsequently decreases. The concentration of dexamethasone in the hypothetical compartment, C_e, slowly increases up until around 17 hours post injection. At around 18 hours, the concentration reaches steady-state with maximal concentration of $C \approx 2.1$ ng/ml and then subsequently decreases.

4.3.2 Effects of Administrating a Single Dose of Dexamethasone in Non-Lactating Cows

The effects of administration of a single dose on the dynamic of metabolic elements in non-lactating cows are shown in Fig 4.7. Simulation results show that the

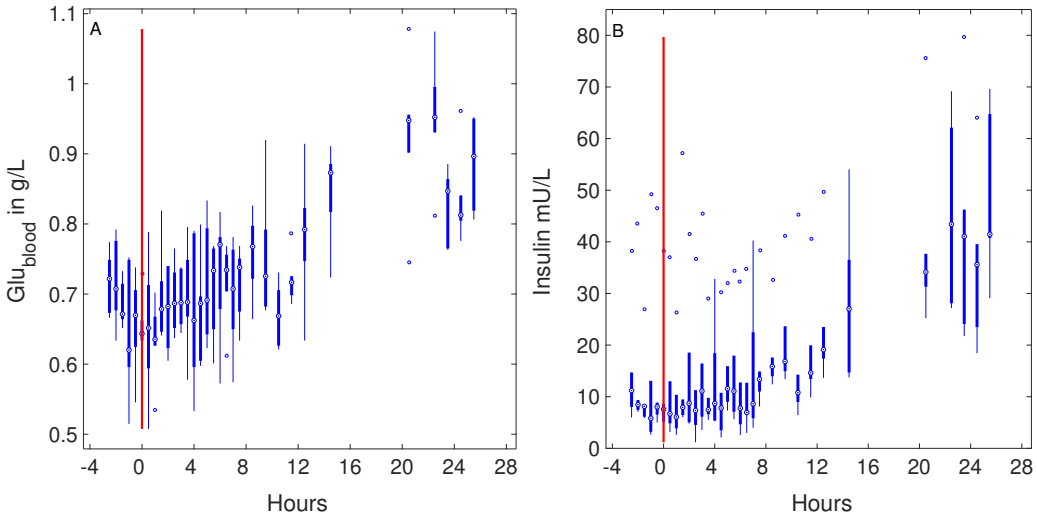

Figure 4.5: **Measured data of glucose and insulin concentrations.** This figure illustrates observed data of glucose and insulin concentrations collected from a clinical study in the Clinic for Ruminants of Freie Universität Berlin. These data were used for parameter estimation of the potassium balance model [14]. The data describe the change of glucose and insulin concentrations on an hourly basis of 6 non-lactating cows that received 0.02 mg/kg dexamethasone 21 isonicotinate by the intramuscular route. The time of administration is depicted by the red line. It can be seen strong inter-individual variations in insulin measurements between the 6 study cows.

stimulatory effect of dexamethasone on alpha cells, eq.(4.3) and eq.(4.7), result in increased glucagon concentration from around 100 ng/ml to around 280 ng/ml, Fig 4.7(E). Hammon et al. [86] reported an increase in glucagon concentration from around 125 ng/L to 175 ng/L in calves treated with dexamethasone administration of 0.03 mg/kg. In [228], the glucagon concentration increased from 150 ng/L to 350 ng/L following dexamethasone administration of 2 mg. As glucagon is a catabolic hormone that regulates glucose levels in the bloodstream, a rise in plasma glucagon concentration increases the supply of gluconeogenic precursors in the liver by stimulating the degradation and mobilization of glycogen and fat. This result is visible in Fig 4.7(D) and Fig 4.7(G), whereby the glucose production is enhanced by hepatic gluconeogenesis process, see Fig 4.7(H). As a result, the plasma glucose concentration temporarily increases from approximately 0.48 g/L to 0.72 g/L and quickly returns to the baseline on the second day, see Fig 4.7(C). The glucose concentration peaks at around 18 hours post drug administration. This time delay that dexamethasone takes until acting at the site of pancreatic alpha cells was modelled by the effect compartment, in which the time of the maximal concentration

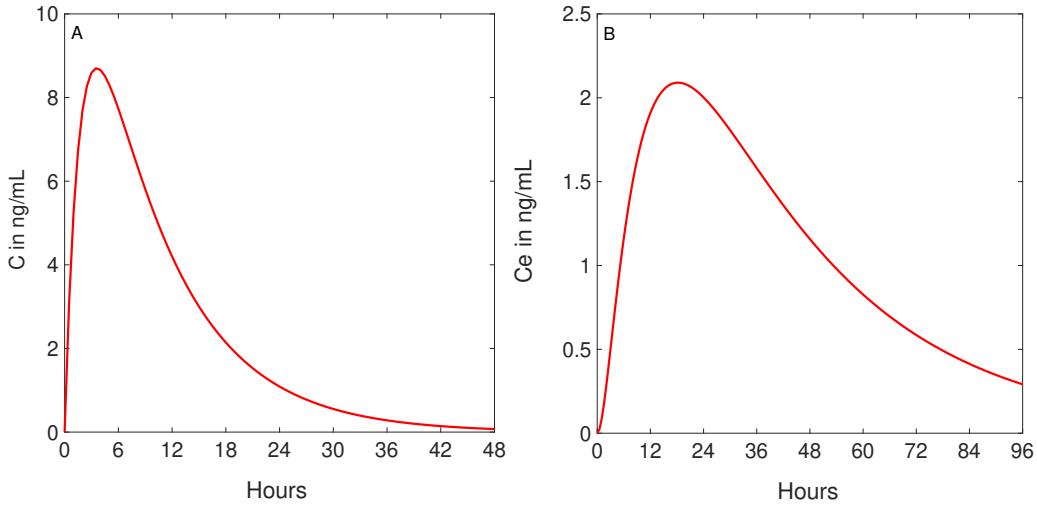

Figure 4.6: **Pharmacokinetics of dexamethasone upon administration of a single dose of 0.02 mg/kg intramuscular injection.** Sub-figure (A) depicts the plasma concentration C of dexamethasone in the central compartment. Sub-figure (B) depicts the concentration C_e of dexamethasone in the hypothetical compartment.

C_e is also around 18 hours post dexamethasone administration, see Fig 4.6(B). The glucose concentration fits to the measurement data as shown in Fig 4.7(A). Here, we scaled down the data of glucose concentration with factor of 0.7 so that they match the baseline of the simulated glucose concentration. The discrepancy in the baseline levels of glucose in the blood between the modelled cow and the cows from the experimental study can be ascribed to several factors such as weight, age, diet, etc.

While insulin primarily stimulates glucose uptake into peripheral tissues, the antagonistic effect of dexamethasone onto this process, eq.(4.4), eq.(4.5) and eq.(4.6), leads to more available glucose in the systemic blood circulation as it can be seen in Fig 4.7(C). Biologically, this occurs through the mechanism by which dexamethasone directly interferes with the insulin signalling cascade in peripheral tissues [208], thereby inducing insulin resistance. The acute elevation in glucose concentration in the blood results in increased insulin concentration. This increase in insulin level is regarded as an adaptation of pancreatic beta cell function to insulin resistance by forcing beta cells to produce a compensatory increase in insulin secretion to maintain glucose homeostasis. In this case, the simulated insulin concentration follows the trend of increasing insulin data as shown in Fig 4.7(F). From this figure, we observe an increase in insulin concentration up to around 40 mU/L on the first day

Table 4.1: Values of rate and effect parameters in the pharmacokinetic-pharmacodynamic model.

Name	Description	Value	Unit
k_a	Absorption rate constant from the central compartment	13.4352	1/d
k_e	Elimination rate constant from the central compartment	2.7086	1/d
k_{eo}	Rate constant describing the rate of change of drug concentration in the effect compartment	0.7	1/d
V_d	Volume of distribution	1.105	L/kg
C_a	Concentration required for half-maximal stimulation of glucagon secretion	1.8	ng/mL
C_b	Concentration required for half-maximal inhibition of glucose uptake	1.8	ng/mL
E_{max}	Maximum stimulatory effect of drug on glucagon secretion	3	-

post dexamethasone administration, and a subsequent return to the baseline on the second day.

As it is evident from Fig 4.7(C) and (F), data of glucose and insulin concentrations resulting from a single dexamethasone administration of 0.02 mg/kg peak almost at the end of the first day post administration. Regardless of the day and the magnitude of this increase, the elevation in both concentrations following a single dexamethasone administration in dairy cows was also observed in early studies. For instance, Jorritsma et al. [99, 199] observed in their studies a significant increase in the mean plasma levels of glucose (3.55 mmol/L = 0.639 g/L) and insulin (13.14 mU/L) on the second day after treatment with a single dexamethasone injection of 0.02 mg/kg 15 days after calving. In another study of healthy Holstein-Friesian dairy cows in late pregnancy treated with a single dexamethasone injection of 0.02 mg/kg, Van der Drift et al. [206] observed a significant increase in the plasma glucose level (median was 4.2 mmol/L = 0.756 g/L) on the second day and insulin level (median was 15 mU/L) on the third day. These discrepancies in the magnitude of increase as well as the day of the peak seem to be dependent on the design of experiment and susceptibility as well as the metabolic condition of the animal under investigation.

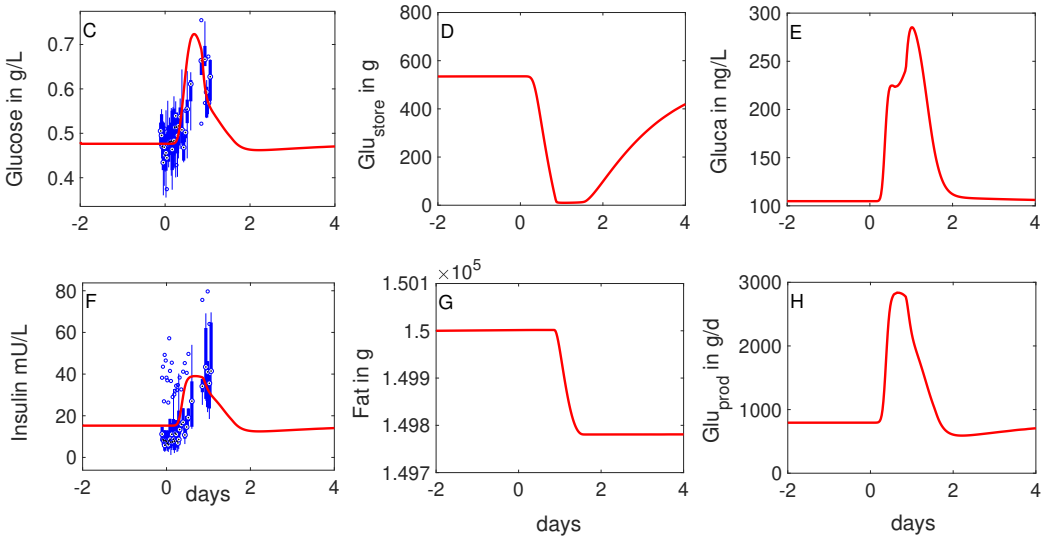

Figure 4.7: **Glucose and insulin changes in non-lactating cows following a single dexamethasone administration of 0.02 mg/kg.** Glucose (C) and insulin (F) concentrations peak almost at the end of the first day post administration. A stimulatory effect of dexamethasone on alpha cells increases glucagon concentration (E), which in turn increases the supply of gluconeogenic precursors in the liver by stimulating the degradation and mobilization of glycogen (D) and fat (G) from the depots, thereby increasing glucose production (H). An inhibitory effect of dexamethasone on body tissues impairs insulin-stimulated glucose uptake, thus allows more glucose in the systemic circulation.

4.3.3 Effects of Administrating a Single Dose of Dexamethasone in Lactating Cows

In this section, we explore the dynamical behaviour over time of the metabolic and the reproductive status in postpartum lactating cows after administrating a single dose of dexamethasone of 0.02 mg/kg.

Effects on the Metabolic Status

We assume that a cow of weight 600 kg gets an amount of DMI and produces an amount of milk as given in Fig 3.5. In addition, we assume that glucose content in DMI is $c_0 = 20\%$. Performed simulations clearly show that for a low amount of glucose in DMI ($c_0 = 20\%$), glucose and insulin concentrations in the blood drop towards their lower physiological limits around peak milk (Fig 3.6 (A),(D)). In order to compensate for the increase in milk production, the cow mobilizes her body reserves as represented in the model by glycogen and fat in the store (Fig 3.6 (B),(E)).

The mobilisation of fat, however, is often associated with negative energy balance. The therapeutic treatment with dexamethasone is expected to up-regulate blood glucose and insulin concentrations in order to decrease the rate of lipolysis. As it is shown in Fig 4.8(A) and (D), the administration of a single dose of dexamethasone of 12 mg on the day 50 postpartum induces a temporary hyperglycemia with a significant increase in glucose concentration over 1 g/L. In their experiment, Shamay et al. [183] reported that a single intramuscular dose of 40 mg dexamethasone in multiparous cows at mid to late lactation caused a 45% reduction in milk yield after 24 hours. This resulted in elevated glucose concentrations in the treated cows to around 1 g/L one day after dexamethasone injection. Glucose was back in the normal range after the second day. Our model-simulated glucose is accompanied by a sharp spike in insulin concentration to around 40 mU/L. Hyperglycemia occurs due to increased glucose production (Fig 4.8(F)), which is stimulated by a rise in dexamethasone-stimulated glucagon secretion. Glucagon concentration sharply increased due to the stimulatory effect of dexamethasone, and subsequently decreased as a response to the significant increase in glucose level, see Fig 4.8(C). Interestingly, although dexamethasone stimulates the mobilization of glycogen and fat from the store, it is evident from Fig 4.8(E) that the rate of lipolysis was decreased. This originates from the fact that milk production is reduced through the mechanism by which dexamethasone impairs the glucose uptake into the mammary tissues. There is only a limited number of studies on the effect of a single dose of dexamethasone on the metabolic status during the postpartum period. All of them, however, report an improvement of the metabolic status in early lactation period. However, all the effects were observed in short terms and there was no long time improvement of the negative energy balance [176].

There are only few conducted studies on the effects of glucocorticoids in combination with or without other drugs on lipolysis in dairy cows, and the findings are inconsistent. In cows treated with dexamethasone on day seven and day eleven postpartum [72, 73], it was shown that in parallel with a significant increase in plasma glucose and insulin concentration, a significant decreases in the plasma concentrations of non-esterified fatty acids and beta-hydroxybutyrate occurs. This decrease can be used as markers of excessive negative energy balance in dairy cows [157]. In other experiments, dexamethasone decreased blood ketone concentrations in ketotic and healthy fresh cows [226, 176]. On the other hand, the administration of a corticosteroid with or without insulin showed to have no therapeutic and preventive effects on ketosis one or two weeks after treatment in early lactation [181]. In other experiments, glucocorticoids did not lead to changes in non-esterified fatty acids concentrations in the blood [206, 99]. These aforementioned findings are discrepant, perhaps due to the difference in dosage, duration of treatment as well as the susceptibility of the cows under investigation. We think that increased lipolysis might occur only when the cow undergoes a consecutive multiple-day dosing of dexamethasone, where the accumulated concentration induces more fat degradation than glucose uptake into the mammary gland. This, however, should be supported

by performing further in vivo and in silico experiments (simulating the model with multiple doses).

Effects on Reproductive Performance

It was shown that an elevated concentration of beta-hydroxybutyric acid is associated with negative enery balance and poor fertility [30, 216]. During negative energy balance phase, fat mobilization increases non-esterified fatty acids and beta-hydroxybutyrate concentrations. These elevations result in impaired *FSH* and *LH* secretion [11, 30], resulting in a negative effect on follicle growth and ovulation. To assess the performance of our model, we administrate a single dose of dexamethasone at two different time points, e.g. days 50 and 52, and compare the two results. Simulation results before drug administration show that for a low glucose content ($c_0 = 20\%$) in DMI the postpartum anestrus interval lasts until day 150, see Fig 4.9 (blue-solid line). After the administration of a single dose of dexamethasone on day 50, simulations show that dexamethasone induces estrous cyclicity with an elongated first cycle and normal cycles thereafter, see Fig 4.9 (red-dotted line). In contrast, administrating a single dose of dexamethasone only two days later fails to reinduce the cyclicity of hormones, see Fig 4.9 (black-dotted line). This discrepancy can be ascribed to the time of administration. In other words, the dexamethasone dose results in a short term increase in glucose and insulin concentrations at days 50 and 52. Based on the linking mechanism of our model, a high insulin concentration stimulates *FSH*, *LH* and *IGF*-1 hormones, see eq.(2.23) and eq.(2.19). It turns out that the sharp increase in insulin temporarily stimulates *LH* and *IGF*-1 around day 52, but in contrast to day 50, the *LH* magnitude does not surpass the threshold that allows follicles to ovulate.

To the best of our knowledge, there are only a few conducted studies about the effects of a single dose of dexamethasone or other glucocorticoids on reproductive performance in dairy cows in early lactation. For instance, Seifi et al. [181] reported that administration of a single dose of isoflupredone alone or in combination with insulin within the first 8 days after calving had no impact on reproductive performance. In other studies, it was reported that excess in glucocorticoid did not affect *LH* concentration of cows [91]. It was also shown in ewe that dexamethasone did not significantly modify reproductive function, in particular, it did not have any effect on *LH* [160]. Maciel et al. showed that dexamethasone did not affect *FSH* and *LH* concentrations, but the total number of follicles (≥ 5 mm) and plasma estradiol concentrations were lower in the treatment group compared to control group [125]. However, in a recent study, Sami et al. [175] were the first to report an improving effect of a single injection of dexamethasone on pregnancy rate and reproductive performance. They concluded from their study that cows treated with an intramuscular injection of 20 mg at day three or ten of lactation had a shorter time to pregnancy than controls. In addition, dexamethasone-treated cows had a better pregnancy rate throughout the lactation period. In particular,

the probability to develop pregnancy on day 120 postpartum was 2 times higher in cows that received dexamethasone in comparison to controls. This study was the first to suggest that a single dose of dexamethasone injection in early lactation might improve reproductive performance.

In general, the effects of glucocorticoids on fertility in dairy cows are not well understood. Future studies should explore mechanisms through which either dexametasone concentration or its signalling pathways in the reproductive system can be changed to improve the reproductive performance.

4.4 Discussion

In this chapter, a pharmacokinetic-pharmacodynamic model was introduced, based on mechanisms underlying homeostasis regulation by dexamethasone. The coupled model takes into account the predominant role of dexamethasone in stimulating glucagon secretion, glycogenolysis and lipolysis and impairing the sensitivity of cells to insulin. Whether the stimulation of endogenous glucose production via gluconeogenesis is a primary dexamethasone effect or a secondary system change via dexamethasone-stimulated glucagon secretion remains unclear. An additional term which accounts for glucagon stimulation, was linked to glu_{prod} to avoid redundancy and overparameterization.

We have shown that the adopted mechanisms are able to induce a temporary hyperglycemia and hyperinsulinemia, which captures the observed data in non-lactating cows. In lactating cows, we have shown that a single dose of dexamethasone reduces the lipolytic effect, owing to the reduction of glucose uptake by mammary gland.

Although our model successfully simulates the acute effect of dexamethasone on the dynamics of metabolic hormones, the simulation of chronic dosing is infeasible due to the lack of mechanisms that describe the long-term effect of dexamethasone treatment on system homeostasis (such as insulin resistance caused via chronic hyperglycemia).

In summary, hyperglycemia and hyperinsulinemia can be simulated following treatment with a single dose of dexamethasone. However, while it is evident that glucocorticoids may acutely decrease or chronically increase insulin secretion in rodents and humans, available studies in dairy cows do not mention any acute decrease in insulin concentration. Since marked differences exist in digestion of carbohydrates and regulation of glucose homeostasis between monogastric animals and ruminating cattle, acute effects of dexamethasone on insulin secretion as well as possible dysfunction of beta cells in chronic treatment regimes should be further investigated in dairy cows.

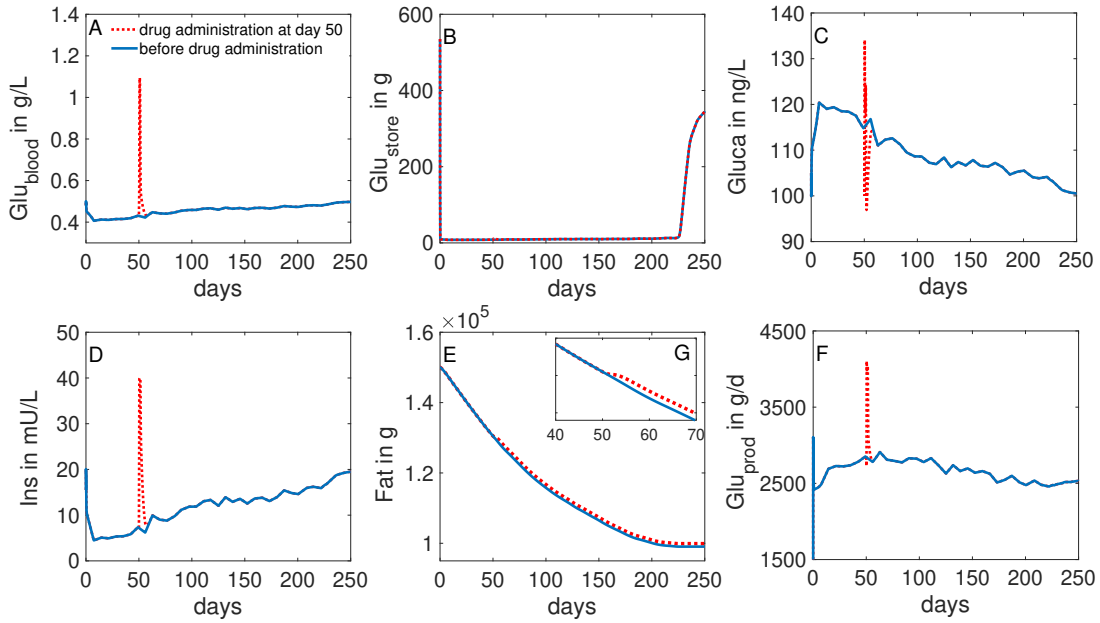

Figure 4.8: **Effects of administrating a single dose of dexamethasone of 0.02 mg/kg on glucose-insulin dynamics in lactating cows.** This figure illustrates the changes in the metabolic components before (blue-solid line) and after (red-dashed line) dexamethasone administration. A sharp increase in glucose (A) and insulin (D) concentrations can be seen after administrating a single dose of dexamethasone of 0.02 mg/kg on day 50. A stimulatory effect of dexamethasone on alpha cells increases glucagon concentration. Glucagon subsequently decreases as a response to the significant increase in the glucose level (C). The increase in glucagon concentration increases the supply of gluconeogenic precursors in the liver by stimulating the degradation and mobilization of glycogen (B) and fat (E) from the depots, thereby increasing glucose production (F). However, it can be seen that the magnitude of decrease in fat is reduced compared to the decrease observed before the administration dexamethasone (G). This originates from the fact that milk production is reduced through the mechanism by which dexamethasone impairs the glucose uptake into the mammary tissues, thus leading to more glucose in the systemic circulation.

Mechanistic pharmacokinetic-pharmacodynamic modeling not only permits assessment of drug effects but also gives additional insights into the interacting components of the model. Improving our biological knowledge about the long term effect of glucocorticoids in dairy cows could entitle the proposed model to be further developed and used as a tool for exploring treatment strategies against ketosis and other diseases related to the metabolic system.

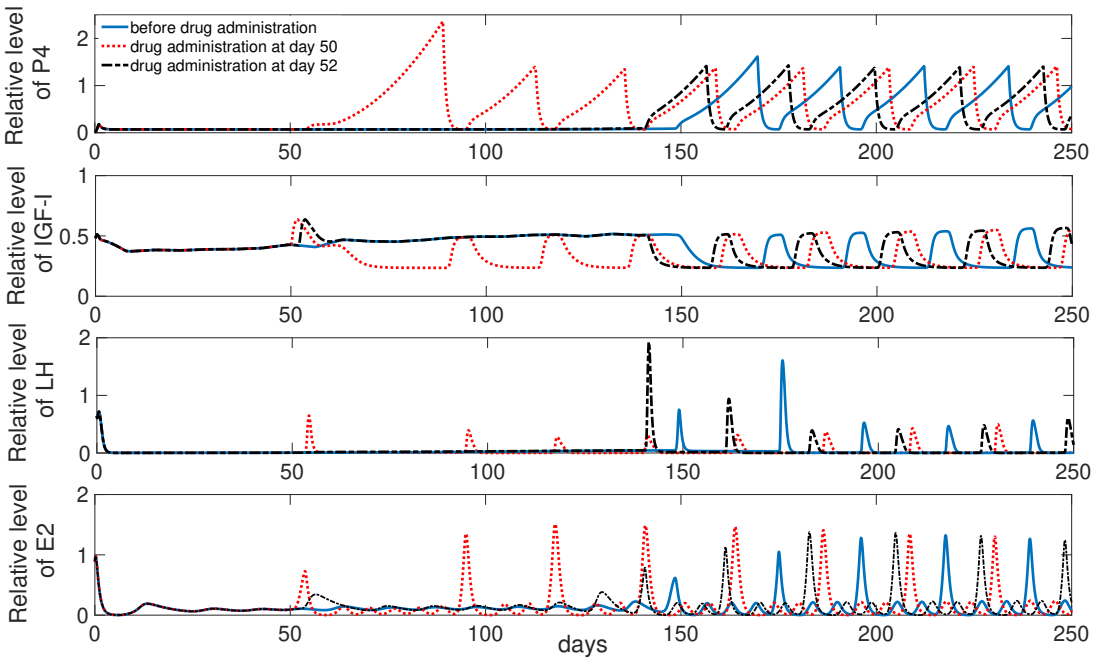

Figure 4.9: **Effects of a single dose of dexamethasone of 0.02 mg/kg on the estrous cycle in lactating cows.** This figure illustrates the dynamic behaviour of *P4*, *IGF*-1, *LH* and *E2* before and after dexamethasone administration. Simulation results before drug administration (blue-solid line) show that the postpartum anestrus interval last until day 150. Administrating a single dose of dexamethasone on day 50 (red-dotted line) induces the cyclicity of *E2*, *LH* and *IGF*-1, thereby reinducing estrous cyclicity with an elongated first cycle and normal cycles thereafter. In contrast, administrating a single dose of dexamethasone only two days later (black-dotted line) fails to reinduce cyclicity of hormones.

Chapter 5

Model Application - Optimal Bayesian Experimental Design

The mechanisms by which the MetRep model is formulated are based on biological assumptions from literature knowledge. These mechanisms are expressed via a large number of unknown parameters one needs to infer from experimental data. But, sometimes experimental data are qualitatively and quantitatively limited, i.e. the available data are not sufficient and do not provide much information about the system. As a result, the model is possibly prone to a certain level of inaccuracy in both parameters and predictions. In contrast, sufficient informative data can play a key role in optimizing and refining the model.

Our aim in this work is to make use of the MetRep model and Bayesian and information theory to systematically analyse and develop hypotheses to guide the design of experiments. This will allow us to define what and when to measure in order to obtain maximum information of the resulting data, and thereby reducing uncertainty in the model parameters and predictions. To this end, we first present an overview of experimental design within the Bayesian framework. Subsequently, we design experiments for non-lactating cows to reduce the uncertainty in the model parameters. Thereafter, we design experiments for lactating cows to reduce the uncertainty in predicting the ovulation time during the postpartum period.

5.1 Background

An experiment is a study or process that results in the collection of data. The results of experiments are not known in advance. Designing an experiment is the process of laying out a detailed experimental plan before performing the experiment. Experimental design is very essential in order to ensure that the right type of data and a sufficient sample size are available to support, refute, or validate a hypothesis as clearly and efficiently as possible. Experimental design has very broad applications across the natural, medical and social sciences, as well as engineer-

ing, business and finance. In recent years, the growing interest in systems biology prompted the emergence of many dynamic computational models, which are developed to test hypotheses about complex biological systems. However, a major challenge with such models is that most of them lack sufficient informative data that limit their predictive power and efficient statistical inference. Recent studies have demonstrated that generally less than half of the parameters are tightly confined by experimental data [82, 66]. This is because the collection of sufficient experimental data can sometimes be a difficult task to conduct, especially in situations where multiple experiments might be difficult, expensive or time-consuming to perform. To overcome this challenge, experimental design emerged as an important approach that can be performed before collecting the data. Hence, the performance of this approach is based on simulated data generated by the model at hand. The ultimate aim of experimental design is the selection of an optimal design from all practically applicable designs. Conducting the experiment based on the selected optimal design is expected to maximize the value of data. The resulting data can be used to better estimate model parameters and predictions. Thus, experimental design answers questions such as, what (i.e. which species) and when to measure, which variables to interrogate, and what experimental conditions to employ.

The design of an experiment involves specifying the purpose of the experiment and defining the variables that can be controlled by the experimenter for the study before the experiment starts. Here variables might include: choosing which species to study and how these species will be measured (e.g., amount, timing, frequency), specifying a length of time for the experiment to be performed [41]. When designing an experiment sometimes experimenters are confronted with some constraints such as a fixed total cost and time. These should be taken into account when choosing the appropriate values of the control variables, especially for situations in which experiments are costly and/or time consuming to conduct. Hence, experimental design can be viewed as an optimisation problem where the resulting optimal design may fulfil the experimental goals more rapidly and hence reduce experimental costs. Therefore, the design of an experiment requires the definition of the design space $\mathbb{D}$, which defines the set of all practically applicable designs, $\mathfrak{D}$, within the limit of available resources. For example, if experimenters are restricted to a limited budget, e.g. δ, then the design space $\mathbb{D}$ is given by

$$\mathbb{D} = \left\{ \mathfrak{D} \subseteq \prod_{i=1}^{n} U_i : \|\mathfrak{D}\| \leq \delta \right\}, \tag{5.1}$$

where $\{U_i\}_{1 \leq i \leq n}$ are the subdomains representing the constraints of the design.

Some common constraints that experimenters often encounter when planning an experiment for sampling species are time and cost budget. Usually, only a limited number of individuals (e.g., n individuals) can be measured. In addition, only a limited number of sampling times (e.g., s times) is allowed. Let us assume that the

experimental measurements consist of readouts,

$$z(t_i) = [z_1(t_i), \cdots, z_j(t_i), \cdots, z_n(t_i)] \in \mathbb{R}^n, \tag{5.2}$$

obtained through sampling species, which can be performed at arbitrary time points $t_1, \cdots, t_i, \cdots, t_s$. We denote the range of indices for time points as,

$$U_1 = \{1, \cdots, i, \cdots, s\},$$

and the range of indices for readout variables as,

$$U_2 = \{1, \cdots, j, \cdots, n\},$$

such that the index pair $(i, j) \in U_1 \times U_2$ refers to the individual measurement. Hence, individual measurements represented by the design $\mathfrak{D}$ can be grouped into datasets,

$$Z^{ind} = \{z_j(t_i) : (i, j) \in \mathfrak{D} \in \mathbb{D}\}. \tag{5.3}$$

Before conducting an experiment, experimenters usually have access to some pieces of information called prior knowledge, which are based on previous studies, domain knowledge or subjective beliefs. In this regards, the Bayesian approach offers an ideal tool to contribute to the design of experiment. It has found its application in experimental design because of the use of the available prior knowledge about a quantity of interest. For instance, the aim of experimental design is to precisely estimate model parameters. Here the prior knowledge about the unknown parameters in the model is combined with the likelihood. The later reflects the amount of information that the data carry about the unknown parameters to estimate the posterior distribution, from which inferences on further quantities of interest can be made. The newly estimated posterior distribution serves as new prior knowledge for the design of the subsequent experiment, see Fig 5.1.

Several works have been developed in both theory and practice to advance the field of experimental design within the Bayesian framework [4, 29, 40, 87, 94, 117, 118, 145, 180, 210]. Early theoretical development of Bayesian experimental design was suggested by Lindley [118], who noted that the design of an experiment should depend on the experimental objectives, e.g., precise estimation of certain parameters, prediction of future responses. In addition, Lindley melded concepts from Bayesian inference and information theory where he measured the initial uncertainty of parameters in terms of the Shannon entropy, which can be updated to the posterior uncertainty after new observations have been collected. Other contributions to Bayesian experimental design were made by Chaloner [40], who further developed Bayesian optimal design theory in a linear regression context and explicitly described how the prior makes a difference between the classical and Bayesian optimal designs. In other words, he noted that optimal Bayesian designs are close

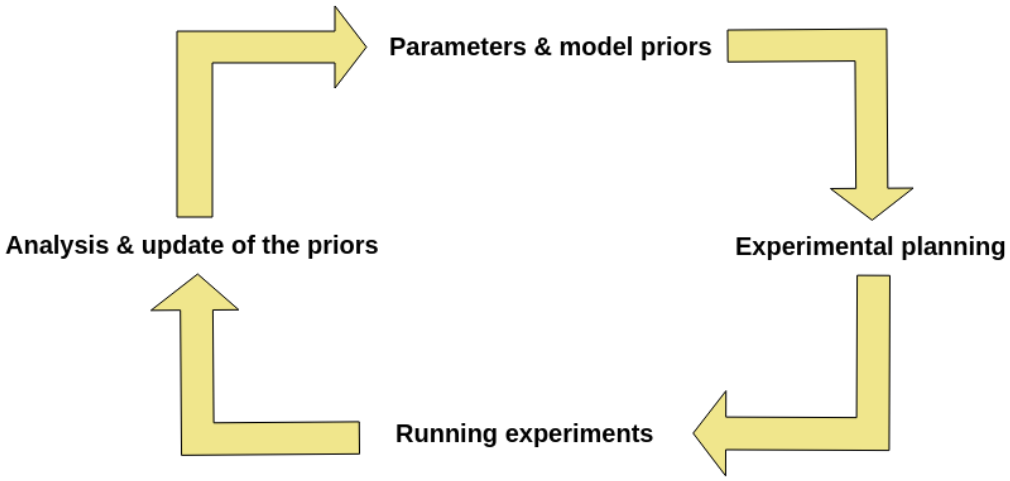

Figure 5.1: **The iterative process for improving the design of experiment.** First, an initial prior knowledge (e.g. about parameters) is used for experimental planning. After carrying out and analysing the output of the experiment, posterior probability is estimated. This serves as new prior knowledge for the design of the subsequent experiment.

to the classical ones when a noninformative prior distribution is used. The applications of Bayesian methodologies to optimal experimental design have been used in several works. For instance, Bussito et. al [29] introduced an efficient method to design informative experiments for selecting biological dynamical models. Vanlier et. al [210], developed a method based on the posterior predictive distribution to asses the predictive power of experiments for models that cope with large parameter uncertainty. Huan et. al [94] employed a Bayesian statistical setting to find optimal experiments via Monte Carlo approximation. Liepe et. al [117] used similar approach as in [94] but improved it in that it is global and not constrained to some local neighbourhood in parameter space and used to assess parameter inference and prediction of system behavior.

5.2 Reducing Uncertainty in Model Parameters

In this section, we formulate an experimental design that aims at reducing uncertainty in the model parameters. First, we formulate the design space, then we present and discuss the calculation results of the mutual information shared between the parameters and measurements. Here we make use of the MetRep model in non-lactating cows to generate the measurements. Finally, we use the experimental outcome to update the prior distribution of one selected parameter of the model.

5.2.1 Formulation of the Experimental Design

To increase our ability to reduce uncertainty in the model parameters, we need to select an optimal design from the design space. If we are concerned with the cost and time to obtain informative measurements, then the design space should take into account two aspects: time points and observed species. Specifically, the selected optimal design should inform us about *when to measure*, i.e. select the optimal sampling times, and *what to measure*, i.e. specify the observed species that provide more information about the model parameters.

For the optimization of the sampling times, we first define the design space with respect to the time period, e.g., from t_1 to t_s during which the experiment is performed. Here t_1 and t_s are the initial time and the final time of observation, respectively. The MetRep model simulates a periodic estrous cycle which averages 21 days in duration. For the sake of verification and confirmation, we perform the experiment over a period of 36 days. This period captures both the follicular and the luteal phase. Sampling can be performed at arbitrary time points, $t_1, \cdots, t_i, t_{i+1} \cdots t_s$. However, in our case we choose to take daily measurements during the period of the observation. This means that $t_{i+1} - t_i = 1$ day and the number of time points $s = 37$. In this case the range of indices for time points is $U_1 = \{1, \cdots, i, i+1, \cdots 37\}$.

The second part of the design space includes the observed species we want to include in our experimental setup. We note that the MetRep model simulates 22 components, some of which are not practically measurable. For this reason, we measure only species that are *practically measurable*. For example, amongst the 22 components of the model we assume that *FSH*, *PGF*, *P4*, *E2*, *INH*, *IGF*, insulin, glucose and glucagon are the only measurable species. Thus, the list of measurable species consists of 9 species, which are

$$\{FSH, PGF, P4, E2, INH, IGF, Ins, Glu_{blood}, Gluca\}. \tag{5.4}$$

In this case, the range of indices for measurements is $U_2 = \{1, \cdots, j, j+1, \cdots 9\}$. These species are time-dependent variables. More generally, the change of these species over time is represented by the initial value problem:

$$\frac{dy(t)}{dt} = f(y(t), \theta),\ y(0) = y_0, \tag{5.5}$$

where the values of species at a specific time point t_i is represented by

$$y(t_i) = [y_1(t_i) \cdots y_9(t_i)] \in \mathbb{R}^9, \tag{5.6}$$

and θ is a vector containing the parameters of the model and y_0 denotes the initial values of the species. If we assume that f is the true deterministic model simulating the species, then the measurements are represented by

$$z(t_i) = y(t_i) + \varepsilon_i,\ i \in U_1, \tag{5.7}$$

and the individual measurement is represented by

$$z_j(t_i) = y_j(t_i) + \varepsilon_{ij},\ (i,j) \in U_1 \times U_2, \tag{5.8}$$

where ε_i and ε_{ij} are uncorrelated random vectors of measurement errors that follow the Gaussian distribution of zero mean and the covariance $\Sigma_{\sigma_i} = \sigma_i^2 \cdot Id_9$ (i.e. $\varepsilon_i \sim \mathcal{N}(0, \Sigma_{\sigma_i})$), where Id_9 is the identity matrix and the variance σ_{ij}^2 (i.e. $\varepsilon_{ij} \sim \mathcal{N}(0, \sigma_{ij}^2)$), respectively. Hence, the measurements of all species can be grouped into datasets,

$$Z^{all} = \left\{ z(t_i) \in \mathbb{R}^9 : i \in U_1 \right\}, \tag{5.9}$$

and the individual measurements represented by the design $\mathfrak{D}$ can be grouped into datasets,

$$Z^{ind} = \left\{ z_j(t_i) \in \mathbb{R} : (i,j) \in \mathfrak{D} \in \mathbb{D} \right\}, \tag{5.10}$$

where $\mathfrak{D}$ is a vector of indices that specify the design point of time and species, and $\mathbb{D}$ is the space of admissible designs.

5.2.2 Results and Discussion

To draw information from all species about the optimal sampling time of measurements, we compute the mutual information, $I(\Theta; Z^{all})$, shared between the model parameters, Θ, and the measurements of all species, Z^{all}. For models of type (5.7), $z \in Z^{all}$ follows the Gaussian distribution of mean y and covariance Σ_σ, i.e. the model likelihood is provided such that $z|\theta \sim \mathcal{N}(y, \Sigma_\sigma)$. In this case, we estimate $I(\Theta; Z^{all})$ via eq.(1.50).

In order to simulate a set of measurements, $\{z^{(q)}\}_{1 \le q \le N_1}$, that are biologically meaningful, we first draw $N_1 + N_2 \in \mathbb{N}$ samples of the parameters $\{\theta^{(q)}\}_{1 \le q \le (N_1+N_2)}$ such that $N_1 < N_2$ from the uniform distribution centred at the nominal value θ_{ref} with 10% standard deviation. Simulating the model (5.5) with the parameters $\theta^{(q)}$ and the initial value $y(0) = y_0$ leads to the solution y. However, some of the solutions are not biologically meaningful. Thus, to filter out the set of parameters $\{\theta^{(q)}\}_{N_1+1 \le q \le N_2}$ that are not biologically meaningful, we apply the approach presented in Section 1.2.3. The accepted parameters are used for the approximation of the prior distribution $p(\theta)$. To graphically illustrate the result of this approach, we plot, as an example, the accepted and rejected solutions of *P4*, see Fig 5.2.

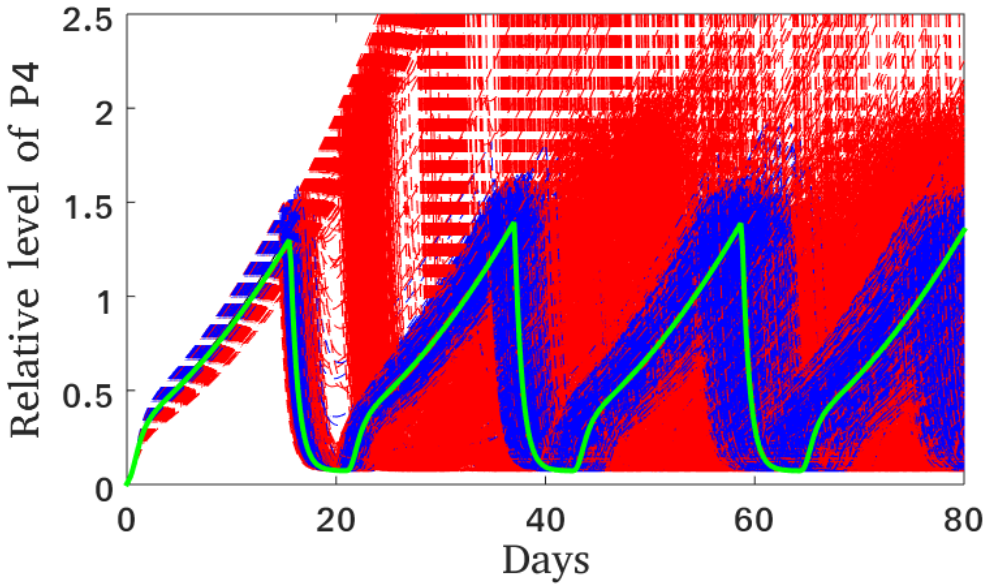

Figure 5.2: **Graphical illustration of the accepted and rejected concentrations of *P4* in non-lactating cows.** This figure compares the dynamic of *P4* concentrations that are biologically meaningful (blue) with concentrations that are not biologically meaningful (red). It can be seen that *P4* concentrations in blue color are slightly deviated from the standard dynamic of *P4* concentration in green color, while *P4* concentrations in red color diverge. These simulation outputs are generated using the approach discussed in Section 1.2.3.

Simulating the model (5.5) using the accepted parameters $\{\theta^{(q)}\}_{1\leq q\leq N_1}$ (as samples from $p(\theta)$), and choosing 10% as the standard deviation, we generate a set of artificial measurements $\{z^{(q)}\}_{1\leq q\leq N_1}$ using eq.(5.7). Thus, this set of measurements can be used to approximate the mutual information $I(\Theta; Z^{all})$ in eq.(1.50).

The calculation result of $I(\Theta; Z^{all})$ is presented in Fig 5.3. The figure shows the daily score of the mutual information shared between the model parameters and the measurements collected for all species. In addition, Fig 5.4 shows the daily score of the information gained $I_{\Theta,z}$, see eq.(1.41), by collecting data z. For the calculation of $I_{\Theta,z}$, we used two random data sets, $z^{(1)} \in Z^{all}$ and $z^{(2)} \in Z^{all}$ to compare the result. Interestingly, we can clearly see that the values of $I_{\Theta,z}$ are higher or less than the values of mutual information, $I(\Theta; Z^{all})$. This variation is ascribed to the fact that the mutual information measures the amount of information contained *on average* over all the possible behaviours of the system, whereas the information gain, $I_{\Theta,z}$, represents the amount of information gain about Θ provided by a single observed data, e.g., $z^{(1)}$ or $z^{(2)}$. Moreover, we can clearly see from the daily scores of the mutual information, Fig 5.3, that the measurements carry more information about the model parameters during the follicular phase than the luteal one. In par-

ticular, the highest and lowest mutual information is recorded on the day 83 (red bar) and 68 (black bar), respectively. This means that collecting data on the day 83 can be expected to significantly decrease the uncertainty in the model parameters compared to data collected on the day 68.

After having determined the optimal time for sampling the measurements, it is beneficial to investigate which species carries high information about the model parameters. In practice, this gives more information to experimenters on how to deal with some restrictions such as a limited budget. For this purpose, we compute the mutual information, $I(\Theta; Z^{ind})$, shared between the model parameters, Θ, and the measurements collected for every species, Z^{ind}. This mutual information is calculated on the day 83 on which the sampling time is optimal. Fig 5.5 (A) shows the scores of the mutual information every species carries about the model parameters. It can be seen that *PGF* and *E2* carry more information about the model parameters than the other species. In addition, species such as *FSH* and *INH* have less information than *PGF* and *E2* but higher than *IGF*-1 and *P4*. Moreover, *Ins, Gluca* and *Glu* contain low information about the model parameters. Fig 5.5 (B) shows the scores of the mutual information every species carries about the model parameters on the day 68. Comparing with the day 83, the information content of species such as *FSH*, *PGF*, *P4*, *E2* and *IGF*-1 is reduced. In particular, this time *PGF* does not provide much information about the model parameters. In contrast, the information content of *INH* remains nearly unchanged. This is also the case for *Ins*, *Gluca* and *Glu* but with low information content.

We expect that species carrying high information can reduce the uncertainty of the parameters more than the ones carrying less information. To illustrate how the information content of species can reduce the uncertainty of the model parameters, we compute the posterior distribution $p(\theta|z)$ for one selected parameter of the model according to eqs.(1.32), (1.33), and (1.34). For the computation, we use the family of samples $\left(\theta^{(q)}, z^{(q)}\right)_{1\leq q\leq N_1}$ comprising the accepted set of parameters and its corresponding set of measurements. In particular, the joint density $p(\theta, z)$ is estimated by choosing the Gaussian kernel, $G\left[(\theta, z), \Sigma\right]$, where $\Sigma = diag(b_\theta^2, b_{z_1}^2, \cdots, b_{z_9}^2)$ is the diagonal bandwidth matrix such that b_θ, $b_{z_1}, \cdots b_{z_9}$ are the bandwidth smoothing parameters. However, in order to avoid the smoothing effect of the *KDE*, we take the Gaussian kernel at (θ, y), i.e. $G\left[(\theta, y), \Sigma_{\theta,\sigma}\right]$ (since $z \sim \mathcal{N}(y, \Sigma_\sigma)$, see eq.(5.7)) for better smoothing, where $\Sigma_{\theta,\sigma} = diag(b_\theta^2, \sigma_1^2, \cdots, \sigma_9^2)$ is the diagonal bandwidth matrix such that $\{\sigma_j\}_{1\leq j\leq 9}$ are the standard deviations of measurements. The choice of the smoothing parameter b_θ is provided by MATLAB's commmand *ksdensity*, which returns the bandwidth of the kernel smoothing window that is the optimal for normal densities.

For the illustration purpose, all visualizations of the prior and posteriors and their uncertainties were done for just one parameter, e.g. the growth rate *E2*, but the

calculation of the mutual information was performed for all parameters. Fig 5.6 depicts the prior distribution (blue line) of the parameter and the corresponding posterior distributions computed using random data collected on the day 68 and day 83. When we update the prior distribution using data containing all species collected on the day 68 (red curve), we observe a negligible decrease in the parameter uncertainty. In contrast, updating the prior distribution using data collected on the day 83 shows a gradual decrease in the parameter uncertainty. Specifically, the more we update the prior distribution using additional species, the more the uncertainty decreases. This gives an idea to what extent experimenters could control the uncertainty of the parameter in line with a limited budget. It is important to mention that the output of an experiment is random, i.e. two collected data, $z^{(1)}$ and $z^{(2)}$ may contain different information content (e.g. see Fig 5.4). To illustrate how the decrease in parameter uncertainty changes according to the amount of information content of data, we update the prior distribution using three different sets of data, see Appendix, Fig 10.

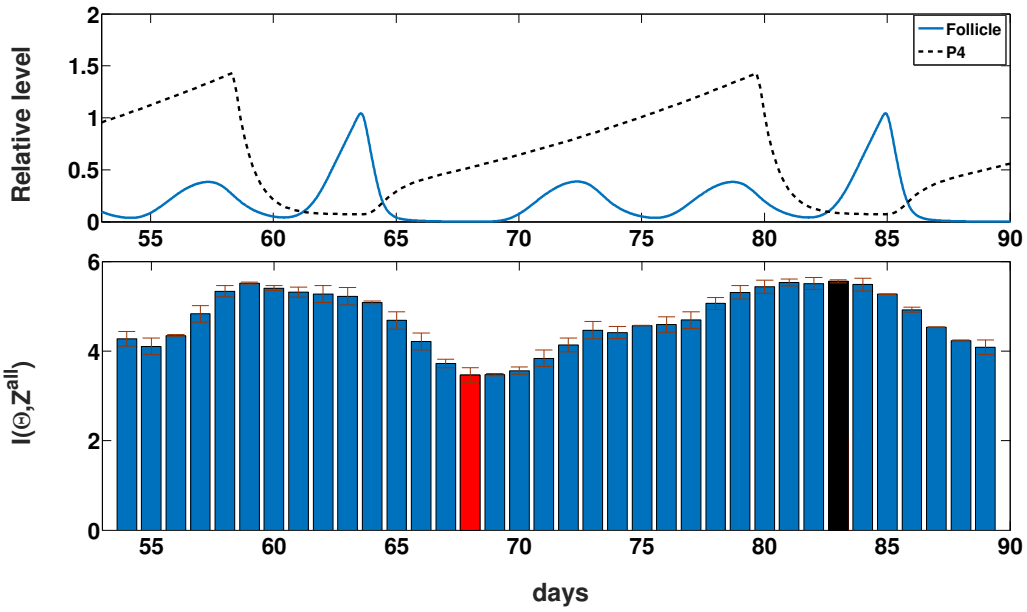

Figure 5.3: **Experiment choice for parameter inference in the MetRep model.** Top: the subfigure illustrates the dynamic of the Follicle and *P4* during one cycle period. Bottom: the subfigure depicts the mutual information, $I(\Theta; Z^{all})$, shared between the model parameters, Θ, and the measurements collected for all species, Z^{all}. High and low mutual information are scored on the day 83 (black barplot) and 68 (red barplot), respectively. The error bars on the mutual information barplots show the variance of the mutual information estimations over 3 independent simulations. It can be observed that the highest mutual information is scored during the follicular phase, while the lowest mutual information is scored at the beginning of the luteal phase.

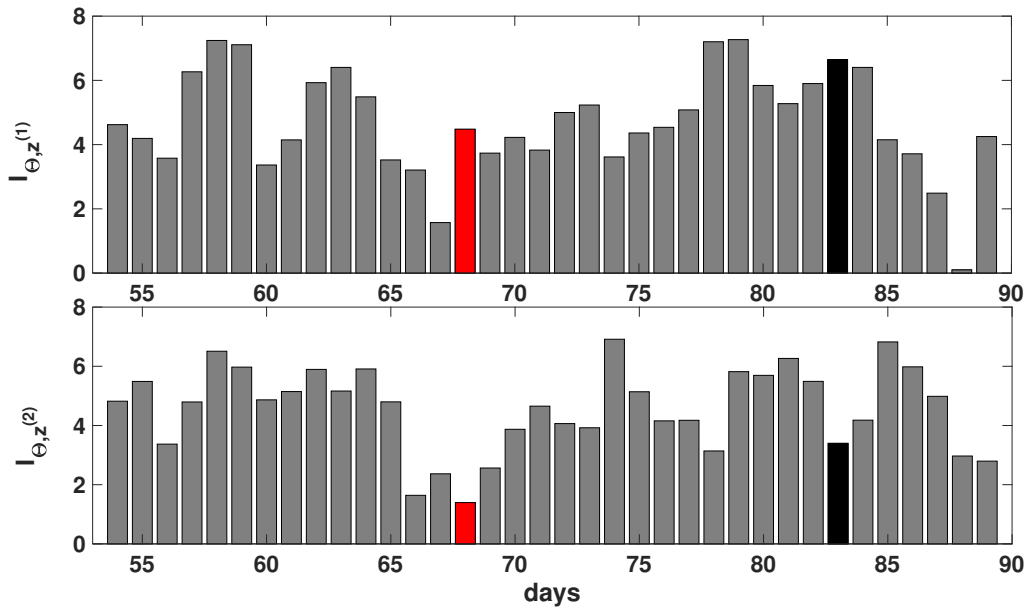

Figure 5.4: **Computed information gain.** This figure compares two computed information gain, $I_{\Theta,z^{(1)}}$ and $I_{\Theta,z^{(2)}}$. We observe that for different realizations $z^{(1)}$ and $z^{(2)}$ of Z^{all} the information gain $I_{\Theta,z^{(j)}}$ for $j \in \{1,2\}$ can be higher or lower than $I(\Theta; Z^{all})$ (e.g. on days 68 and 83), which is the expected information gain, i.e. averaged over all possible outcomes of Z^{all}.

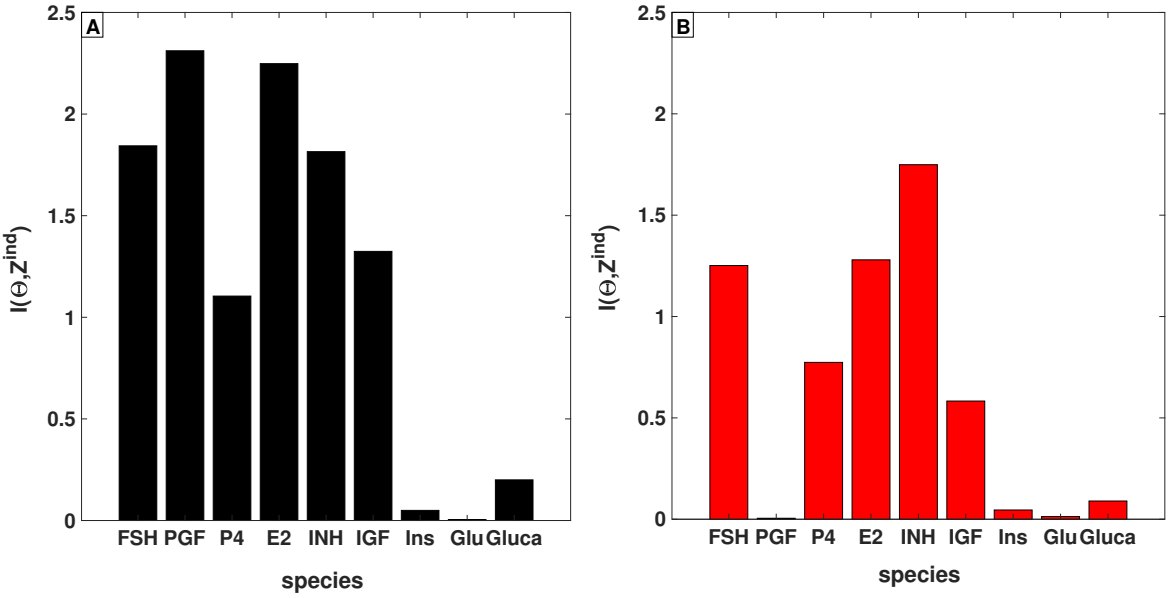

Figure 5.5: **The mutual information between the model parameters and the measurements of the individual species.** The figure compares the individual information content on the day 83 (A) and 68 (B). From both subfigures, we can observe that *Ins*, *Glu* and *Gluca* do not provide much information about the model parameters. This is also the case for *PGF* on the day 68.

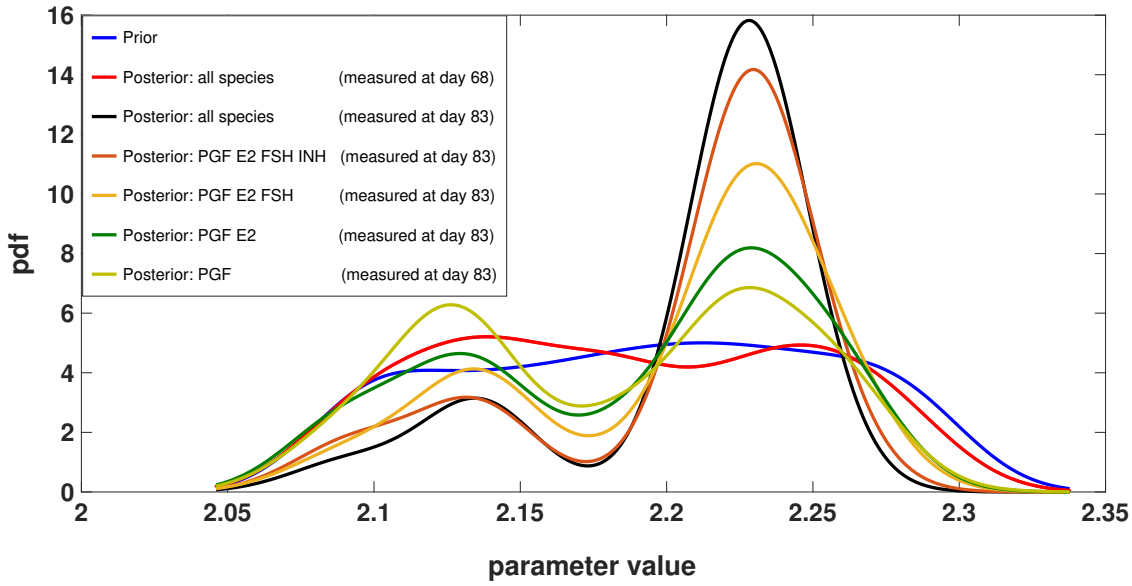

Figure 5.6: **The prior and posterior distributions of the parameter.** This figure shows the prior distribution of the growth rate of *E2* (in blue) and the estimated posterior distributions. The posterior distributions in red and black are estimated based on data containing all species collected, respectively, on the day 68 and 83. The other posterior distributions are estimated based on data containing some selected species collected on the day 83. It can be seen that the more we update the prior distribution using additional species, the more we observe a decrease in the uncertainty. This is also the case for Fig 10.

5.3 Reducing Uncertainty in Model Prediction

In the third chapter of this thesis, we discussed the effect of NEB on the reproductive performance of dairy cows. In particular, we showed that minimising the interval of NEB after calving induces the re-initiation of ovarian cyclicity in a short period. In addition, early studies reported that a shorter postpartum anestrus interval to first ovulation is positively associated with conception rate later during the breeding period [30]. Moreover, minimizing the interval to first ovulation provides more time for completion of multiple ovarian cycles prior to insemination, which in turn improves the conception rate [32]. In addition, we also presented a nutritional strategy to mitigate the effects and the extension of NEB. In particular, we showed that a higher glucose content in the diet results in an improved energy balance during the postpartum period.

The focus of the experimental design in the section is somewhat different to the one in the previous section, since our aim is no longer to reduce the uncertainty of model parameters but of the model prediction. In this case, the time of first ovulation T_{ov} during lactation period. Consequently, we will no longer attempt to maximize the mutual information $I(\Theta; Z^{all})$, which represents the experimental information gain on the parameter from the measurements, but the mutual information $I(T_{ov}; Z^{all})$, which measures the experimental information gain on the ovulation time T_{ov} from the measurements.

In the following, we make use of the MetRep model to design an experiment that provides a criterion for predicting the time of first ovulation during lactation period. In this regards, we simulate the model for lactating cows with a fraction of glucose content in the DMI, $c_0 = 25\%$, to generate the measurements. In this case, the model predicts the first ovulation on day 45 postpartum, (see Fig 3.10). To start, we first formulate the design space, we then present and discuss the results of the experimental outcome.

5.3.1 Formulation of the Experimental Design

In this section, the formulation of the design space includes the same components as that of the previous section, i.e. time points of sampling and species to be measured. As in the previous section, we also assume that only 9 species are measurable which are *FSH*, *PGF*, *P4*, *E2*, *INH*, *IGF*, insulin, glucose and glucagon. Thus, the range of indices for measurements is $U_2 = \{1, \cdots, j, j+1, \cdots 9\}$. But in this section, we consider a slight change in the sampling times of measurements. First, we perform the experiment from the second week postpartum, i.e. the day $t_1 = 7$ until the day $t_n = 68$. This interval includes the time of first ovulation (i.e. day 45) which is predicted by the model. In addition, we perform the sampling of measurements on a weekly basis during the period of the observation. In this case, the total points of sampling time is 8, which is represented by $U_1 = \{1, \cdots, i, i+1, \cdots 8\}$.

Analogously to the previous section, the measurements of all species can be grouped into datasets,

$$Z^{all} = \left\{ z(t_i) \in \mathbb{R}^9 : i \in U_1 \right\}, \tag{5.11}$$

and the individual measurements represented by the design $\mathfrak{D}$ can be grouped into datasets,

$$Z^{ind} = \left\{ z_j(t_i) \in \mathbb{R} : (i,j) \in \mathfrak{D} \in \mathbb{D} \right\}, \tag{5.12}$$

where $\mathfrak{D}$ is a vector of indices that specify the design point of time and species, $\mathbb{D}$ is the space of admissible designs.

5.3.2 Results and Discussion

Now that we have formulated the design space, we turn to the computation of the mutual information, $I(T_{ov}; Z^{all})$, shared between the random variable T_{ov} describing the time of first ovulation and the measurements of all species Z^{all}. In this case, it is not evident how to provide the likelihood function, $p(z|t_{ov})$. Thus, the estimation of the mutual information, $I(T_{ov}; Z^{all})$, can only be achieved following eq.(1.51). In this regards, we need to generate a family of samples $(t_{ov}^{(k)}, z^{(k)})_{1 \le k \le N}$ representing the time of first ovulation and the measurements. To do so, we consider the model:

$$\begin{aligned} \varphi : \Theta \times \mathbb{R}^+ &\longrightarrow \mathbb{R}^+ \times \mathbb{R}^+ \\ (\theta, y_0) &\longmapsto (t_{ov}, y), \end{aligned}$$

where θ is the model parameters, y_0 is the initial condition of the model, y is the simulated species via the model (5.5), and t_{ov} is the simulated time of the first ovulation. The time t_{ov} is chosen as the earliest time point at which the (relative) *P4*-level is larger than a threshold $T_{P4} = 1$,

$$t_{ov} := \min_{t \ge 0} (P4(t) \ge T_{P4}).$$

We follow the same procedure as in the previous section, see 5.2.2, where we first filter out the species' concentrations, y, that are not biologically meaningful and their corresponding time of ovulation, t_{ov}. Fig 5.7 shows the accepted and rejected solutions of *P4* concentration. By considering 10% as the standard deviation, the accepted simulated species, y, are utilized to generate measurements, $z \in Z^{all}$, according to eq.(5.8). Thus, repeating the same procedure for a large number of times, e.g., N times, we can generate the family of samples, $(t_{ov}^{(k)}, z^{(k)})_{1 \le k \le N}$.

It should be noted that for the purpose of predicting the time of first ovulation, we are interested only in the ovulation times $\{t_{ov}^{(k)}\}_{1 \le k \le N}$ occurring after collecting the measurements during the postpartum period. This constraint should be embedded

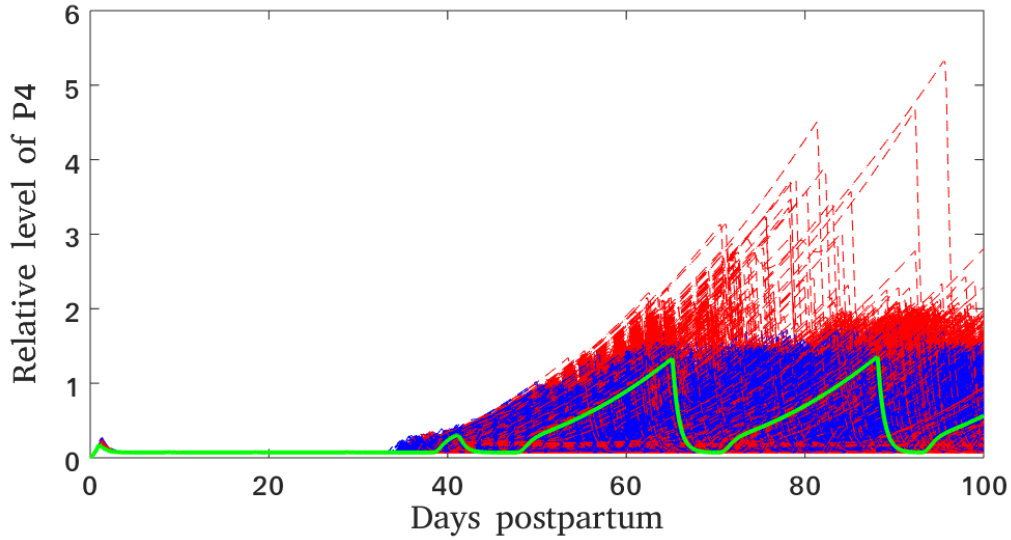

Figure 5.7: **Graphical illustration of the accepted and rejected concentrations of *P4* during postpartum for lactating cows.** This figure compares the dynamic of *P4* concentrations that are biologically meaningful (blue) with concentrations that are not biologically meaningful (red). It can be seen the cyclicity of *P4* concentrations in blue color are are similar to the standard dynamic of *P4* concentration in green color, while *P4* concentrations in red color strongly diverge. These simulation outputs are generated using the approach discussed in Section 1.2.3.

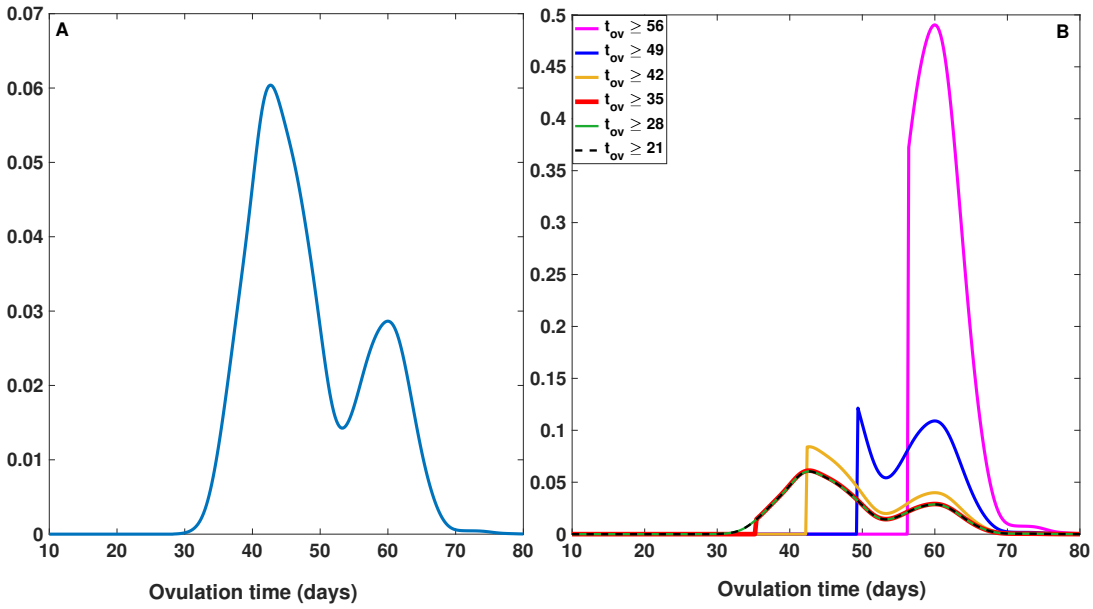

Figure 5.8: **Graphical illustration of the approximated prior distribution via the *KDE* approach.** The subfigure (A) presents the approximated prior distribution, $\hat{p}(t_{ov})$, based on the set $\{t_{ov}^{(k)}\}_{1\leq k\leq N}$ of the ovulation times occurring between the day 0 to 80. This approximation is performed using the Gaussian kernel function. The subfigure (B), shows the approximated prior distributions based on the set $\{t_{ov}^{(k)}\}_{1\leq k\leq N}$ such that $t_{ov} \geq t_i$, where $t_i \in \{7, 21, 28, 35, 42, 49, 56\}$. It can be seen that the density of the time of ovulation when measuring at t_j is more informative than when measuring at t_i, where $t_i < t_j$.

into the density $p(t_{ov})$ when computing the mutual information. In other words, the density $p(t_{ov})$ used for the computation of mutual information should be formulated as follows,

$$p(t_{ov}) = \begin{cases} 0 & \text{if } t_{ov} < t_i, \\ \hat{p}(t_{ov}) & \text{if } t_{ov} \geq t_i, \end{cases}$$

where t_i is the day of collecting measurements and $\hat{p}(t_{ov})$ is the approximated distribution of $p(t_{ov})$ using the *KDE* approach based on samples $\{t_{ov}^{(k)}\}_{1\leq k\leq N}$ such that $t_i \leq t_{ov}^{(k)}$. Fig 5.8 shows the result of the approximation of $p(t_{ov})$ using the Gaussian kernel. It can be seen that the prior density of the time of ovulation when measuring at t_j is more informative than when measuring at t_i, for $t_i < t_j$, which is meaningful since we gathered information about the ovulation time by simply waiting longer, the ovulation time did not occur in the interval $[t_i, t_j]$.

Fig 5.9 (A) depicts the weekly score of mutual information shared between T_{ov} and Z^{all}. The result shows that the highest mutual information value is recorded on the day 49, whereas the lowest score is on the day 7. In addition, Fig 5.9 (B) shows the calculation of mutual information shared between T_{ov} and the individual species represented by Z^{ind} on the day 49 (for the day 7 see Appendix, Fig 11). This result indicates that *P4* carries high information about the time of first ovulation comparing to the other species. This result supports previous studies [26, 34, 30, 70], which suggest the potential value of monitoring *P4* levels in postpartum dairy cows as an aid to the assessment of reproductive activity. During the first weeks of postpartum period, the dynamical change in *P4* profile can indicate the time at which the estrous cycle resumes. In other words, the anestrus postpartum period is characterized by a low level of *P4* concentration. As the metabolic status improves, the *P4* concentration relatively increases until reaching the normal profile. This profile is characterized by *P4* levels greater than 5 ng/ml during the luteal phase that lasts for 10-14 days, [26, 34]. It can be also seen from Fig 5.9 (B) that species such *IGF*-1, *INH*, *E2* and *FSH* carry almost equal information (but less than *P4*) about the first time of ovulation. In contrast, the other species such as *PGF*, *Ins*, *Glu* and *Gluca* provide less information about the time of first ovulation.

We learned from Fig 5.9 (A) that sampling species on the day 49 can be expected to provide high information for predicting the time of first ovulation. To illustrate how the information content of species can reduce the uncertainty of prediction, we estimate the posterior distributions, $p(t_{ov}|z)$, based on data z collected on the day 49. The posterior distributions are estimated similarly as in the previous section by choosing the Gaussian kernel. Fig 5.10 shows the prior distribution (in blue) of the possible ovulation times after collecting data z on the day 49 (grey line), i.e. $t_{ov} \geq 49$. The model prediction of the ovulation time is indicated by the brown line. In addition, the figure shows the estimated posterior distributions based on data z containing one or more species. For instance, when updating the prior distribution using data z containing only the information content of *P4*, the uncertainty of prediction is reduced (red dotted curve). Naturally, the more we include additional information from other species into the data z, the more the uncertainty is reduced. In other words, the posterior distribution based on data containing high information of *P4*, *IGF*-1, *INH*, *E2*, *FSH* indicates that it is highly probable that the ovulation occurs around the day 56-57. This is also what the model predicts (brown line). On the other hand, we observe no significant decrease in the uncertainty when adding low information from species such as *PGF*, *Ins*, *Glu*, *Gluca*. To explore how the magnitude of uncertainty can be reduced by other random data, we update the prior distribution based on two random data collected on the day 49, see Appendix, Fig 12. From this figure, the information content embedded into the two data resulted in different predictions and magnitude of uncertainties.

Comparing to the day 49, the mutual information is low on the day 7, see Fig 5.9

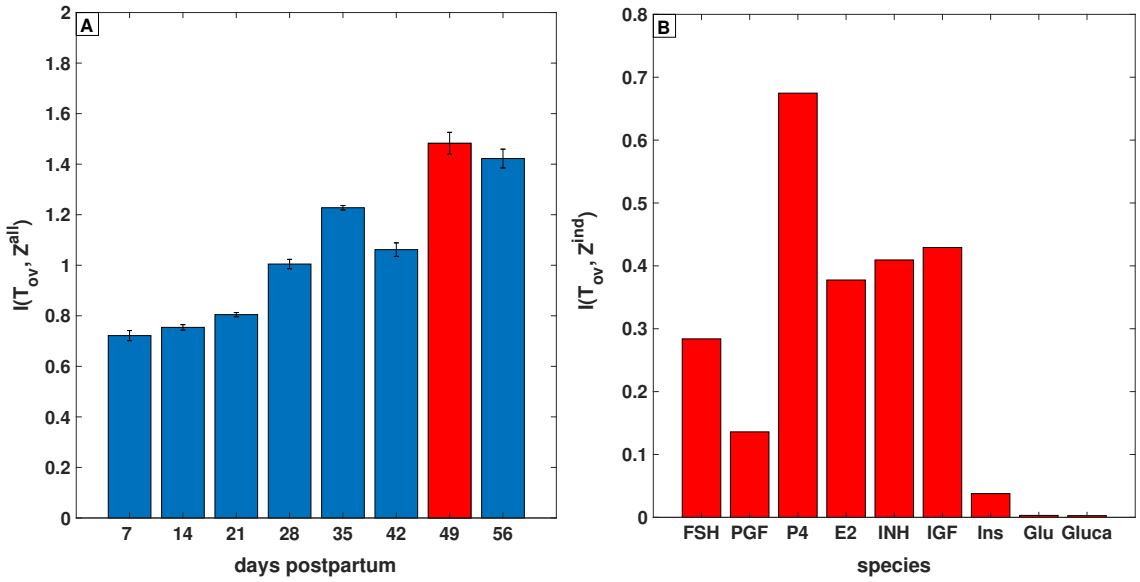

Figure 5.9: **The mutual information shared between the time of ovulation and the species.** The subfigure (A) presents the weekly mutual information shared between the time of ovulation and all species. High and low mutual information are scored on the day 49 (red barplot) and 7, respectively. The error bars on the mutual information barplots show the variance of the mutual information estimations over 3 independent simulations. The subfigure (B) presents the mutual information shared between the time of ovulation and each species. The information content of *P4* suggests that high information about the time of ovulation can be provided by measuring *P4*.

(A). This means that collecting species on this day will unlikely reduce the uncertainty. To verify this, we estimate the posterior distribution based on data collected on the day 7. Fig 13 (a) and (b) show the prior distribution (in blue) of the possible ovulation times after collecting data on the day 7 (grey line), i.e. $t_{ov} \geq 7$. The model prediction of the ovulation time is indicated by the brown line. Moreover, the figure shows the estimated posterior distributions based on data containing one or more species. Clearly, it can be seen that the resulting posterior distributions show a little decrease in the uncertainty.

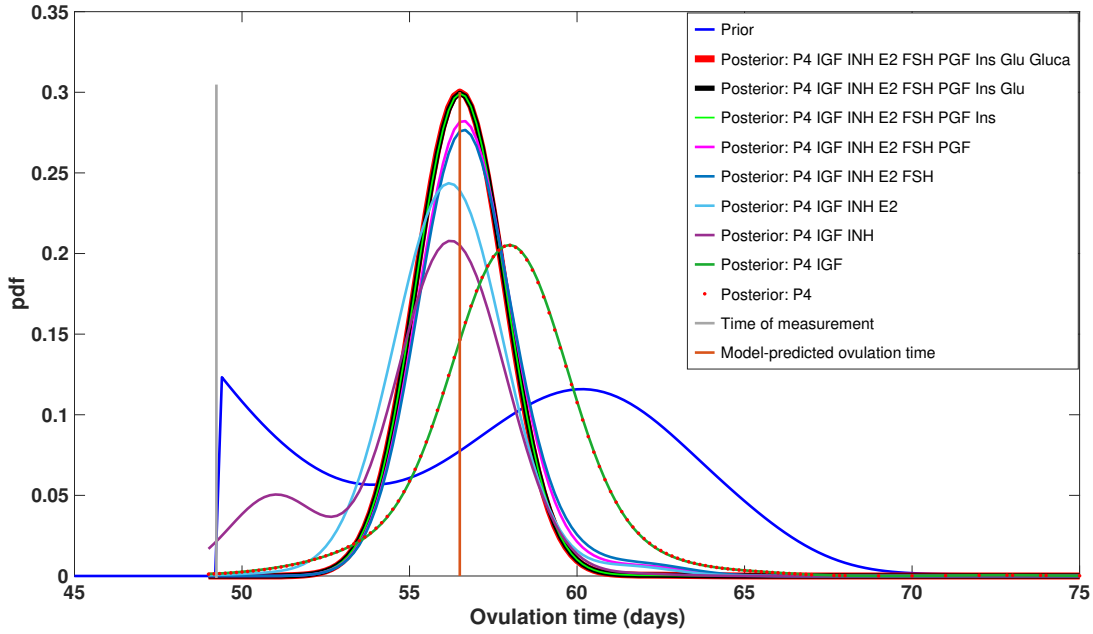

Figure 5.10: **The prior and posterior distributions of the time of first ovulation.** This figure shows the prior distribution (in blue) of the possible ovulation times occurring after the day 49. The time of measurement and the model prediction of the ovulation time are represented by the grey and brown lines, respectively. The estimated posterior distributions are based on data containing one or more species. Updating the prior distribution using data containing only *P4* results in decreased uncertainty (red dotted curve). It can be seen that the more we include additional information from other species into the data, the more the uncertainty is reduced. In addition, we observe no significant decrease in the uncertainty when including low information from species such as *PGF*, *Ins*, *Glu*, *Gluca*.

Conclusion

To understand the interaction between nutrition, metabolism and reproduction, a unified approach was followed, similar to [137, 138], where these fields of interest are integrated into one mathematical framework. Following this approach, a mathematical model of bovine metabolism and reproduction has been developed based on previously published and validated ODE models [195, 14]. Literature information about mechanistic interactions of fertility and metabolism is contradictory and redundant. Therefore, we decided to include as few mechanisms as possible to realize the coupling of the two models.

The developed model simulates the interplay of follicular development and its hormonal regulation with the glucose-insulin system. By conducting numerical simulations relying on it, it was confirmed that an appropriate nutritional intake is fundamental in mitigating the effects and the extension of NEB in order to reduce the incidence of metabolic disorders in high producing cows and to avoid subsequent fertility problems.

The present model enables the user to explore the relationship between nutrition and reproduction by performing related parameter studies. The local sensitivity analysis with respect to the onset of luteal activity after calving is just one example for such an analysis, which can easily be extended to other quantities of interest.

To explore the effect of drug therapy on glucose metabolism in dairy cows, the model has been linked to a pharmacokinetic model. Based on mechanisms underlying homeostasis regulation by dexamethasone, the model successfully captures the effect of one single dose of dexamethasone on the physiological behaviour of the system. Although this model has been formulated to deal with only one single dose of dexamethasone, this model can be further improved for the simulation of multidoses of dexamethasone.

Assuming that the current model simulates the "true" dynamical behaviour of the system, the model enables the user to select the optimal design of experiments. In this thesis, we focused on designing experiments that lead us to reduce the uncertainty in the model parameters for non-lactating cows and the uncertainty in predicting the first ovulation time during postpartum for lactating cows.

So far, it is fair to say that the model presented here is only a starting point. In other words, it can be considered as an early attempt towards developing in silico feeding and therapeutic strategies for diseases related to the metabolic system. It will certainly be modified and improved in the future for further application. For example, the current version of the model can be improved to become a risk assessment tool for the quantification of the flow rate of contaminant from the DMI to milk. Ultimately, improving the current version of the model in the future will promote the principle of the 3Rs (Replacement, Reduction and Refinement of animal testing). This principle allows to address important scientific questions without the use of animal experiments.

Appendix

Table 1: **Species in the metabolic model.** The initial values are used to solve the differential equations.

Name	Description	Initial value	Unit
Glu_{blood}	Glucose concentration in the blood	0.48	g/L
Glu_{liver}	Glucose generated in the liver	110	g
Glu_{store}	Glucose stored as glycogen	535	g
Fat	Body fat	150	kg
Ins	Insulin concentration in the blood	15.5	mU/L
$Gluca$	Glucagon concentration in the blood	105	ng/L

Table 2: **Physiological ranges of blood plasma glucose, insulin and glucagon levels.**

Species	Range	Reference
Glu_{blood}	0.39–0.59 g/L (2.22–3.30 mmol/L)	[2]
Ins	2–50 mU/L	[223, 222]
$Gluca$	50–120 ng/L	[223, 222]

Table 3: **Rates in the metabolic model.**

Name	Description	Unit
$glu_{feed-bl}$	Glucose in the DMI available for direct absorption	g/d
$glu_{feed-gng}$	Glucose generated from glucogenic substances in the DMI	g/d
glu_{bl-lv}	Glucose absorbed from the blood into liver cells	g/d
glu_{st-lv}	Glucose generated from glycogen (glycogenolysis)	g/d
glu_{lv-st}	Glucose stored as glycogen (glycogenesis)	g/d
glu_{lv-fat}	Glucose converted to triglycerides (lipogenesis)	g/d
glu_{fat-lv}	Glucose synthesized from glycerol	g/d
glu_{prod}	Glucose released from the liver to the blood	g/d
$glu_{bl-usage}$	Glucose usage for maintenance and milk production	g/d
$glu_{lv-usage}$	Glucose usage for liver metabolism	g/d
ins_{sec}	Insulin secretion	mU/(L·d)
ins_{deg}	Insulin degradation	mU/(L·d)
$gluca_{sec}$	Glucagon secretion	ng/(L·d)
$gluca_{deg}$	Glucagon degradation	ng/(L·d)

Table 4: Values of rate and effect parameters.

Symbol	Value	Unit	Explanation
c_0	0.08	–	Relative glucose content in the DMI
c_1	0.08	–	Fraction of directly absorbable glucose
c_2	84211	mU/(L·d)	Rate constant for insulin secretion
c_3	2105	1/d	Rate constant for insulin degradation
c_4	70182	ng/(L·d)	Rate constant for glucagon secretion
c_5	350.87	1/d	Rate constant for glucagon degradation
c_6	50	(g·L)/(mU·d)	Rate constant for glucose absorption from blood into liver cells
c_7	180	L/(mU·d)	Rate constant for glycogenesis
c_8	0.22683	L/(mU·d)	Rate constant for lipogenesis
c_9	1350	(g·L)/(ng·d)	Rate constant for glycogenolysis
c_{10}	3.5272	(g·L)/(ng·d)	Rate constant for gluconeogenesis
c_{11}	0.0684	L/(ng·d)	Rate constant for glucose release from the liver to the blood
c_{12}	1000	g/d	Glucose usage for maintenance
c_{13}	72	g/kg	Glucose usage for milk production
c_{14}	5	1/d	Glucose usage for liver metabolism
c_{17}	0.4	[IGF]/d	Basal IGF-1 synthesis rate in the blood
c_{18}	1	[IGF]/d	P4- and insulin-regulated IGF-1 synthesis rate
c_{19}	1.7	1/d	IGF-1 clearance rate
c_{20}	3.49	1/d	Maximum effect of LH on follicular function
c_{21}	1	[LH]	Maximum threshold of LH to stimulate follicular function
c_{22}	3	–	Maximum effect of insulin on FSH synthesis in the pituitary
c_{23}	1.05	–	Maximum effect of insulin on LH synthesis in the pituitary
c_{24}	1.5	[Oxy]/d	Maximum rate of additional oxytocin synthesis during lactation
c_{25}	0.0007	$1/d^2$	Clearance of additional oxytocin during lactation
V	22.8	L	Extracellular volume of blood

Table 5: Values of threshold parameters

Symbol	Value	Unit	Explanation
T_1	0.5	g/L	Threshold of glucose in the blood to stimulate insulin secretion
T_2	0.5	g/L	Threshold of glucose in the blood to inhibit glucagon secretion
T_3	0.45	g/L	Threshold of glucose in the blood to stimulate the absorption of glucose into liver cells
T_4	10	L	Threshold of milk to inhibit glycogenesis
T_5	10	L	Threshold of milk to inhibit lipogenesis
T_6	1000	g	Threshold of glygogen store to stimulate lipogenesis
T_7	10	g	Threshold of glycogen store to stimulate glycogenolysis
T_8	10	g	Threshold of glycogen store to stimulate gluconeogenesis
T_9	150	kg	Threshold of fat to stimulate gluconeogenesis
T_{10}	0.5	g/L	Threshold of glucose in the blood to stimulate non-mammary utilization
T_{11}	0.3	[P4]	Threshold of P4 to inhibit IGF-1 synthesis
T_{12}	15	mU/L	Threshold of insulin to stimulate IGF-1 synthesis
T_{14}	0.5	[IGF]	Threshold of IGF-1 to stimulate the responsiveness of follicles to LH
T_{15}	15	mU/L	Threshold of insulin to stimulate FSH synthesis
T_{16}	16	mU/L	Threshold of insulin to stimulate LH synthesis

Table 6: Initial values for species in the BovCycle model.

No	Component	Initial value	Unit
1	GnRH in the hypothalamus	0.667	[GnRH]
2	GnRH in the pituitary	0.551	[GnRH]
3	FSH in the pituitary	0.316	[FSH]
4	FSH in the blood	0.395	[FSH]
5	LH in the pituitary	1	[LH]
6	LH in the blood	0.642	[LH]
7	Follicle	1	[Follicle]
8	$PGF2_\alpha$	0.00506	[$PGF2_\alpha$]
9	Corpus luteum	0	[CL]
10	Progesterone	0.004	[P4]
11	Estradiol	0.89	[E2]
12	Inhibin	0.826	[Inhibin]
13	Enzyme	0	[Enzyme]
14	Oxytocin (non-lactating case)	0.0183	[Oxy]
–	Oxytocin (lactating case)	2.5	[Oxy]
15	Insulin-like growth factor 1 (IGF-1)	0.48	[IGF]
16	Intra ovarian factor (IOF)	0.35	[IOF]

Table 7: Values of parameters that have been changed compared to [195].

Symbol	Value in [195]	New value	Unit	Explanation
c_{LH}	12	2	1/d	LH clearance rate constant
c_{P4}	0	0.1	[P4]/d	P4 baseline concentration in the blood
ex_{CL}^{CL}	2	30	–	Exponent of CL to stimulate self-growth
ex_{PGF}^{Enz}	5	1	–	Exponent of enzyme to stimulate prostaglandin $F2_\alpha$ synthesis
ex_{PGF}^{Oxy}	2	10	–	Exponent of oxytocin to stimulate prostaglandin $F2_\alpha$ synthesis
ex_{Enz}^{P4}	5	1	–	Exponent of P4 to stimulate enzyme synthesis
ex_{IOF}^{PGF}	5	10	–	Exponent of prostaglandin $F2_\alpha$ to stimulate interovarian factor synthesis
ex_{IOF}^{CL}	10	1	–	Exponent of CL to stimulate interovarian factor synthesis
$T_{FSH}^{Follicle}$	0.57	1.497	[FSH]	Threshold of FSH to stimulate follicular function
$T_{Follicle}^{FSH}$	0.22	0.322	[Follicle]	Threshold of follicular function to downscale FSH threshold
T_{CL}^{CL}	0.1	0.2807	[CL]	Threshold of CL to stimulate self-growth
c_{CL}^{CL}	0.0334	0.0335	[CL]/d	Maximum increase of CL simulated by itself.
c_{LH}^{CL}	0.334	0.4	[CL]/d	Maximum increase of CL simulated by LH.

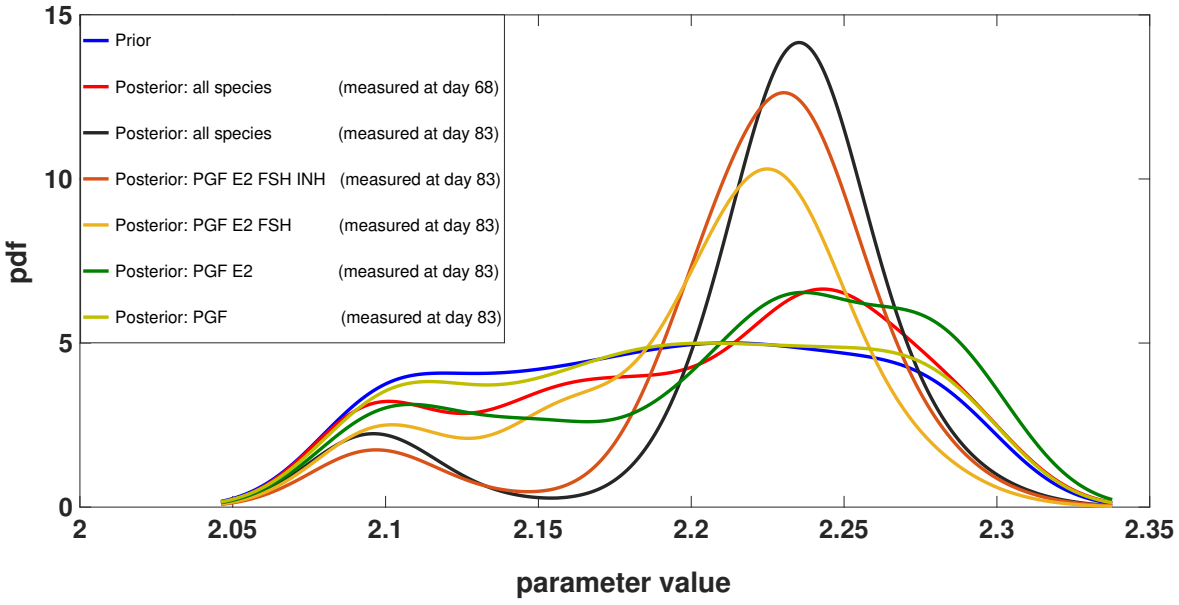
Prior
Posterior: all species (measured at day 68)
Posterior: all species (measured at day 83)
Posterior: PGF E2 FSH INH (measured at day 83)
Posterior: PGF E2 FSH (measured at day 83)
Posterior: PGF E2 (measured at day 83)
Posterior: PGF (measured at day 83)
pdf
parameter value
0
5
10
15
2
2.05
2.1
2.15
2.2
2.25
2.3
2.35

(a)

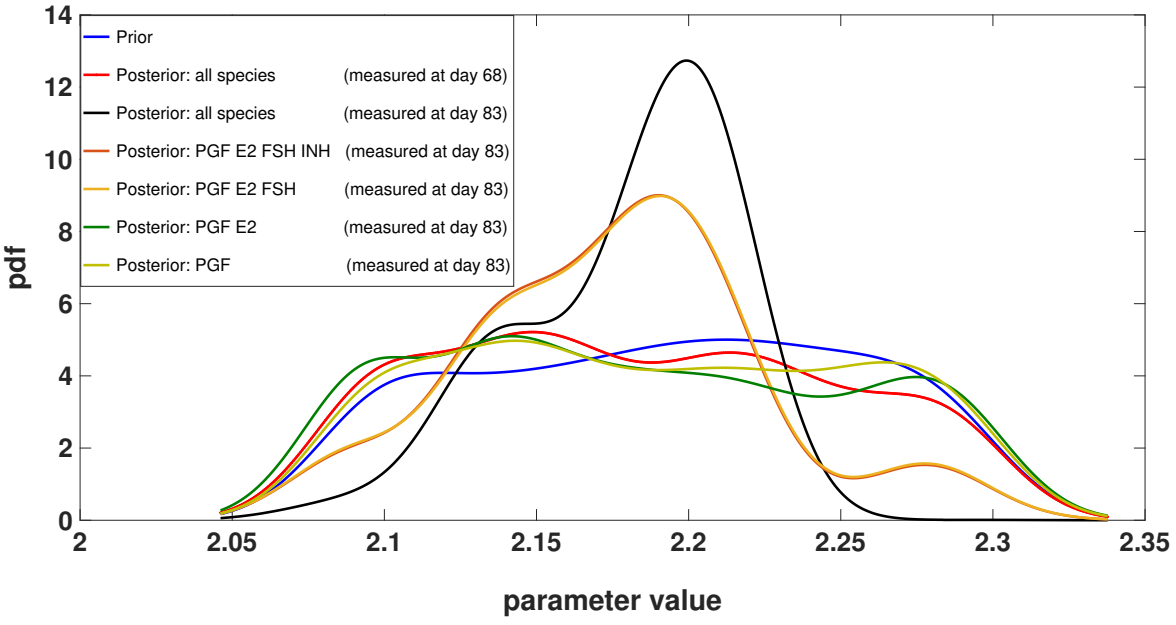
Prior
Posterior: all species (measured at day 68)
Posterior: all species (measured at day 83)
Posterior: PGF E2 FSH INH (measured at day 83)
Posterior: PGF E2 FSH (measured at day 83)
Posterior: PGF E2 (measured at day 83)
Posterior: PGF (measured at day 83)
pdf
parameter value
0
2
4
6
8
10
12
14
2
2.05
2.1
2.15
2.2
2.25
2.3
2.35

(b)

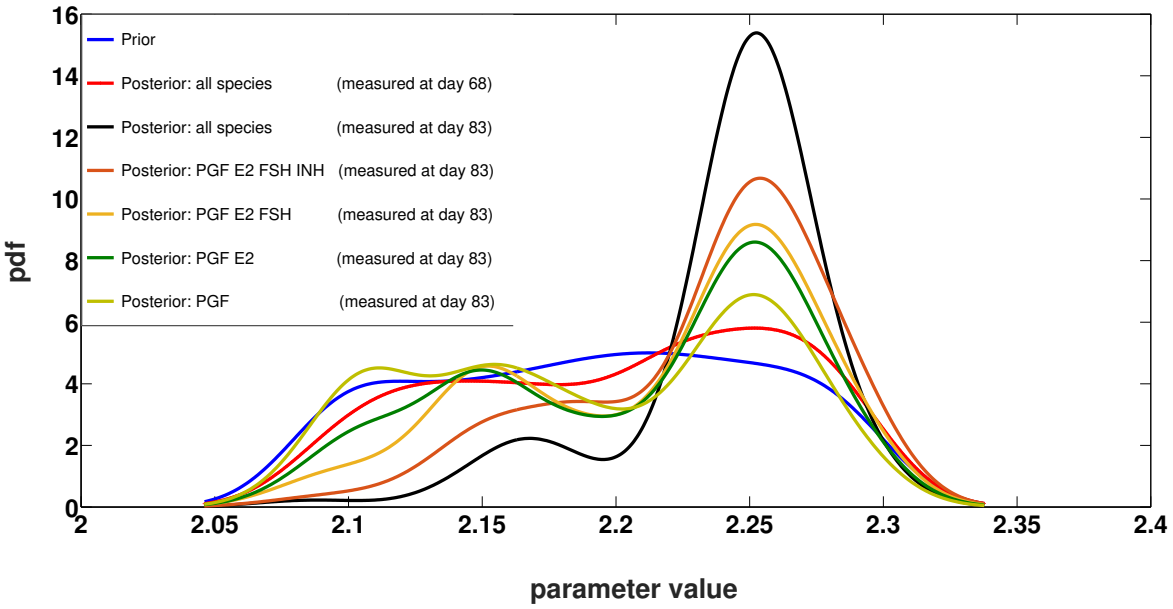

(c)

Figure 10: **The prior and posterior distributions of the parameter.** This figure shows the prior distribution of the growth rate of E2 (in blue) and the estimated posterior distributions based on three different data (subfigures (a), (b) and (c)). The posterior distributions in red and black are estimated based on data containing all species collected, respectively, on the day 68 and 83. The other posterior distributions are estimated based on data containing some selected species collected on the day 83. The information content of the three data resulted in different estimated posterior distribution. For example, the subfigure (a) shows that the updated prior distribution using data containing all species collected on the day 68 (red curve), results in a slight decrease in the parameter uncertainty. In contrast, the subfigures (b) and (c) show no decrease in the parameter uncertainty when using data containing all species collected on the day 68 (red curve). On the other hand, it can be seen from the subfigures (a), (b) and (c) a decrease in the parameter uncertainty when using data containing all species collected on the day 83 (red curve).

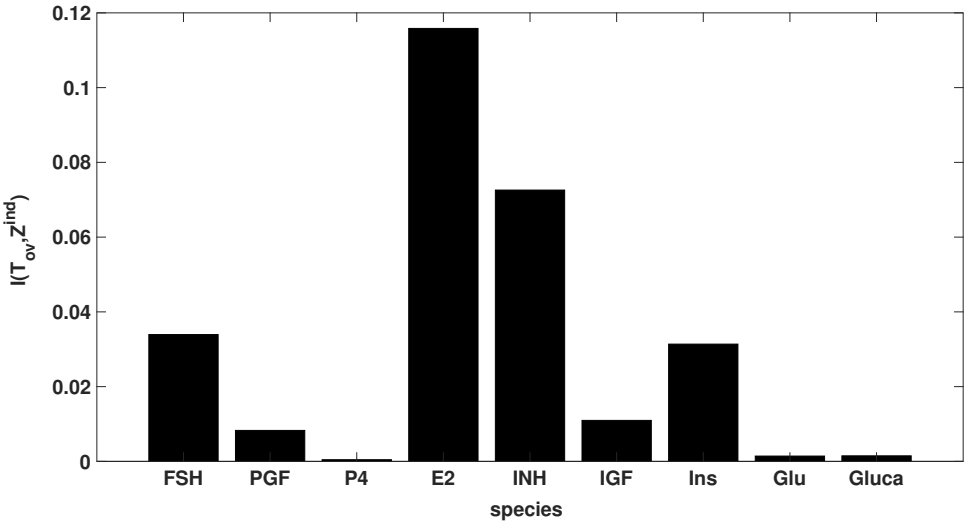

Figure 11: The mutual information shared between the time of ovulation and each species on the day 7.

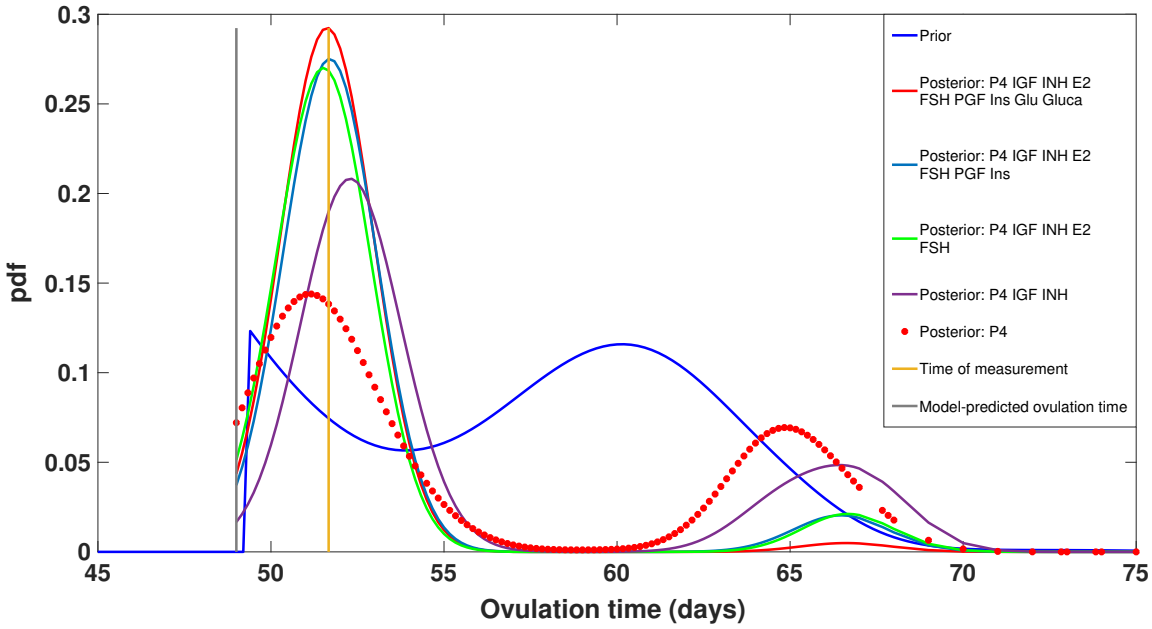

(a)

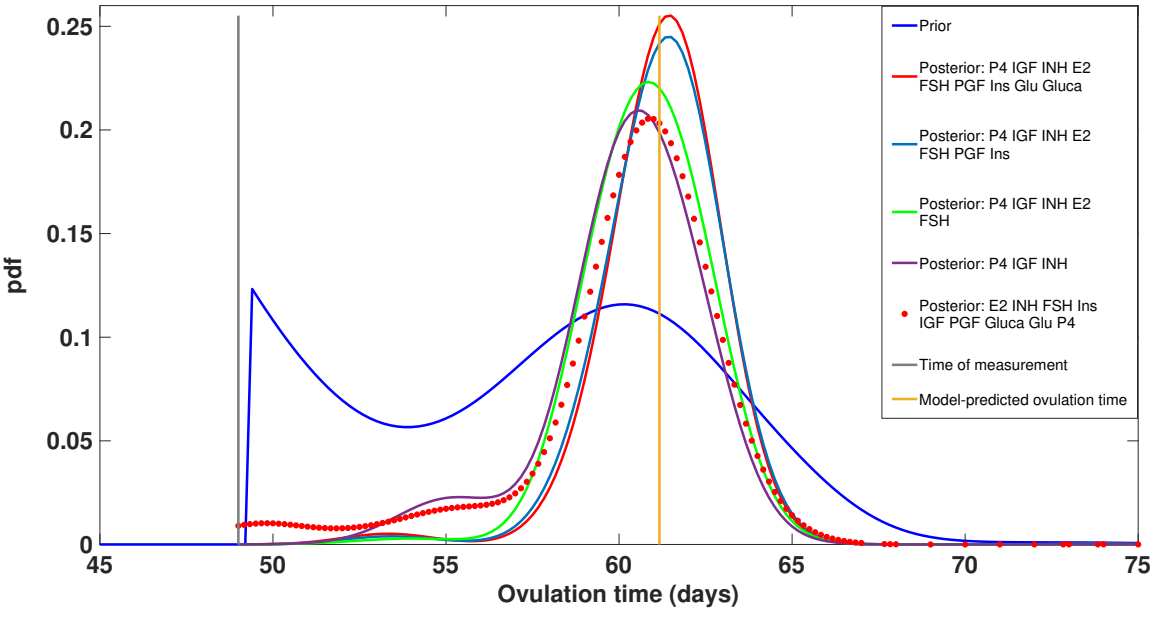

(b)

Figure 12: **The prior and posterior distributions of the time of first ovulation.** This figure shows the prior distribution (in blue) of the possible ovulation times occurring after the day 49. The estimated posterior distributions are based on two different data containing one or more species (subfigure (a) and (b)). The information content embedded into the two data resulted in different prediction and different magnitude of the uncertainty. The time of measurement and the model prediction of the ovulation time are represented by the grey and brown lines, respectively. It can be seen that the more we include additional information from other species into the data, the more the uncertainty is reduced.

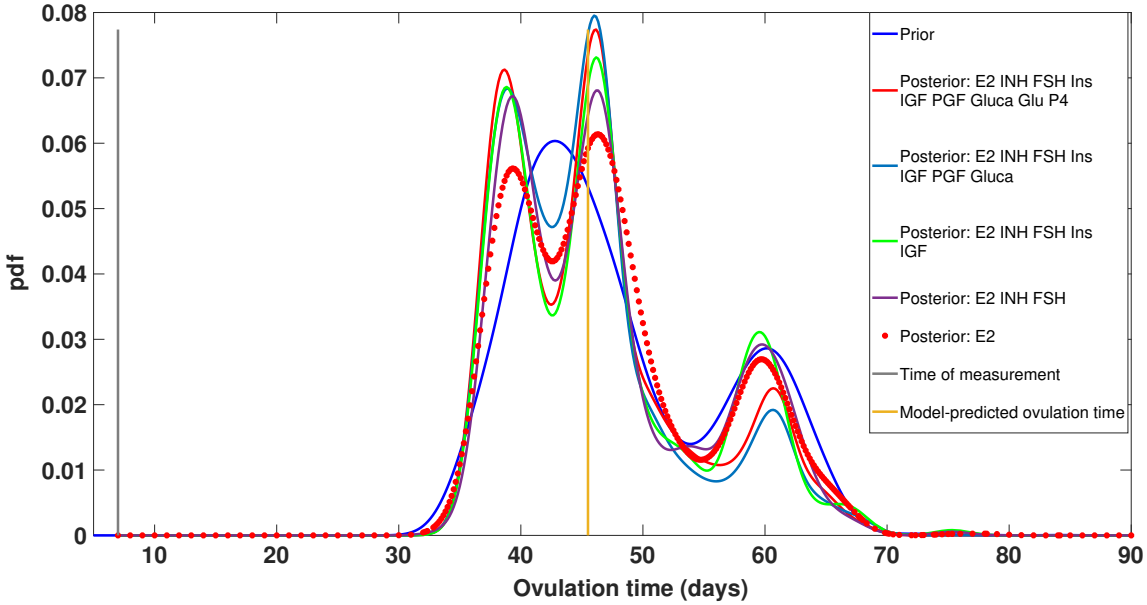

(a)

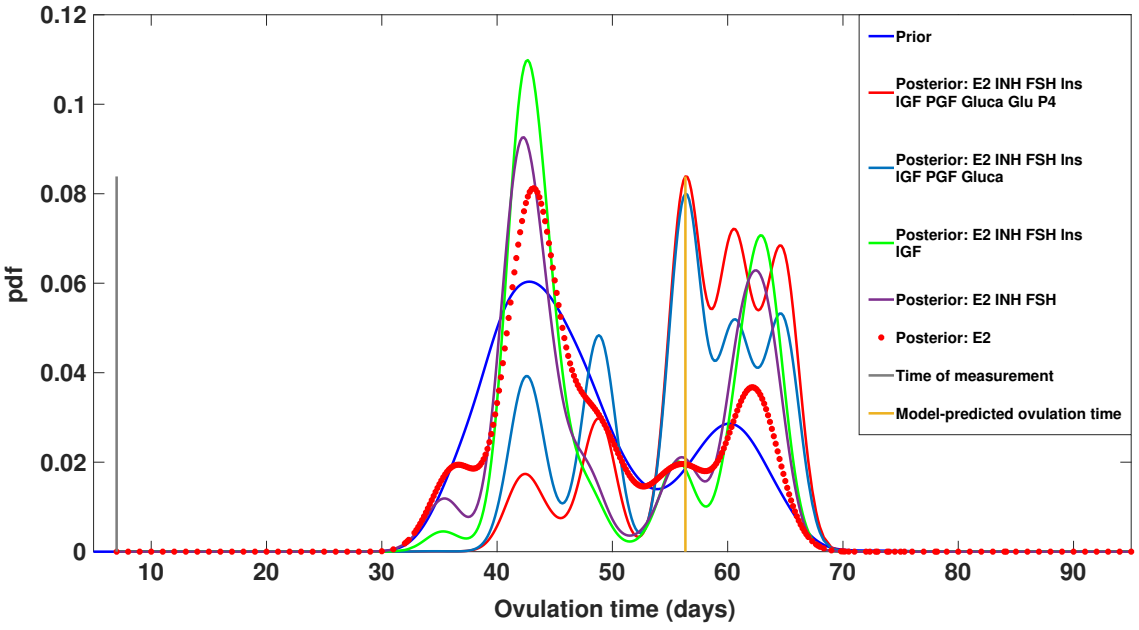

(b)

Figure 13: **The prior and posterior distributions of the time of first ovulation.** This figure shows the prior distribution (in blue) of the possible ovulation times occurring after the day 7. The time of measurement and the model prediction of the ovulation time are represented by the grey and brown lines, respectively. The estimated posterior distributions are based on two different data containing one or more species (subfigure (a) and (b)). Since measuring species on the day 7 resulted in less information about the the ovulation time, it can be seen clearly that updating the prior distribution with the two different data set did not decrease the uncertainty of the ovulation time.

Bibliography

[1] `https://www.mathworks.com/help/matlab/ref/ode15s.html`. Accessed: 01-02-2019.

[2] Laboratory reference values. University of Leipzig, Department of Large Animal Medicine, `http://www.vetmed.uni-leipzig.de/ik/wmedizin/labor/diagnostik/referenzwerte/rind.htm`.

[3] H. S. Al-Sallami, V. V. Pavan Kumar, C. B. Landersdorfer, J. B. Bulitta, and S. B. Duffull. The time course of drug effects. *Pharmaceutical Statistics: The Journal of Applied Statistics in the Pharmaceutical Industry*, 8(3):176–185, 2009.

[4] B. Amzal, F. Y. Bois, E. Parent, and C. P. Robert. Bayesian-optimal design via interacting particle systems. *Journal of the American Statistical association*, 101(474):773–785, 2006.

[5] A. Andrews, R. Laven, and I. Maisey. Treatment and control of an outbreak of fat cow syndrome in a large dairy herd. *The Veterinary Record*, 129(10):216–219, 1991.

[6] J. R. Aschenbach, N. B. Kristensen, S. S. Donkin, H. M. Hammon, and G. B. Penner. Gluconeogenesis in dairy cows: the secret of making sweet milk from sour dough. *IUBMB Life*, 62(12):869–877, 2010.

[7] V. S. Ayyar, D. C. DuBois, R. R. Almon, and W. J. Jusko. Mechanistic multi—tissue modeling of glucocorticoid-induced leucine zipper regulation: Integrating circadian gene expression with receptor-mediated corticosteroid pharmacodynamics. *Journal of Pharmacology and Experimental Therapeutics*, 363(1):45–57, 2017.

[8] R. L. Baldwin. *Modeling ruminant digestion and metabolism*. Springer Science & Business Media, 1995.

[9] D. E. Bauman and W. B. Currie. Partitioning of nutrients during pregnancy and lactation: a review of mechanisms involving homeostasis and homeorhesis. *Journal of dairy science*, 63(9):1514–1529, 1980.

[10] J. D. Baxter and P. H. Forsham. Tissue effects of glucocorticoids. *The American journal of medicine*, 53(5):573–589, 1972.

[11] S. Beam and W. Butler. Effects of energy balance on follicular development and first ovulation in postpartum dairy cows. *Journal of Reproduction and fertility–Supplement*, pages 411–424, 1999.

[12] E. A. Bender. *An introduction to mathematical modeling*. Courier Corporation, 2012.

[13] J. Berg, J. Tymoczko, and L. Stryer. Glycogen metabolism. biochemistry, 2002.

[14] M. Berg, J. Plöntzke, S. Leonhard Marek, M. K. Elisabeth, and S. Röblitz. A dynamic model to simulate potassium balance in dairy cows. *Journal of Dairy Science*, 100(12):9799–9814, 2017.

[15] E. Bergman, R. Brockman, and C. Kaufman. Glucose metabolism in ruminants: comparison of whole-body turnover with production by gut, liver, and kidneys. *Federation Proceedings*, 33(7):1849–1854, 1974.

[16] J. M. Bernardo. Expected information as expected utility. *the Annals of Statistics*, pages 686–690, 1979.

[17] S. J. Bertics, R. R. Grummer, C. Cadorniga Valino, and E. E. Stoddard. Effect of prepartum dry matter intake on liver triglyceride concentration and early lactation. *Journal of dairy science*, 75(7):1914–1922, 1992.

[18] H. M. T. Boer, C. Stötzel, S. Röblitz, P. Deuflhard, R. F. Veerkamp, and H. Woelders. A simple mathematical model of the bovine estrous cycle: follicle development and endocrine interactions. *Journal of Theoretical Biology*, 278(1):20–31, 2011.

[19] J. Bolaños, J. Molina, and M. Forsberg. Effect of blood sampling and administration of acth on cortisol and progesterone levels in ovariectomized zebu cows (bos indicus). *Acta Veterinaria Scandinavica*, 38(1):1–7, 1997.

[20] G. E. Box and N. R. Draper. *Empirical model-building and response surfaces*. John Wiley & Sons, 1987.

[21] R. Brockman. Roles of glucagon and insulin in the regulation of metabolism in ruminants: A review. *The Canadian Veterinary Journal*, 19(3):55, 1978.

[22] R. P. Brockman. Effects of insulin and glucose on the production and utilization of glucose in sheep (ovis aries). *Comparative Biochemistry and Physiology Part A: Physiology*, 74(3):681–685, 1983.

[23] R. Bruckmaier and J. Blum. Oxytocin release and milk removal in ruminants. *Journal of Dairy Science*, 81(4):939–949, 1998.

[24] J. Brunstedt and J. H. Nielsen. Direct long-term effect of hydrocortisone on insulin and glucagon release from mouse pancreatic islets in tissue culture. *Acta endocrinologica*, 96(4):498–504, 1981.

[25] J. C. Buckingham. Glucocorticoids: exemplars of multi-tasking. *British journal of pharmacology*, 147(S1):S258–S268, 2006.

[26] D. Bulman and G. Lamming. The use of milk progesterone analysis in the study of oestrus detection, herd fertility and embryonic mortality in dairy cows. *British Veterinary Journal*, 135(6):559–567, 1979.

[27] D. C. Bulman and G. Lamming. Milk progesterone levels in relation to conception, repeat breeding and factors influencing acyclicity in dairy cows. *Journal of Reproduction and Fertility*, 54(2):447–458, 1978.

[28] D. C. Bulman and P. Wood. Abnormal patterns of ovarian activity in dairy cows and their relationships with reproductive performance. *Animal Science*, 30(2):177–188, 1980.

[29] A. G. Busetto, A. Hauser, G. Krummenacher, M. Sunnåker, S. Dimopoulos, C. S. Ong, J. Stelling, and J. M. Buhmann. Near-optimal experimental design for model selection in systems biology. *Bioinformatics*, 29(20):2625–2632, 2013.

[30] W. Butler. Nutritional interactions with reproductive performance in dairy cattle. *Animal Reproduction Science*, 60:449–457, 2000.

[31] W. Butler, R. Everett, and C. Coppock. The relationships between energy balance, milk production and ovulation in postpartum holstein cows. *Journal of Animal Science*, 53(3):742–748, 1981.

[32] W. Butler and R. Smith. Interrelationships between energy balance and postpartum reproductive function in dairy cattle. *Journal of dairy science*, 72(3):767–783, 1989.

[33] W. R. Butler. Energy balance relationships with follicular development, ovulation and fertility in postpartum dairy cows. *Livestock Production Science*, 83(2):211–218, 2003.

[34] W. Butterfield and A. Lishman. Progesterone profiles of postpartum dairy cows as an aid to diagnosis and treatment of reproductive disorders. *South African journal of animal science*, 20(4):155–160, 1990.

[35] V. Cabrera. Economics of fertility in high-yielding dairy cows on confined tmr systems. *Animal*, 8(s1):211–221, 2014.

[36] T. Cacoullos. Estimation of a multivariate density. *Annals of the Institute of Statistical Mathematics*, 18(1):179–189, 1966.

[37] R. Canfield and W. Butler. Energy balance and pulsatile lh secretion in early postpartum dairy cattle. *Domestic Animal Endocrinology*, 7(3):323–330, 1990.

[38] J. E. Chacón and T. Duong. *Multivariate kernel smoothing and its applications*. Chapman and Hall/CRC, 2018.

[39] L. Chagas, J. Bass, D. Blache, C. Burke, J. Kay, D. Lindsay, M. Lucy, G. Martin, S. Meier, F. Rhodes, et al. Invited review: New perspectives on the roles of nutrition and metabolic priorities in the subfertility of high-producing dairy cows. *Journal of Dairy Science*, 90(9):4022–4032, 2007.

[40] K. Chaloner et al. Optimal bayesian experimental design for linear models. *The Annals of Statistics*, 12(1):283–300, 1984.

[41] K. Chaloner and I. Verdinelli. Bayesian experimental design: A review. *Statistical Science*, pages 273–304, 1995.

[42] A. Chuthaputti and H. Fletcher. Effect of hydrocortisone on terbutaline stimulated insulin release from isolated pancreatic islets. *Research communications in chemical pathology and pharmacology*, 57(3):329–341, 1987.

[43] C. Cobelli and E. Carson. An introduction to modelling methodology. In *Modeling methodology for physiology and medicine*, pages 1–13. Elsevier, 2001.

[44] N. R. Council et al. *Nutrient requirements of dairy cattle: 2001*. National Academies Press, 2001.

[45] T. D O'Brien, P. Westermark, and K. H. Johnson. Islet amyloid polypeptide and insulin secretion from isolated perfused pancreas of fed, fasted, glucose-treated, and dexamethasone-treated rats. *Diabetes*, 40(12):1701–1706, 1991.

[46] A. Danfær. A dynamic model of nutrient digestion and metabolism in lactating dairy cows. *Beretning fra Statens Husdyrbrugsforsøg*, 671, 1990.

[47] A. Danfær. Nutrient metabolism and utilization in the liver. *Livestock Production Science*, 39(1):115–127, 1994.

[48] S. R. Daniels. The consequences of childhood overweight and obesity. *The future of children*, 16(1):47–67, 2006.

[49] B. Davani, A. Khan, M. Hult, E. Mårtensson, S. Okret, S. Efendic, H. Jörnvall, and U. C. Oppermann. Type 1 11β-hydroxysteroid dehydrogenase mediates glucocorticoid activation and insulin release in pancreatic islets. *Journal of Biological Chemistry*, 275(45):34841–34844, 2000.

[50] M. Day, K. Imakawa, D. Zalesky, R. Kittok, and J. E. Kinder. Effects of restriction of dietary energy intake during the prepubertal period on secretion of luteinizing hormone and responsiveness of the pituitary to luteinizing

hormone-releasing hormone in heifers. *Journal of animal science*, 62(6):1641–1648, 1986.

[51] G. De Boer. *Glucagon, insulin, and growth hormone in the regulation of metabolism in dairy cows during lactation and ketosis*, 1984.

[52] M. H. DeGroot et al. Uncertainty, information, and sequential experiments. *The Annals of Mathematical Statistics*, 33(2):404–419, 1962.

[53] F. Delaunay, A. Khan, A. Cintra, B. Davani, Z. C. Ling, A. Andersson, C. Ostenson, J. Gustafsson, S. Efendic, and S. Okret. Pancreatic beta cells are important targets for the diabetogenic effects of glucocorticoids. *The Journal of clinical investigation*, 100(8):2094–2098, 1997.

[54] G. Dellino and C. Meloni. *Uncertainty management in simulation-optimization of complex systems*. Springer, 2015.

[55] J. Dijkstra, J. M. Forbes, and J. France. *Quantitative aspects of ruminant digestion and metabolism*. CABI, 2005.

[56] G. DIMITRIADIS, B. LEIGHTON, M. PARRY BILLINGS, S. SASSON, M. YOUNG, U. KRAUSE, S. BEVAN, P. Terrence, G. WEGENER, and E. A. NEWSHOLME. Effects of glucocorticoid excess on the sensitivity of glucose transport and metabolism to insulin in rat skeletal muscle. *Biochemical Journal*, 321(3):707–712, 1997.

[57] M. Diskin, D. Mackey, J. Roche, and J. Sreenan. Effects of nutrition and metabolic status on circulating hormones and ovarian follicle development in cattle. *Animal Reproduction Science*, 78(3):345–370, 2003.

[58] L. Donaldson. Effect of continued daily injections of oxytocin on oestrous cycle length and reproductive tract morphology in the cow. *Journal of reproduction and fertility*, 18(2):259–263, 1969.

[59] L. Donaldson, J. Bassett, and G. Thorburn. Peripheral plasma progesterone concentration of cows during puberty, oestrous cycles, pregnancy and lactation, and the effects of under-nutrition or exogenous oxytocin on progesterone concentration. *Journal of Endocrinology*, 48(4):599–614, 1970.

[60] L. Donaldson and A. Takken. The effect of exogenous oxytocin on corpus luteum function in the cow. *Journal of reproduction and fertility*, 17(2):373–383, 1968.

[61] S. S. Donkin. Control of hepatic gluconeogenesis during the transition period. In *2016 Florida Ruminant Nutrition Symposium*, page 111, 2016.

[62] C. Dym. *Principles of mathematical modeling*. Elsevier, 2004.

[63] M. H. Ebou, A. Singh Estivalet, J. M. Launay, J. Callebert, F. Tronche, P. Ferré, J. F. Gautier, G. Guillemain, B. Bréant, B. Blondeau, et al. Glucocorticoids inhibit basal and hormone-induced serotonin synthesis in pancreatic beta cells. *PloS one*, 11(2):e0149343, 2016.

[64] J. Elliot. The glucose economy of the lactating dairy cow [metabolism]. In *Proceedings Cornell Nutrition Conference for Feed Manufacturers*, 1976.

[65] P. Érdi and J. Tóth. *Mathematical models of chemical reactions: theory and applications of deterministic and stochastic models*. Manchester University Press, 1989.

[66] K. Erguler and M. P. Stumpf. Practical limits for reverse engineering of dynamical systems: a statistical analysis of sensitivity and parameter inferability in systems biology models. *Molecular BioSystems*, 7(5):1593–1602, 2011.

[67] J. Exton. Regulation of gluconeogenesis by glucocorticoids. *Monographs on endocrinology*, 12:535–546, 1979.

[68] J. H. Exton, N. Friedmann, E. H. A. Wong, J. P. Brineaux, J. D. Corbin, and C. R. Park. Interaction of glucocorticoids with glucagon and epinephrine in the control of gluconeogenesis and glycogenolysis in liver and of lipolysis in adipose tissue. *Journal of Biological Chemistry*, 247(11):3579–3588, 1972.

[69] N. H. Fine, C. L. Doig, Y. S. Elhassan, N. C. Vierra, P. Marchetti, M. Bugliani, R. Nano, L. Piemonti, G. A. Rutter, D. A. Jacobson, et al. Glucocorticoids reprogram β-cell signaling to preserve insulin secretion. *Diabetes*, 67(2):278–290, 2018.

[70] Y. Folman, M. Kaim, Z. Herz, and M. Rosenberg. Comparison of methods for the synchronization of estrous cycles in dairy cows. 2. effects of progesterone and parity on conception1. *Journal of dairy science*, 73(10):2817–2825, 1990.

[71] N. Friggens, G. Emmans, I. Kyriazakis, J. Oldham, and M. Lewis. Feed intake relative to stage of lactation for dairy cows consuming total mixed diets with a high or low ratio of concentrate to forage. *Journal of Dairy Science*, 81(8):2228–2239, 1998.

[72] M. Fürll and B. Fürll. Glukokortikoid-(prednisolon-) wirkungen auf einige blut, harn und leberparameter bei kühen in der zweiten woche des postpartums. *Tierärztl Prax*, 26:262–8, 1998.

[73] M. Fürll, H. Kirbach, and B. Knobloch. Glukokortikosteroideinfluß auf die fastenstimulierte lipolyse und die leberfunktion bei kühen. *Tierärztl Prax*, 21:399–403, 1993.

[74] P. Gaignage, G. Lognay, D. Bosson, D. Vertongen, P. Dreze, M. Marlier, and M. Severin. Dexamethasone bovine pharmacokinetics. *European journal of drug metabolism and pharmacokinetics*, 16(3):219–221, 1991.

[75] P. Garnsworthy, J. Gong, D. Armstrong, J. Newbold, M. Marsden, S. Richards, G. Mann, K. Sinclair, and R. Webb. Nutrition, metabolism, and fertility in dairy cows: 3. amino acids and ovarian function. *Journal of Dairy Science*, 91(11):4190–4197, 2008.

[76] C. Geyer. Introduction to markov chain monte carlo. *Handbook of markov chain monte carlo*, 20116022:45, 2011.

[77] J. Gong, W. Lee, P. Garnsworthy, and R. Webb. Effect of dietary-induced increases in circulating insulin concentrations during the early postpartum period on reproductive function in dairy cows. *Reproduction*, 123(3):419–427, 2002.

[78] R. Gorewit, E. Wachs, R. Sagi, and W. Merrill. Current concepts on the role of oxytocin in milk ejection. *Journal of Dairy Science*, 66(10):2236–2250, 1983.

[79] R. C. Gorewit. Lactation biology and methods of increasing efficiency. In N. R. C. U. C. on Technological Options to Improve the Nutritional Attributes of Animal Products, editor, *Designing Foods: Animal Product Options in the Marketplace*, pages 208–223. National Academy Press, 1988.

[80] V. Grill and M. Rundfeldt. Abnormalities of insulin responses after ambient and previous exposure to glucose in streptozocin-diabetic and dexamethasone-treated rats: role of hyperglycemia and increased b-cell demands. *Diabetes*, 35(1):44–51, 1986.

[81] R. R. Grummer. Impact of changes in organic nutrient metabolism on feeding the transition dairy cow. *Journal of Animal Science*, 73(9):2820–2833, 1995.

[82] R. N. Gutenkunst, J. J. Waterfall, F. P. Casey, K. S. Brown, C. R. Myers, and J. P. Sethna. Universally sloppy parameter sensitivities in systems biology models. *PLoS computational biology*, 3(10):e189, 2007.

[83] C. Gutierrez, J. Gong, T. Bramley, and R. Webb. Effects of genetic selection for milk yield on metabolic hormones and follicular development in postpartum dairy cattle. *J. Reprod. Fertil. Abst Ser*, 24:32, 1999.

[84] K. M. Habegger, K. M. Heppner, N. Geary, T. J. Bartness, R. Dimarchi, and M. H. Tschöp. The metabolic actions of glucagon revisited. *Nature Reviews Endocrinology*, 6:689–697, 2010.

[85] T. Hamada. Importance of blood glucose and ketones in the evaluation of nutritional state of the ruminant. *JARQ (Japan)*, 1984.

[86] H. Hammon, C. Philipona, Y. Zbinden, J. Blum, and S. Donkin. Effects of dexamethasone and growth hormone treatment on hepatic gluconeogenic enzymes in calves. *Journal of dairy science*, 88(6):2107–2116, 2005.

[87] C. Han and K. Chaloner. Bayesian experimental design for nonlinear mixed-effects models with application to hiv dynamics. *Biometrics*, 60(1):25–33, 2004.

[88] P. Hartmann and D. Kronfeld. Mammary blood flow and glucose uptake in lactating cows given dexamethasone1. *Journal of dairy science*, 56(7):896–902, 1973.

[89] J. H. Herbein, R. J. Aielle, L. I. Eckler, R. E. Pearson, and R. M. Akers. Glucagon, insulin, growth hormone, and glucose concentrations in blood plasma of lactating dairy cows. *Journal of Dairy Science*, 68:320–325, 1985.

[90] A. V. Hill. The possible effects of the aggregation of the molecules of haemoglobin on its dissociation curves. *j. physiol.*, 40:4–7, 1910.

[91] M. Hockett, F. Hopkins, M. Lewis, A. Saxton, H. Dowlen, S. Oliver, and F. Schrick. Endocrine profiles of dairy cows following experimentally induced clinical mastitis during early lactation. *Animal reproduction science*, 58(3-4):241–251, 2000.

[92] N. Holford. Pharmacodynamic principles and the time course of delayed and cumulative drug effects. *Translational and Clinical Pharmacology*, 26(2):56–59, 2018.

[93] N. H. Holford and L. B. Sheiner. Understanding the dose-effect relationship. *Clinical pharmacokinetics*, 6(6):429–453, 1981.

[94] X. Huan and Y. M. Marzouk. Simulation-based optimal bayesian experimental design for nonlinear systems. *Journal of Computational Physics*, 232(1):288–317, 2013.

[95] M. Hucka, A. Finney, H. Sauro, H. Bolouri, J. Doyle, H. Kitano, and et al. The systems biology markup language (sbml): a medium for representation and exchange of biochemical network models. *Bioinformatics*, 19(4):524–531, 2003.

[96] N. Janovick, Y. Boisclair, and J. Drackley. Prepartum dietary energy intake affects metabolism and health during the periparturient period in primiparous and multiparous holstein cows. *Journal of Dairy Science*, 94(3):1385–1400, 2011.

[97] I. K. Jeong, S. H. Oh, B. J. Kim, J. H. Chung, Y. K. Min, M. S. Lee, M. K. Lee, and K. W. Kim. The effects of dexamethasone on insulin release and biosynthesis are dependent on the dose and duration of treatment. *Diabetes research and clinical practice*, 51(3):163–171, 2001.

[98] J. Y. Jin and W. J. Jusko. Pharmacodynamics of glucose regulation by methylprednisolone. ii. normal rats. *Biopharmaceutics & drug disposition*, 30(1):35–48, 2009.

[99] R. Jorritsma, J. Thanasak, M. Houweling, J. Noordhuizen, and K. Müller. Effects of a single dose of dexamethasone-21-isonicotinate on the metabolism of heifers in early lactation. *The Veterinary record*, 155(17):521–523, 2004.

[100] S. C. Kalhan and P. A. Adam. Inhibitory effect of prednisone on insulin secretion in man: model for duplication of blood glucose concentration. *The Journal of Clinical Endocrinology & Metabolism*, 41(3):600–610, 1975.

[101] J. Kallrath. *Modeling languages in mathematical optimization*, volume 88. Springer Science & Business Media, 2013.

[102] A. Kawai and N. Kuzuya. On the role of glucocorticoid in glucose-induced insulin secretion. *Hormone and Metabolic Research*, 9(05):361–365, 1977.

[103] C. Kawashima, K. Kida, K. G. Hayashi, C. A. Montoya, E. Kaneko, N. Matsunaga, T. Shimizu, M. Matsui, Y. I. Miyake, D. Schams, et al. Changes in plasma metabolic hormone concentrations during the ovarian cycles of japanese black and holstein cattle. *Journal of Reproduction and Development*, 53(2):247–254, 2007.

[104] A. Khan, C. Ostenson, P. Berggren, and S. Efendic. Glucocorticoid increases glucose cycling and inhibits insulin release in pancreatic islets of ob/ob mice. *American Journal of Physiology-Endocrinology and Metabolism*, 263(4):E663–E666, 1992.

[105] N. Kraus Friedmann. Hormonal regulation of hepatic gluconeogenesis. *Physiological Reviews*, 64(1):170–259, 1984.

[106] N. B. Kristensen, A. Danfær, and N. Agergaard. Absorption and metabolism of short-chain fatty acids in ruminants. *Archives of Animal Nutrition*, 51(2-3):165–175, 1998.

[107] D. Kronfeld. Major metabolic determinants of milk volume, mammary efficiency, and spontaneous ketosis in dairy cows1. *Journal of Dairy Science*, 65(11):2204–2212, 1982.

[108] T. Kuo, A. McQueen, T. C. Chen, and J. C. Wang. Regulation of glucose homeostasis by glucocorticoids. In *Glucocorticoid Signaling*, pages 99–126. Springer, 2015.

[109] M. Kusenda, M. Kaske, M. Piechotta, L. Locher, A. Starke, K. Huber, and J. Rehage. Effects of dexamethasone-21-isonicotinate on peripheral insulin action in dairy cows 5 days after surgical correction of abomasal displacement. *Journal of veterinary internal medicine*, 27(1):200–206, 2013.

[110] C. Lambillotte, P. Gilon, and J. C. Henquin. Direct glucocorticoid inhibition of insulin secretion. an in vitro study of dexamethasone effects in mouse islets. *The Journal of clinical investigation*, 99(3):414–423, 1997.

[111] G. Lamming, D. C. Wathes, and A. Peters. Endocrine patterns of the postpartum cow. *Journal of reproduction and fertility. Supplement*, 30:155–170, 1981.

[112] R. Landgraf, J. Schulz, K. Eulenberger, and J. Wilhelm. Plasma levels of oxytocin and vasopressin before, during and after parturition in cows. *Experimental and Clinical Endocrinology & Diabetes*, 81(03):321–328, 1983.

[113] A. Lange, R. Schwieger, J. Plöntzke, S. Schäfer, and S. Röblitz. Follicular competition in cows: the selection of dominant follicles as a synergistic effect. *Journal of Mathematical Biology*, 2018.

[114] C. J. Langmead. *Generalized queries and bayesian statistical model checking in dynamic bayesian networks: Application to personalized medicine*, 2009.

[115] R. Leng et al. Glucose synthesis in ruminants. *Adv. Vet. Sci.*, 14:209–260, 1970.

[116] L. Li, Z. Q. Li, C. H. Deng, M. R. Ning, H. Q. Li, S. S. Bi, T. Y. Zhou, and W. Lu. A mechanism-based pharmacokinetic/pharmacodynamic model for cyp3a1/2 induction by dexamethasone in rats. *Acta Pharmacologica Sinica*, 33(1):127, 2012.

[117] J. Liepe, S. Filippi, M. Komorowski, and M. P. Stumpf. Maximizing the information content of experiments in systems biology. *PLoS computational biology*, 9(1):e1002888, 2013.

[118] D. V. Lindley. On a measure of the information provided by an experiment. *The Annals of Mathematical Statistics*, pages 986–1005, 1956.

[119] H. K. Lon, D. Liu, and W. J. Jusko. Pharmacokinetic/pharmacodynamic modeling in inflammation. *Critical Reviews^{TM} in Biomedical Engineering*, 40(4), 2012.

[120] C. A. Longano and H. P. Fletcher. Insulin release after acute hydrocortisone treatment in mice. *Metabolism-Clinical and Experimental*, 32(6):603–608, 1983.

[121] P. Lovendahl, C. Ridder, and N. C. Friggens. Limits to prediction of energy balance from milk composition measures at individual cow level. *Journal of dairy science*, 93(5):1998–2006, 2010.

[122] M. Lucy. Regulation of ovarian follicular growth by somatotropin and insulin-like growth factors in cattle1. *Journal of Dairy Science*, 83(7):1635–1647, 2000.

[123] M. Lucy. Reproductive loss in high-producing dairy cattle: where will it end? *Journal of dairy science*, 84(6):1277–1293, 2001.

[124] M. Lucy. Functional differences in the growth hormone and insulin-like growth factor axis in cattle and pigs: implications for post-partum nutrition and reproduction. *Reproduction in Domestic Animals*, 43(s2):31–39, 2008.

[125] S. Maciel, C. Chamberlain, R. Wettemann, and L. Spicer. Dexamethasone influences endocrine and ovarian function in dairy cattle1. *Journal of dairy science*, 84(9):1998–2009, 2001.

[126] D. Mackey, A. Wylie, J. Sreenan, J. Roche, and M. Diskin. The effect of acute nutritional change on follicle wave turnover, gonadotropin, and steroid concentration in beef heifers. *Journal of Animal Science*, 78(2):429–442, 2000.

[127] D. R. Mackey, J. M. Sreenan, J. F. Roche, and M. G. Diskin. Effect of acute nutritional restriction on incidence of anovulation and periovulatory estradiol and gonadotropin concentrations in beef heifers. *Biology of Reproduction*, 61(6):1601–1607, 1999.

[128] L. Majdoub, M. Vermorel, and I. Ortigues Marty. Intraruminal propionate supplementation modifies hindlimb energy metabolism without changing the splanchnic release of glucose in growing lambs. *British Journal of Nutrition*, 89(1):39–50, 2003.

[129] W. J. Malaisse, F. Malaisse Lagae, E. F. Mc Craw, and P. H. Wright. Insulin secretion in vitro by pancreatic tissue from normal, adrenalectomized, and cortisol-treated rats. *Proceedings of the Society for Experimental Biology and Medicine*, 124(3):924–928, 1967.

[130] T. Mancini, E. Tronci, I. Salvo, F. Mari, A. Massini, and I. Melatti. Computing biological model parameters by parallel statistical model checking. In *International Conference on Bioinformatics and Biomedical Engineering*, pages 542–554. Springer, 2015.

[131] J. Marco, C. Calle, D. Román, M. Díaz Fierros, M. L. Villanueva, and I. Valverde. Hyperglucagonism induced by glucocorticoid treatment in man. *New England Journal of Medicine*, 288(3):128–131, 1973.

[132] P. Marjoram, J. Molitor, V. Plagnol, and S. Tavaré. Markov chain monte carlo without likelihoods. *Proceedings of the National Academy of Sciences*, 100(26):15324–15328, 2003.

[133] O. Martin, F. Blanc, J. Agabriel, C. Disenhaus, J. Dupont, C. Ponsart, P. Paccard, J. Pires, S. Freret, S. Elis, et al. A bovine reproductive physiology model to predict interactions between nutritional status and reproductive management. In *Proceedings of the 2012 Meeting of the Animal Science Modelling Group, Canadian Journal of Animal Science*, 2012.

[134] O. Martin and D. Sauvant. Dynamic model of the lactating dairy cow metabolism. *Animal*, 1(8):1143–1166, 2007.

[135] J. McArt, D. Nydam, and G. Oetzel. Epidemiology of subclinical ketosis in early lactation dairy cattle. *Journal of dairy science*, 95(9):5056–5066, 2012.

[136] M. McMahon, J. Gerich, and R. Rizza. Effects of glucocorticoids on carbohydrate metabolism. *Diabetes/metabolism reviews*, 4(1):17–30, 1988.

[137] J. McNamara. Ruminant nutrition symposium: A systems approach to integrating genetics, nutrition, and metabolic efficiency in dairy cattle. *Journal of Animal Science*, 90(6):1846–1854, 2012.

[138] J. P. McNamara and S. L. Shields. Reproduction during lactation of dairy cattle: integrating nutritional aspects of reproductive control in a systems research approach. *Animal Frontiers*, 3(4):76–83, 2013.

[139] S. Meier, J. R. Roche, E. S. Kolver, and R. C. Boston. A compartmental model describing changes in progesterone concentrations during the oestrous cycle. *Journal of Dairy Research*, 76(2):249–256, 2009.

[140] L. Menten and M. Michaelis. Die kinetik der invertinwirkung. *Biochem Z*, 49:333–369, 1913.

[141] V. Momongan and G. Schmidt. Oxytocin levels in the plasma of holstein-friesian cows during milking with and without a premilking stimulus1. *Journal of Dairy Science*, 53(6):747–751, 1970.

[142] V. G. Momongan. *The effect of milking stimulus and stage of lactation on the levels of oxytocin in the blood during the milking process.* Phd thesis, Cornell University, Ithaca, NY, 1969.

[143] P. Monget and G. Martin. Involvement of insulin-like growth factors in the interactions between nutrition and reproduction in female mammals. *Human Reproduction*, 12(suppl_1):33–52, 1997.

[144] S. A. Morgan, M. Sherlock, L. L. Gathercole, G. G. Lavery, C. Lenaghan, I. J. Bujalska, D. Laber, A. Yu, G. Convey, R. Mayers, et al. 11β-hydroxysteroid dehydrogenase type 1 regulates glucocorticoid-induced insulin resistance in skeletal muscle. *Diabetes*, 2009.

[145] P. Müller. Simulation based optimal design. *Handbook of Statistics*, 25:509–518, 2005.

[146] M. Murphy, W. Enright, M. Crowe, K. McConnell, L. Spicer, M. Boland, and J. Roche. Effect of dietary intake on pattern of growth of dominant follicles during the oestrous cycle in beef heifers. *Journal of Reproduction and Fertility*, 92(2):333–338, 1991.

[147] R. A. Nafikov and D. C. Beitz. Carbohydrate and lipid metabolism in farm animals. *The Journal of Nutrition*, 137(3):702–705, 2007.

[148] T. Nakaya and K. Yano. Visualising crime clusters in a space-time cube: An exploratory data-analysis approach using space-time kernel density estimation and scan statistics. *Transactions in GIS*, 14(3):223–239, 2010.

[149] J. A. Negrão and P. G. Marnet. Milk yield, residual milk, oxytocin and cortisol release during machine milking in gir, gir× holstein and holstein cows. *Reproduction Nutrition Development*, 46(1):77–85, 2006.

[150] I. Newton and C. Huygens. *Mathematical principles of natural philosophy*. Encyclopaedia Britannica, 1987.

[151] B. Nonnecke, J. Burton, and M. Kehrli. Associations between function and composition of blood mononuclear leukocyte populations from holstein bulls treated with dexamethasone1. *Journal of dairy science*, 80(10):2403–2410, 1997.

[152] A. Ogawa, J. H. Johnson, M. Ohneda, C. T. McAllister, L. Inman, T. Alam, and R. H. Unger. Roles of insulin resistance and beta-cell dysfunction in dexamethasone-induced diabetes. *The Journal of clinical investigation*, 90(2):497–504, 1992.

[153] G. Oldham and C. Howard. Suppression of bovine lymphocyte responses to mitogens following in vivo and in vitro treatment with dexamethasone. *Veterinary immunology and immunopathology*, 30(2-3):161–177, 1992.

[154] S. Ollier, F. Beaudoin, N. Vanacker, and P. Lacasse. Effect of reducing milk production using a prolactin-release inhibitor or a glucocorticoid on metabolism and immune functions in cows subjected to acute nutritional stress. *Journal of dairy science*, 99(12):9949–9961, 2016.

[155] G. Opsomer. Interaction between metabolic challenges and productivity in high yielding dairy cows. *Japanese Journal of Veterinary Research*, 63(Supplement 1):S1–S14, 2015.

[156] G. Opsomer, M. Coryn, H. Deluyker, and A. d. Kruif. An analysis of ovarian dysfunction in high yielding dairy cows after calving based on progesterone profiles. *Reproduction in Domestic Animals*, 33(3-4):193–204, 1998.

[157] P. A. Ospina, J. A. McArt, T. R. Overton, T. Stokol, and D. V. Nydam. Using nonesterified fatty acids and β-hydroxybutyrate concentrations during the transition period for herd-level monitoring of increased risk of disease and decreased reproductive and milking performance. *Veterinary Clinics: Food Animal Practice*, 29(2):387–412, 2013.

[158] E. Parzen. On estimation of a probability density function and mode. *The annals of mathematical statistics*, 33(3):1065–1076, 1962.

[159] R. Pfuhl, O. Bellmann, C. Kuehn, F. Teuscher, K. Ender, and J. Wegner. Beef versus dairy cattle: a comparison of feed conversion, carcass composition, and meat quality. *Archives Animal Breeding*, 50(1):59–70, 2007.

[160] D. Phillips and I. Clarke. Effects of the synthetic glucocorticoid dexamethasone on reproductive function in the ewe. *Journal of endocrinology*, 126(2):289–295, 1990.

[161] R. Pivonello, M. De Leo, P. Vitale, A. Cozzolino, C. Simeoli, M. C. De Martino, G. Lombardi, and A. Colao. Pathophysiology of diabetes mellitus in cushing's syndrome. *Neuroendocrinology*, 92(Suppl. 1):77–81, 2010.

[162] S. R. Pring, M. Owen, J. R. King, K. D. Sinclair, R. Webb, A. P. Flint, and P. C. Garnsworthy. A mathematical model of the bovine oestrous cycle: Simulating outcomes of dietary and pharmacological interventions. *Journal of Theoretical Biology*, 313:115–126, 2012.

[163] O. Radostits, C. Gay, D. Blood, and K. Hinchcliff. Ketosis in ruminants. *Veterinary medicine: A textbook of the diseases of cattle, sheep, pigs, goats and horses*, pages 1452–1462, 2000.

[164] A. Rafacho, L. M. Gonçalves Neto, J. C. Santos Silva, P. Alonso Magdalena, B. Merino, S. R. Taboga, E. M. Carneiro, A. C. Boschero, A. Nadal, and I. Quesada. Pancreatic alpha-cell dysfunction contributes to the disruption of glucose homeostasis and compensatory insulin hypersecretion in glucocorticoid-treated rats. *PLoS One*, 9(4):e93531, 2014.

[165] H. Randy and G. Graf. Factors affecting endogenous plasma oxytocic activity in lactating holstein cows. *Journal of Dairy Science*, 56(4):446–450, 1973.

[166] H. Randy, G. Graf, and T. Bibb. relationship between plasma oxytocin and reproductive status in lactating bovine. *Amer Dairy Science Assoc*, 54(5), 1971.

[167] A. Rawan, S. Yoshioka, H. Abe, and T. Acosta. Insulin-like growth factor-1 regulates the expression of luteinizing hormone receptor and steroid production in bovine granulosa cells. *Reproduction in Domestic Animals*, 50(2):283–291, 2015.

[168] C. Reynolds. Glucose balance in cattle. florida ruminant nutrition symposium. http://dairy.ifas.ufl.edu/rns/2005/Reynolds.pdf, 2005.

[169] C. Reynolds, P. Aikman, B. Lupoli, D. Humphries, and D. Beever. Splanchnic metabolism of dairy cows during the transition from late gestation through early lactation. *Journal of Dairy Science*, 86(4):1201–1217, 2003.

[170] J. A. Rice. Mathematical statistics and data analysis. 2007. *Duxbury Press*, 1996.

[171] M. Richards, J. Spitzer, and M. Warner. Effect of varying levels of postpartum nutrition and body condition at calving on subsequent reproductive performance in beef cattle. *Journal of Animal Science*, 62(2):300–306, 1986.

[172] M. Richards, R. Wettemann, and H. Schoenemann. Nutritional anestrus in beef cows: body weight change, body condition, luteinizing hormone in serum and ovarian activity. *Journal of Animal Science*, 67(6):1520–1526, 1989.

[173] J. F. Roche. The effect of nutritional management of the dairy cow on reproductive efficiency. *Animal Reproduction Science*, 96(3):282–296, 2006.

[174] M. Rosenblatt. Remarks on some nonparametric estimates of a density function. *The Annals of Mathematical Statistics*, pages 832–837, 1956.

[175] M. Sami, N. Farzaneh, M. Mohri, and H. A. Seifi. Effects of dexamethasone and insulin alone or in combination on reproduction in dairy cows in early lactation. *Revue de Medecine Veterinaire*, 168, 2017.

[176] M. Sami, M. Mohri, and H. A. Seifi. Effects of dexamethasone and insulin alone or in combination on energy and protein metabolism indicators and milk production in dairy cows in early lactation–a randomized controlled trial. *PloS one*, 10(9):e0139276, 2015.

[177] R. Scaramuzzi, D. Baird, B. Campbell, M. A. Driancourt, J. Dupont, J. Fortune, R. Gilchrist, G. Martin, K. McNatty, A. McNeilly, et al. Regulation of folliculogenesis and the determination of ovulation rate in ruminants. *Reproduction, Fertility and Development*, 23(3):444–467, 2011.

[178] U. Schröder and R. Staufenbiel. Invited review: Methods to determine body fat reserves in the dairy cow with special regard to ultrasonographic measurement of backfat thickness. *Journal of Dairy Science*, 89(1):1–14, 2006.

[179] D. W. Scott. *Multivariate density estimation: theory, practice, and visualization*. John Wiley & Sons, 2015.

[180] P. Sebastiani and H. P. Wynn. Maximum entropy sampling and optimal bayesian experimental design. *Journal of the Royal Statistical Society: Series B (Statistical Methodology)*, 62(1):145–157, 2000.

[181] H. A. Seifi, S. LeBlanc, E. Vernooy, K. Leslie, and T. Duffield. Effect of isoflupredone acetate with or without insulin on energy metabolism, reproduction, milk production, and health in dairy cows in early lactation. *Journal of dairy science*, 90(9):4181–4191, 2007.

[182] G. Selk, R. Wettemann, K. Lusby, J. Oltjen, S. Mobley, R. Rasby, and J. Garmendia. Relationships among weight change, body condition and reproductive performance of range beef cows. *Journal of Animal Science*, 66(12):3153–3159, 1988.

[183] A. Shamay, F. Shapiro, H. Barash, I. Bruckental, and N. Silanikove. *Effect of dexamethasone on milk yield and composition in dairy cows.* EDP Sciences, 2000.

[184] H. Shamoon, V. Soman, and R. S. Sherwin. The influence of acute physiological increments of cortisol on fuel metabolism and insulin binding to monocytes in normal humans. *The Journal of Clinical Endocrinology & Metabolism*, 50(3):495–501, 1980.

[185] C. E. Shannon. A mathematical theory of communication. *Bell system technical journal*, 27(3):379–423, 1948.

[186] P. She. *Regulation of carbohydrate metabolism by exogenous glucagon in lactating cows*, 1997.

[187] L. B. Sheiner, D. R. Stanski, S. Vozeh, R. D. Miller, and J. Ham. Simultaneous modeling of pharmacokinetics and pharmacodynamics: application to d-tubocurarine. *Clinical Pharmacology and Therapeutics*, 25(3):358–371, 1979.

[188] R. Short and R. Bellows. Relationships among weight gains, age at puberty and reproductive performance in heifers. *Journal of Animal Science*, 32(1):127–131, 1971.

[189] N. Shpigel, R. Chen, Y. Avidar, and E. Bogin. Use of corticosteroids alone or combined with glucose to treat ketosis in dairy cows. *Journal of the American Veterinary Medical Association*, 208(10):1702–1704, 1996.

[190] S. A. Sisson, Y. Fan, and M. M. Tanaka. Sequential monte carlo without likelihoods. *Proceedings of the National Academy of Sciences*, 104(6):1760–1765, 2007.

[191] B. Slavin, J. Ong, and P. Kern. Hormonal regulation of hormone-sensitive lipase activity and mrna levels in isolated rat adipocytes. *Journal of lipid research*, 35(9):1535–1541, 1994.

[192] C. Staples, J. Burke, and W. Thatcher. Influence of supplemental fats on reproductive tissues and performance of lactating cows1. *Journal of Dairy Science*, 81(3):856–871, 1998.

[193] R. Stewart, L. Spicer, T. Hamilton, B. Keefer, L. Dawson, G. Morgan, and S. Echternkamp. Levels of insulin-like growth factor (igf) binding proteins, luteinizing hormone and igf-i receptors, and steroids in dominant follicles during the first follicular wave in cattle exhibiting regular estrous cycles. *Endocrinology*, 137(7):2842–2850, 1996.

[194] M. Stone et al. Application of a measure of information to the design and comparison of regression experiments. *The Annals of Mathematical Statistics*, 30(1):55–70, 1959.

[195] C. Stötzel, J. Plöntzke, W. Heuwieser, and S. Röblitz. Advances in modeling of the bovine estrous cycle: Synchronization with pgf2α. *Theriogenology*, 78(7):1415–1428, 2012.

[196] M. Stumvoll, B. J. Goldstein, and T. W. van Haeften. Type 2 diabetes: principles of pathogenesis and therapy. *The Lancet*, 365(9467):1333–1346, 2005.

[197] Y. N. Sun, L. I. McKay, D. C. DuBois, W. J. Jusko, and R. R. Almon. Pharmacokinetic/pharmacodynamic models for corticosteroid receptor down-regulation and glutamine synthetase induction in rat skeletal muscle by a receptor/gene-mediated mechanism. *Journal of Pharmacology and Experimental Therapeutics*, 288(2):720–728, 1999.

[198] M. A. Tanner and W. H. Wong. Data-based nonparametric estimation of the hazard function with applications to model diagnostics and exploratory analysis. *Journal of the American Statistical Association*, 79(385):174–182, 1984.

[199] J. Thanasak, R. Jorritsma, A. Hoek, J. P. Noordhuizen, V. P. Rutten, and K. E. Müller. The effects of a single injection of dexamethasone-21-isonicotinate on the lymphocyte functions of dairy cows at two weeks post partum. *Veterinary research*, 35(1):103–112, 2004.

[200] J. Thissen, O. Schakman, and H. Gilson. Mechanisms of glucocorticoid-induced myopathy. *Bone*, 45:S123–S124, 2009.

[201] J. P. Thissen, L. E. Underwood, and J. M. Ketelslegers. Regulation of insulin-like growth factor–i in starvation and injury. *Nutrition reviews*, 57(6):167–176, 1999.

[202] V. Thorup, D. Edwards, and N. Friggens. On-farm estimation of energy balance in dairy cows using only frequent body weight measurements and body condition score. *Journal of dairy science*, 95(4):1784–1793, 2012.

[203] T. Toni and M. P. Stumpf. Simulation-based model selection for dynamical systems in systems and population biology. *Bioinformatics*, 26(1):104–110, 2009.

[204] T. Toni, D. Welch, N. Strelkowa, A. Ipsen, and M. P. Stumpf. Approximate bayesian computation scheme for parameter inference and model selection in dynamical systems. *Journal of the Royal Society Interface*, 6(31):187–202, 2009.

[205] P. Toutain, R. Brandon, M. Alvinerie, R. Garcia Villar, and Y. Ruckebusch. Dexamethasone in cattle: pharmacokinetics and action on the adrenal gland. *Journal of veterinary pharmacology and therapeutics*, 5(1):33–43, 1982.

[206] S. G. van der Drift, M. Houweling, M. Bouman, A. P. Koets, A. G. Tielens, M. Nielen, and R. Jorritsma. Effects of a single glucocorticoid injection on propylene glycol-treated cows with clinical ketosis. *The Veterinary Journal*, 204(2):144–149, 2015.

[207] D. Van Raalte, A. Mari, M. Bunck, V. Nofrate, W. Dokter, U. Nassander, et al. Acute and subacute exposure to glucocorticoids differentially impair various aspects of beta-cell function in healthy males (1468-p). 68th sessions american diabetes association. *San Francisco*, 2008.

[208] D. Van Raalte, D. Ouwens, and M. Diamant. Novel insights into glucocorticoid-mediated diabetogenic effects: towards expansion of therapeutic options? *European journal of clinical investigation*, 39(2):81–93, 2009.

[209] D. van Ravenzwaaij, P. Cassey, and S. D. Brown. A simple introduction to markov chain monte carlo sampling. *Psychonomic bulletin & review*, 25(1):143–154, 2018.

[210] J. Vanlier, C. A. Tiemann, P. A. Hilbers, and N. A. van Riel. A bayesian approach to targeted experiment design. *Bioinformatics*, 28(8):1136–1142, 2012.

[211] S. V. Vaseghi. *Advanced digital signal processing and noise reduction*. John Wiley & Sons, 2008.

[212] I. Vetharaniam, A. Peterson, K. McNatty, and T. Soboleva. Modelling female reproductive function in farmed animals. *Animal Reproduction Science*, 122(3):164–173, 2010.

[213] J. L. Vicini, F. C. Buonomo, J. J. Veenhuizen, M. A. Miller, D. R. Clemmons, and R. J. Collier. Nutrient balance and stage of lactation affect responses of insulin, insulin-like growth factors i and ii, and insulin-like growth factor-binding protein 2 to somatotropin administration in dairy cows. *The Journal of Nutrition*, 121(10):1656–1664, 1991.

[214] A. Villa Godoy, T. Hughes, R. Emery, L. Chapin, and R. Fogwell. Association between energy balance and luteal function in lactating dairy cows. *Journal of Dairy Science*, 71(4):1063–1072, 1988.

[215] E. J. Wagenmakers, M. Lee, T. Lodewyckx, and G. J. Iverson. Bayesian versus frequentist inference. In *Bayesian evaluation of informative hypotheses*, pages 181–207. Springer, 2008.

[216] R. Walsh, J. Walton, D. Kelton, S. LeBlanc, K. Leslie, and T. Duffield. The effect of subclinical ketosis in early lactation on reproductive performance of postpartum dairy cows. *Journal of dairy science*, 90(6):2788–2796, 2007.

[217] S. Walsh, D. Matthews, J. Browne, N. Forde, M. Crowe, M. Mihm, M. Diskin, and A. Evans. Acute dietary restriction in heifers alters expression of genes regulating exposure and response to gonadotrophins and igf in dominant follicles. *Animal Reproduction Science*, 133(1):43–51, 2012.

[218] S. Walsh, E. Williams, and A. Evans. A review of the causes of poor fertility in high milk producing dairy cows. *Animal Reproduction Science*, 123(3):127–138, 2011.

[219] Z. Wang, W. M. Bennet, R. Wang, M. A. Ghatei, and S. R. Bloom. Evidence of a paracrine role of neuropeptide-y in the regulation of insulin release from pancreatic islets of normal and dexamethasone-treated rats. *Endocrinology*, 135(1):200–206, 1994.

[220] L. Wasserman. *All of statistics: a concise course in statistical inference*. Springer Science & Business Media, 2013.

[221] D. Wathes, G. Pollott, K. Johnson, H. Richardson, and J. Cooke. Heifer fertility and carry over consequences for life time production in dairy and beef cattle. *Animal*, 8(s1):91–104, 2014.

[222] C. Weber, C. Hametner, A. Tuchscherer, B. Losand, E. Kanitz, W. Otten, S. Singh, R. Bruckmaier, F. Becker, W. Kanitz, et al. Variation in fat mobilization during early lactation differently affects feed intake, body condition, and lipid and glucose metabolism in high-yielding dairy cows. *Journal of dairy science*, 96(1):165–180, 2013.

[223] C. Weber, C. Schäff, U. Kautzsch, S. Börner, S. Erdmann, S. Görs, M. Röntgen, H. Sauerwein, R. Bruckmaier, C. Metges, et al. Insulin-dependent glucose metabolism in dairy cows with variable fat mobilization around calving. *Journal of dairy science*, 99(8):6665–6679, 2016.

[224] S. P. Weinstein, C. M. Wilson, A. Pritsker, and S. W. Cushman. Dexamethasone inhibits insulin-stimulated recruitment of glut4 to the cell surface in rat skeletal muscle. *Metabolism*, 47(1):3–6, 1998.

[225] J. N. Weiss. The hill equation revisited: uses and misuses. *The FASEB Journal*, 11(11):835–841, 1997.

[226] A. Wierda, J. Verhoeff, J. Dorresteijn, T. Wensing, et al. Effects of two glucocorticoids on milk yield and biochemical measurements in healthy and ketotic cows. *The Veterinary record*, 120(13):297–299, 1987.

[227] J. Wiltbank, W. Rowden, J. Ingalls, and D. Zimmerman. Influence of postpartum energy level on reproductive performance of hereford cows restricted in energy intake prior to calving. *Journal of Animal Science*, 23(4):1049–1053, 1964.

[228] J. K. Wise, R. Hendler, and P. Felig. Influence of glucocorticoids on glucagon secretion and plasma amino acid concentrations in man. *The Journal of clinical investigation*, 52(11):2774–2782, 1973.

[229] J. Yelich, R. Wettemann, H. Dolezal, K. Lusby, D. Bishop, and L. Spicer. Effects of growth rate on carcass composition and lipid partitioning at puberty and growth hormone, insulin-like growth factor i, insulin, and metabolites before puberty in beef heifers. *Journal of Animal Science*, 73(8):2390–2405, 1995.

[230] J. W. Young, D. R. Trott, P. J. Berger, S. P. Schmidt, and J. A. Smith. Gluconeogenesis in ruminants: glucose kinetic parameters in calves under standardized conditions. *The Journal of Nutrition*, 104(8):1049–1055, 1974.

Zusammenfassung

Experimentelle Studien haben gezeigt, dass die Ernährung von Kühen eine wichtige Rolle bei der Regulation der Reproduktionshormone sowie bei der Follikelreifung spielt. Bei Milchkühen führt eine negative Energiebilanz zu Beginn der Laktationsperiode zu einer verzögerten Aufnahme des Reproduktionszyklus. Niedrige Glukose- und Insulinkonzentrationen im Blut resultieren in Hormonungleichgewichten und führen infolge dessen zu einer verzögerten Aufnahme der zyklischen Aktivität nach dem Kalben.

In dieser Arbeit werden mathematische Modelle auf der Basis von Differentialgleichungen verwendet, um die Glukose-Insulin-Dynamik und den Östruszyklus zu simulieren. In Kombination beschreiben diese Modelle, wie sich die Futtermenge und deren Glukosegehalt auf die Reproduktionshormone und die Follikelreifung auswirken. Die Simulationsergebnisse für verschiedene Glukosegehalte im Futter bei laktierenden und nichtlaktierenden Kühen werden mit Ergebnissen experimenteller Studien verglichen. Weiterhin werden akute und chronische Futterreduktionen bei nichtlaktierenden Kühen untersucht. Für laktierende Kühe, welche nach der Kalbung unter Energiemangel leiden, werden die Futtermenge und der Glukosegehalt variiert und es wird gezeigt, dass die resultierenden Hormonzyklen in Abhängigkeit von Glukoseaufnahme und Körpergewicht stark variieren. Insgesamt zeigen die Berechnungen, dass ein Futtermanagement einen Einfluss auf metabolische Funktionen hat und die Fruchtbarkeit in Milchkühen beeinflusst.

Um die Anwendbarkeit des mathematischen Modells zu belegen, wird der Effekt einer Einzeldosis Dexamethason auf das Glukose-Insulin-System simuliert. Hierzu wird das mathematische Modell mit einem Pharmakokinetik-Modell gekoppelt, welches die Wirkung von Dexamethason auf das modellierte System beschreibt. Als weitere praktisch wichtige Anwendung wird das mathematische Modell für das Design von Experimenten eingesetzt. Bayessche Inferenz und informationstheoretische Konzepte geben Auskunft darüber, wann gemessen werden sollte, also über die Auswahl optimaler Messzeitpunkte, sowie darüber, was gemessen werden soll, also welche Modellspezies. Diese Information gestattet es, für nichtlaktierende Kühe die Unsicherheit in den Modellparametern zu reduzieren und für laktierende Kühe die Unsicherheit in der Vorhersage des frühesten Ovulationszeitpunktes nach der Kalbung zu minimieren.

Zusammengefasst repräsentiert diese Arbeit einen wichtigen Schritt in Richtung der Entwicklung von Fütterungsstrategien und Behandlungsoptionen in silico und leistet somit einen Beitrag zur Reduzierung von Tierversuchen.

Summary

Experimental studies have reported that nutrition plays a crucial role in regulating reproductive hormones and follicular development in cattle. In lactating cows, a negative energy balance at the onset of milk production after calving has been associated with similar problems. Here, elongated periods of anovulation have been observed resulting from an attenuation of the pulse frequency of the luteinizing hormone caused by lower concentrations of blood glucose and insulin.

In this thesis, differential equation models are used to simulate the glucose-insulin dynamics and the bovine estrous cycle. Combined, these models describe how the amount and the composition of food, in particular its glucose content, affect the reproductive hormones and the follicular development. Simulation results for different nutritional regimes in lactating and non-lactating dairy cows are examined and compared with experimental studies. For example, we study acute and chronic dietary restrictions; this is done for non-lactating cows. For lactating cows, which postpartum suffer from energetic deficiencies, we vary the amount of food and its glucose content. The resulting versions of the estrous cycle differ distinctly depending on the nutritional glucose and the body weight. The computations show that an improved food management that reduces incidences of metabolic disorder can increase the fertility of dairy cows.

Regarding the applicability of the resulting mathematical model, we simulate the effect of one single dose of dexamethasone on the physiological behaviour of the system, especially glucose metabolism. This is realized by linking the mathematical model to a pharmacokinetic model which describes the fate of dexamethasone in the system. Another application is the use of the mathematical model in designing experiments. In particular, we make use of the model, together with Bayesian inference and information theory to select the optimal design. The latter is expected to inform us about when to measure, i.e. select the optimal sampling times of measurement, and what to measure, i.e. specify observed species. These information allow us to reduce the uncertainty in the model parameters for non-lactating cows and the uncertainty in predicting the ovulation time during postpartum for lactating cows.

In summary, this work represents an important step towards the development of nutritional strategies and treatment options in silico and thus contributes to the reduction of animal testing.

Selbständigkeitserklärung

Hiermit bestätige ich, dass ich die vorliegende Arbeit selbständig verfasst habe. Ich versichere, dass ich ausschließlich die angegebenen Quellen und Hilfen in Anspruch genommen habe.

Berlin, den 19. March 2019

Mohamed Omari

Acknowledgment

First of all, I would like to express my sincere gratitude to my supervisor Susanna Röblitz for not only introducing me into the exciting field of Mathematical Systems Biology and offering me the possibility of writing this thesis, but also for her inspiring enthusiasm for research, her valuable input & feedback, and her endless support & kindness, and also for her guidance & patience throughout the last four years of my PhD.

I would also like to express my gratitude and appreciation to the current and former colleagues of the Computational Systems Biology Group at Zuse Institut Berlin (ZIB) for sharing their scientific knowledge/personal life topics with me inside and outside the research group. In particular, Rainald Ehrig for being always available to provide various supports in terms of academical and personal issues I faced during my stay at ZIB. I am also thankful to Julia Plöntzke for the support regarding the modelling work of this thesis, Stefanie Winkelmann for the kind assistance, Ilja Klebanov and Alexander Sikorski for being cool colleagues and for their valuable thoughts and numerous stimulating discussion in developing the chapter of Bayesian Experimental Design. I would also like to thank Stefanie Kasielke and Pooja Gupta for being nice officemates and for the kind help and support they provided. In addition, my thanks goes to Lisa Fischer and Mascha Berg for being friendly colleagues and for the help and support they also provided. I am also thankful to Stefan Schäfer, Robert Schwieger for the fun and cool time we had inside and outside ZIB, Marian Moldenhauer for the time we spent exchanging nice topics and ideas and the other members of ZIB including the administrative staff.

Furthermore, my gratitude also goes to the Steering Board members of the Graduate Research Training Program, PharMetrX, Charlotte Kloft and Wilhelm Huisinga for introducing me into the exciting field of Pharmacometrics. Additionally, A special thanks are due to all of my friends and colleagues whom I met through this exciting program and also enjoyed my time during my stay in Berlin: Lisa Ehmann, Sulav Duwal, Miro Eigenmann, Imke Ortland, Anke-Katrin Volz, Eva Göbgen, Jane Knöchel, Saskia Fuhrmann, Francis Williams Ojara, Maximilian Schmitt and André Byrla.

I must also thank all of my friends in Berlin area for all various support and sharing

all the nice moments as well as the ups and downs and for being a great persons through an important part of my life: Christian Lehr, Gabriela Onandia, Carlos Acame, Garabet Kazanjian, Neveen Eshtewy, Tobias Hohenbrink, Anne Schneider, Philipp Rauneker, Muhammad Arshad, Miaomiao Ma.

And finally, I would like to express my deepest gratitude to my family, in particular, my lovely parents, my sister and my brother for their continuous encouragement and all kinds of support whenever necessary.